2005-06

Sensibility study of St Andrew Bay rapid response system for Naval applications

Pauly, Patrice

Monterey, California. Naval Postgraduate School

NAVAL POSTGRADUATE SCHOOL

MONTEREY, CALIFORNIA

THESIS

SENSITIVITY STUDY OF ST ANDREW BAY RAPID RESPONSE SYSTEM FOR NAVAL APPLICATIONS

by

Patrice Pauly

June 2005

Thesis Advisor:	Peter Chu
Second Reader:	Steven D. Haeger

Approved for public release; distribution is unlimited

THIS PAGE INTENTIONALLY LEFT BLANK

REPORT DOCUMENTATION PAGE			Form Approved OMB No. 0704-0188
Public reporting burden for this collection of information is estimated to average 1 hour per response, including the time for reviewing instruction, searching existing data sources, gathering and maintaining the data needed, and completing and reviewing the collection of information. Send comments regarding this burden estimate or any other aspect of this collection of information, including suggestions for reducing this burden, to Washington headquarters Services, Directorate for Information Operations and Reports, 1215 Jefferson Davis Highway, Suite 1204, Arlington, VA 22202-4302, and to the Office of Management and Budget, Paperwork Reduction Project (0704-0188) Washington DC 20503.			
1. AGENCY USE ONLY ***(Leave blank)***	**2. REPORT DATE** June 2005	**3. REPORT TYPE AND DATES COVERED** Master's Thesis	
4. TITLE AND SUBTITLE: sibility study of St Andrew Bay rapid response system for naval applications.			**5. FUNDING NUMBERS**
6. AUTHOR(S) Patrice Pauly			
7. PERFORMING ORGANIZATION NAME(S) AND ADDRESS(ES) Naval Postgraduate School Monterey, CA 93943-5000			**8. PERFORMING ORGANIZATION REPORT NUMBER**
9. SPONSORING /MONITORING AGENCY NAME(S) AND ADDRESS(ES) N/A			**10. SPONSORING/MONITORING AGENCY REPORT NUMBER**
11. SUPPLEMENTARY NOTES The views expressed in this thesis are those of the author and do not reflect the official policy or position of the Department of Defense or the U.S. Government.			
12a. DISTRIBUTION / AVAILABILITY STATEMENT Approved for public release; distribution is unlimited			**12b. DISTRIBUTION CODE**

13. ABSTRACT (maximum 200 words)

Rapid assessment of littoral ocean physical and chemical conditions has represented a great challenge in recent years. For the physical part, time constraint may limit to using the barotropic mode. But because rain can be significant in St Andrew Bay system, Florida, fresh water, even when rivers lack, is a prevailing salinity regulator through ground seepage. Therefore, studying the baroclinicity and forcing mechanisms should provide a reasonable guidance help for deciding which will be ignored or included when modeling the area of interest. For the chemical part, considering either national security relevance or shipping hazard, a release of chemicals used in nearby offshore oil platform stands in the domain of possibilities.

A coupled hydrodynamic and chemical model, WQMAP and CHEMMAP developed at the Applied Sciences Associates, is used in this study with WQMAP for evaluating baroclinicity and forcing mechanism impacts and with CHEMAP for estimating the consequences of a hypothetical release of chemical. A stochastic model was applied for determining probable distribution and concentration resulting from the release at a given location.

14. SUBJECT TERMS St Andrew Bay– Baroclinicity – WQMAP – CHEMMAP - chemical			**15. NUMBER OF PAGES** 116
			16. PRICE CODE
17. SECURITY CLASSIFICATION OF REPORT Unclassified	**18. SECURITY CLASSIFICATION OF THIS PAGE** Unclassified	**19. SECURITY CLASSIFICATION OF ABSTRACT** Unclassified	**20. LIMITATION OF ABSTRACT** UL

NSN 7540-01-280-5500 Standard Form 298 (Rev. 2-89)
Prescribed by ANSI Std. 239-18

THIS PAGE INTENTIONALLY LEFT BLANK

Approved for public release; distribution is unlimited

SENSIBILITY STUDY OF ST ANDREW BAY RAPID RESPONSE SYSTEM FOR NAVAL APPLICATIONS.

Patrice Pauly
Lieutenant Commander, French Navy
B.S., French naval academy, 1992

Submitted in partial fulfillment of the
requirements for the degree of

MASTER OF SCIENCE IN PHYSICAL OCEANOGRAPHY

from the

NAVAL POSTGRADUATE SCHOOL
June 2005

Author: Patrice Pauly

Approved by: Peter Chu
Thesis Advisor

Steven D. Haeger
Second Reader

Mary L. Batteen
Chairman, Department of Oceanography

THIS PAGE INTENTIONALLY LEFT BLANK

ABSTRACT

Rapid assessment of littoral ocean physical and chemical conditions has represented a great challenge in recent years. For the physical part, time constraint may limit to using the barotropic mode. But because rain can be significant in St Andrew Bay system, Florida, fresh water, even when rivers lack, is a prevailing salinity regulator through ground seepage. Therefore, studying the baroclinicity and forcing mechanisms should provide a reasonable guidance help for deciding which will be ignored or included when modeling the area of interest. For the chemical part, considering either national security relevance or shipping hazard, a release of chemicals used in nearby offshore oil platform stands in the domain of possibilities.

A coupled hydrodynamic and chemical model, WQMAP and CHEMMAP developed at the Applied Sciences Associates, is used in this study with WQMAP for evaluating baroclinicity and forcing mechanism impacts and with CHEMAP for estimating the consequences of a hypothetical release of chemical. A stochastic model was applied for determining probable distribution and concentration resulting from the release at a given location.

THIS PAGE INTENTIONALLY LEFT BLANK

TABLE OF CONTENTS

THIS PAGE INTENTIONALLY LEFT BLANK

LIST OF FIGURES

THIS PAGE INTENTIONALLY LEFT BLANK

LIST OF TABLES

THIS PAGE INTENTIONALLY LEFT BLANK

ACKNOWLEDGMENTS

My first thought goes to the Service Hydrographique de la Marine (SHOM) and the Etablissement Principal du Service Hydrographique de la Marine (EPSHOM) which endlessly supported my master program at NPS. I would like to thank both Mr. Steven D. Haeger from the Naval Oceanographic Office for his assistance in the shaping of my work and NAVO which funded my study. I wish to thank Mr. Matthew Ward from Applied Science Associates, Inc. for his technical assist. He easily shared his skills for teaching me how to handle the models he provided and his expertise in the analysis process.

I would like to thank the NPS faculty for the time and the knowledge they shared with me during the two years I have spent in Monterey. Among them, I would particularly emphasize my gratitude towards Professor Peter Chu for his continuous support, his advice and the guidance he provided throughout the months I worked on my thesis. I am also deeply grateful for his endorsement during my PhD exam.

Lastly, I would like to pledge my wife Katy with my doubtless awareness for all the sacrifices she granted to. I would like to apologize for the time I spent working in stead of taking care of her and our children. For their constant support and the manner they light my life up, I ensure them of my true love. No words will ever reflect the pride I have to stand besides them.

THIS PAGE INTENTIONALLY LEFT BLANK

I. INTRODUCTION

The U.S. Navy has requirements for the prediction of currents and tides worldwide in geographical basins ranging from open ocean to continental shelf, estuary, and rivers. The Naval Oceanographic Office (NAVOCEANO) implements and runs several types of 2D and 3D circulation models for many geographical domains around the world. Most of these are run in operational modes and generate daily products for the Fleet. Although the mission is to provide nowcasts and forecasts worldwide (deep and shallow water), many operations take place in coastal bays and rivers. The model products in these domains support a wide variety of applications ranging from Special Operations, Mine Warfare, Expeditionary Warfare, Object Drift, Search and Rescue, Chemical and Oil Spill. St Andrew Bay system, hosting the Naval Surface Warfare Center, is a perfect theatre of this study because it has the intra-coastal highways, and is in the neighborhood of offshore oil drilling platforms. Rapid environmental assessment is important for this region.

High resolution, 3D baroclinic nested littoral-open ocean models are usually used to assess complex littoral zone oceanography with forcing functions. The purpose of this study is to determine if a 2D *barotropic,* un-nested littoral circulation model can satisfy certain Navy applications in coastal bays dominated by tides and local wind forcing within time scales ranging from "instantaneous" (what a diver will feel in the water) to days (the drift of floating objects). Savings in model implement, tuning, and validation are of outmost importance when using rapid response systems as authorities requires shrinking time delay between accident occurrence and the first decision.

Applied Science Associate, Inc. (ASA) out of Narragansett, Rhode Island has developed a three-dimensional, time dependent hydrodynamic model, the Water Quality Mapping and Analysis Package (WQMAP) coupled with rapid response model for oil spill tracking (OILMAP), search and rescue operations (SARMAP) or chemical release (CHEMMAP). The possibility of running these hydrodynamic models either in 2D- or 3D-version, the fact they have been used for years by NAVOCEANO, increased the significance of their use.

The lack of in-situ measured data did not constrain this study as we focused on the effects each forcing mechanism induced to the system. We hence built up a control run as a reference picture for circulation pattern, current speed and vertical salinity distributions. A careful scrutiny of local forcing pinpointed their ability in influencing the circulation in St Andrew Bay system and the consequences of each forcing mechanism on the system were examined. We finally choose to run the hydrochemical model CHEMMAP as rapid response system to evaluate the response of St Andrew Bay to a hazardous chemical release.

II. ST ANDREW BAY OCEANOGRAPHY

The continental shelf of the Gulf of Mexico includes the broad Western Florida Shelf that extends to 200 km in width (Roberts et al., 1999). Major relief along the shelf in this region is associated with roughly shore-parallel ridges, related to the positions of former shorelines during the rise of sea level after the latest Pleistocene glacial maximum. The northeastern Gulf of Mexico continental shelf off the panhandle of Florida, Alabama, and Mississippi ranges in width from 25 to 125 km, and depths at the shelf break range from 60 to 100 m.

Shelf circulation in the Gulf of Mexico exhibits distinct patterns in different regions. Off western Florida, the circulation is complex, influenced largely by wind and Loop Current forcing. In the northeastern Gulf of Mexico, flow appears to be responsive to wind forcing. Average flow along the inner shelf is onshore near the bottom and offshore in the upper water column (Wiseman and Sturges, 1999).

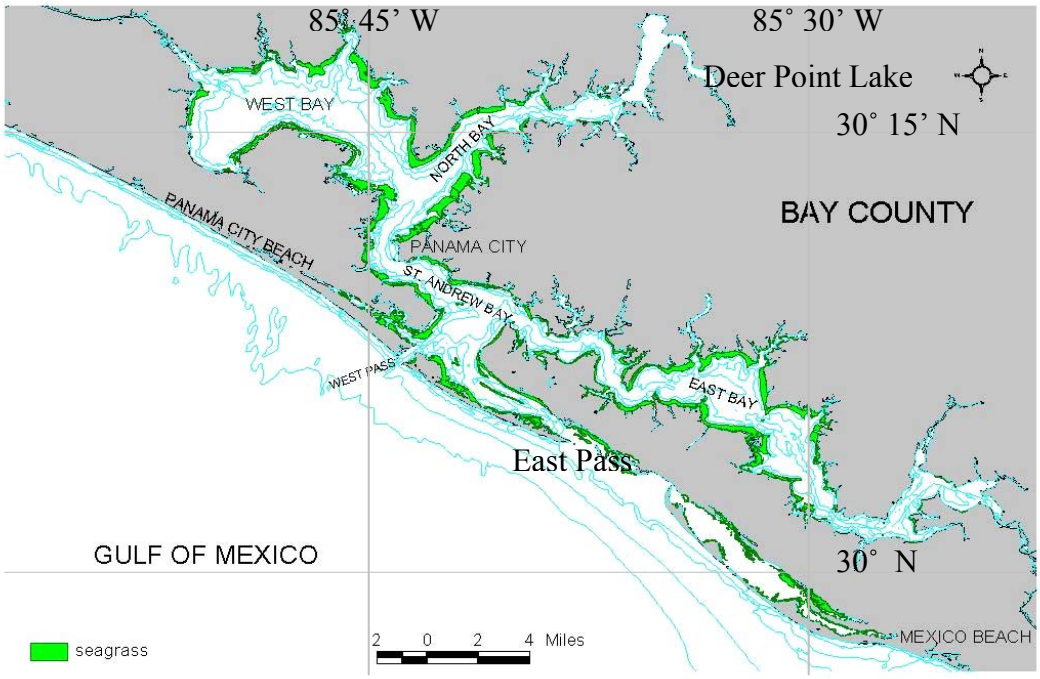

Figure 1. St Andrew Bay system (http://science.gulfcoast.edu/lindafitzhugh/St.%20Andrew%20Bay.jpg) the 20-May-05

A. ST ANDREW BAY SYSTEM

The St Andrew Bay system is located in the western part of Florida State close to Pensacola. It is a long, narrow and rather shallow (water column extends from 4 to 10 m) bay oriented in the northwestern direction. Deer Point Lake located at the northern edge of North Bay, provides the major freshwater inflow into the estuary, along with a number of smaller creeks. Two major passes, East Pass and West Pass, have provided surface water connections via its central part (St Andrew Bay) with the Gulf of Mexico. West Pass was artificially cut in 1934 in Shell Island as the primary navigation channel to the Gulf, while most exchange between the estuary and the Gulf had historically occurred through East Pass. East Pass was recently filled in (1998), however, by the movement of shoreline sediments. Dredging was conducted for reopening the pass in 2001. None of these channel widths exceed 1 km. St Andrew Bay system also links the Intracoastal Waterway on both the very end of the East Bay and the West Bay. The waterway depth is constantly maintained at 4m which causes some water exchanges to occur at these locations.

Drainages into these bays are small and mainly due to groundwater seepage. For example, it is suggested that almost two thirds of the creeks which flow into Deer Point Lake are supposed to be spring fed (Musgrove et al., 1965). Nevertheless their influence can be crucial when modeling the whole system.

In terms of estuarine classification, the four basins are generally positive, i.e., drainage inflow exceeds evaporation (Pritchard, 1952) except in St Andrew bay where neutral conditions, due to its connection with the Gulf, are found (Ichyie and Jones, 1961). The bottom contours are part of the WQMAP geographic information system (GIS) layer and have been provided by NOAA. They depict a 5.2m average depth for St Andrew bay, the mean depth respectively being 2.1, 1.7 and 2m for East, North and West bays.

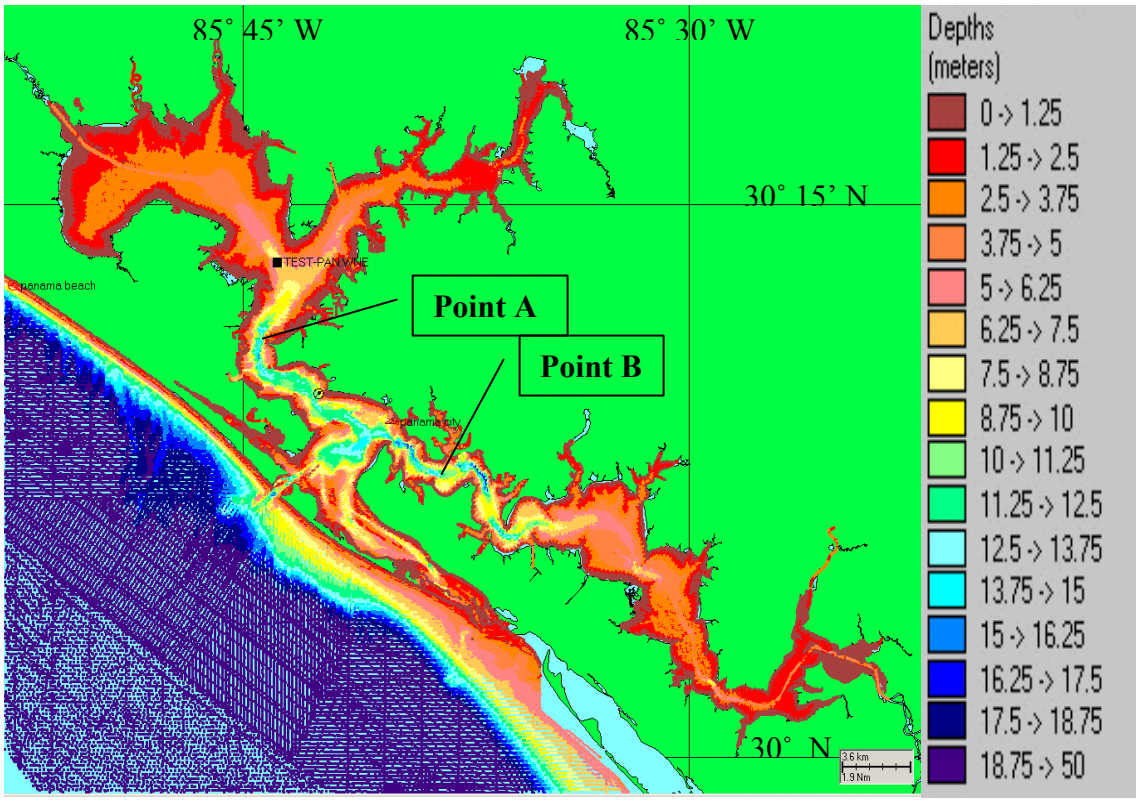

Figure 2. St Andrew Bay bathymetry

Temperature is rather uniform within the water column through out the bay system with very small vertical variations even in summer (the depth is too shallow for the thermocline to really develop). But its seasonal variability is evident. A five year-study of surface temperature from both inside and outside the bay, conducted using NOAA time series data, shows that the mean temperature varies between 15º C in winter and 30º C in summer. The comparison of these two 5-year-long time series (between 2000 and 2004) portrays a strong zonal sensibility and the difference ranges from 0 during winter time up to 2.5º C during summer (Fig. 3). The rather shallow bay allows the water column to heat up very quickly; the maximum difference is reached no later than March and lasts almost 9 months.

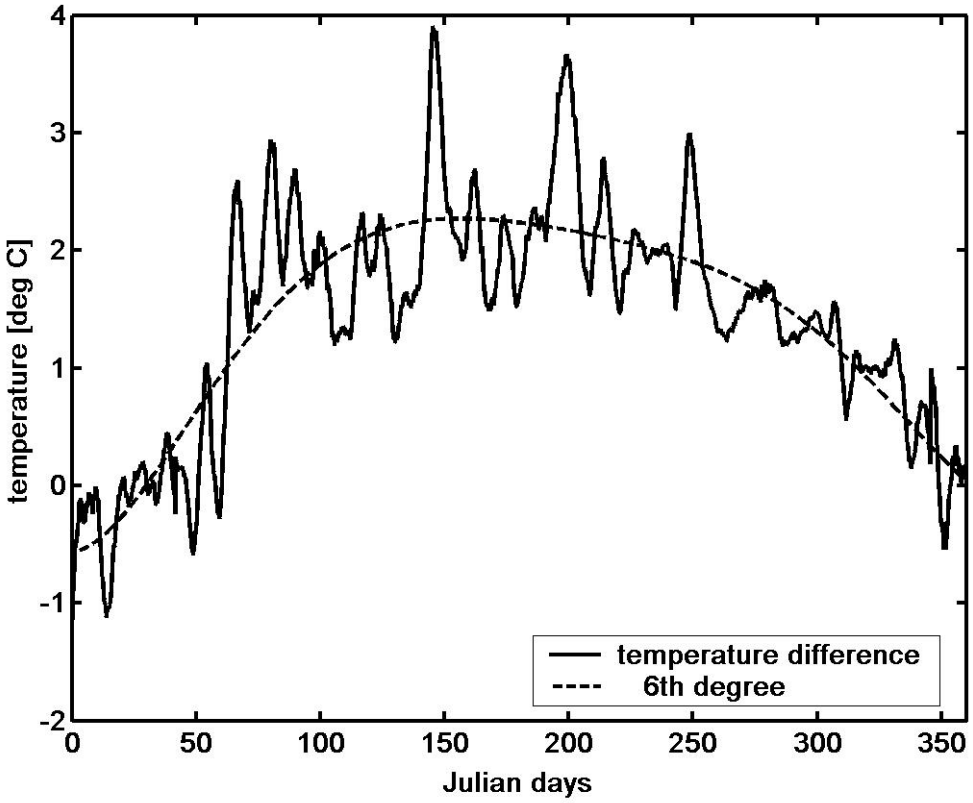

Figure 3. Temperature difference between St Andrew Bay and Gulf inner shelf

Salinity, however, presents some zonal features. Close to the Gulf of Mexico connection, the salinity is almost constant within the water column (gradient of 0.17 psu/m) and reaches its highest value (34.3 psu). Its value can drop down to 9 psu at surface nearby with a gradient of 3.3 psu/m (Ichyie, 1961; Blumberg and Kim, 2000). Nethertheless, the 24 h variation of salinity does not correlate closely with variations of the tidal current, specifically away from the bay entrance. The salinity follows the net flows caused by wind driven currents and freshwater inflow events. The hydrographic study conducted by Ichyie (1961) proved the water column stability being time independent and mainly subjected to salinity vertical variations (Sverdrup et al., 1942).

A. TIDES

The Panama City Beach (30º 12.8'N – 85º 52.7'W) and the St Andrew Bay (30º 09.1'N – 85º 40.0'W) data study shows that according to the form ratio (ratio between diurnal -K1+O1- and semidiurnal -M2+S2-), the tidal constituents are diurnal (ratio greater than 3). High and low water times study show the tidal waves first enter the bay through East Pass (5 minutes difference between East and West Pass) which correlates the general motion of tidal waves. The maximum current is found in the West Pass and can exceed 0.5m/s. It then decreases as low as 0.15m/s at the western end of West Bay. Most of the time, ebb currents duration is longer than flood current duration, mainly due to the effect of drainage, source of a quasi permanent outward current in the upper layer if any (Pritchard, 1952). This process causes "tidal pumping" phenomenon (Fischer et al, 1979).

Compound tides, often important in shallow water and hence on inner shelves, are generated by the nonlinear interactions of the primary constituents. The long-period tidal constituents are not resolvable in the month-long series, and contributes little (1.1 cm) to the tidal elevation. It is crucial to understand any seasonal effects which may occur on tides. Tidal results from a yearly sea-level time series were compared with those from a monthly subset of the sea-level time series to examine the seasonal effects. Additionally, this provides insight into the effects of unresolved tidal constituents contained in shorter time series. Overall, none of the major diurnal and semidiurnal tidal constituents differed more than 1 cm between the year- and month-long series except K1 constituent which varies significantly.

The five main constituents have been computed though 12 successive month-long time series collected in 2004 outside St Andrew Bay and are associated with a 95% confidence interval. This general trend is consistent with the observations of the last 5 years and denotes the occurrence of a seasonal dependence of both K1 and S2 constituents. A study, conducted in 2003 by Alvarez (personal publication), shows that sea breezes may be considered as a major source of the seasonal variability in the K1 tidal dynamics in near-coastal shallow regions this fact being explained as follows: if the

K1 tidal response to boundary forcing is subjected to the sea-breeze impact, the superposition of the K1 signal and the S1 signal, independent of what is its origin, will produce a seasonal modulation of the K1 tidal dynamics and, hence, seasonal variations in the K1 tidal characteristics. This finding results from the well-known expression for an amplitude- and phase-modulated oscillation. This statement is supported by experiments conducted in the Bay of Cadiz. However, the S1 coefficient does not show up during a monthly computation (the frequency step is too small for separating S1 from K1) and only portrays an amplitude of 0.3cm (2% of the K1 constituent) in the year-long time series study. It is also to notice that the confidence interval is very large during September as the data were impacted by a series of storm and a hurricane.

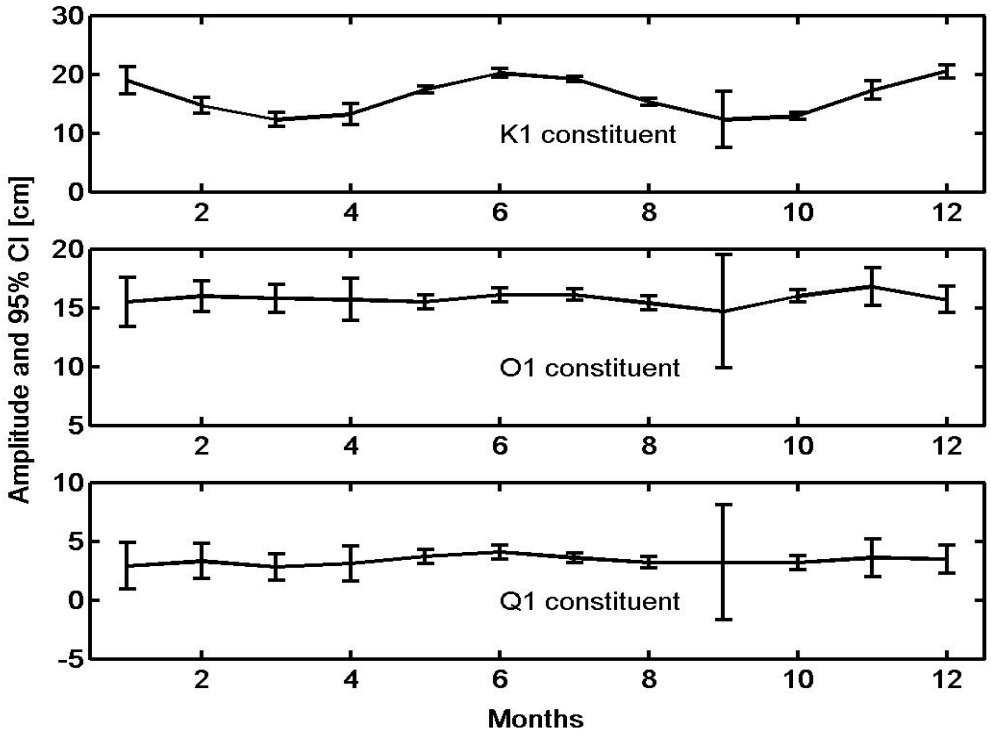

Figure 4. Diurnal constituents seasonal variability (at Panama City Beach)

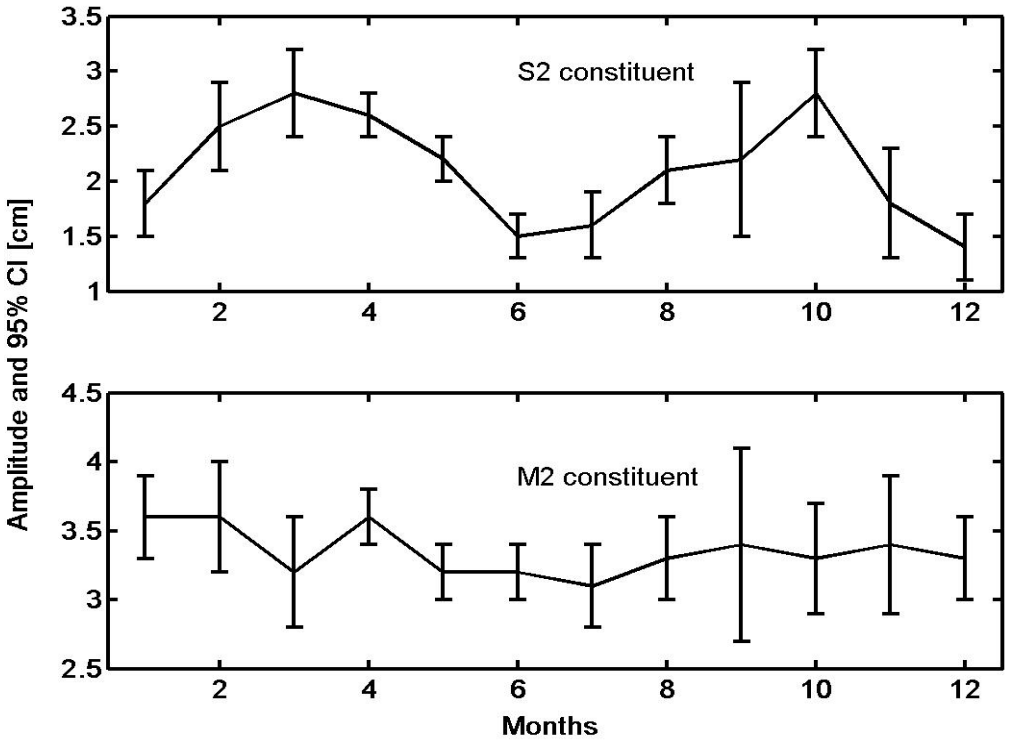

Figure 5. Semi-diurnal constituents seasonal variability (at Panama City Beach)

The only difference between both tidal analyses is the existence of residual semidiurnal energy, which accounts for small, erratic oscillations in the residual of the month-long series. While these residual oscillations are small compared to the dominant tidal constituents, it illustrates the problem of tidal analysis resolution inherent in short record lengths.

B. FRESHWATER SUPPLY

Freshwater discharge in the Gulf of Mexico totals approximately 1110 km^3 per year and is dominated by the Mississippi and Atchafalaya rivers, which contribute 55% of this discharge (Solis and Powell, 1999). The extent of the impact of this discharge, both vertically and horizontally, is variable and modulated by discharge rate and processes that disperse the plume, primarily wind stress. The river water accumulates in the inner shelf, forming a low salinity band that supports a persistent baroclinic flow to

the south (Atkinson et al., 1983). The mid shelf zone (21-40 m isobaths) is vertically homogeneous during the fall (September, October, November) and winter (December, January, February), due to enhanced wind mixing and decreased runoff. This region undergoes a transition to a vertically stratified state in the spring (March, April, May) and summer (June, July, August) as wind mixing decreases and runoff increases (Atkinson et al., 1983). In addition to runoff, groundwater sources have been shown to be important in the SE region of United States and prevail in the St Andrew bay system.

C. WAVE CONDITIONS

Waves largely correlating the wind direction, they primarily come from the east (23.5%). 2004 measurements from buoy 42039, located at 28.80N-86.06W, largely confirm the average computed from 1996 to 2001, the correlation coefficient being 0.77.

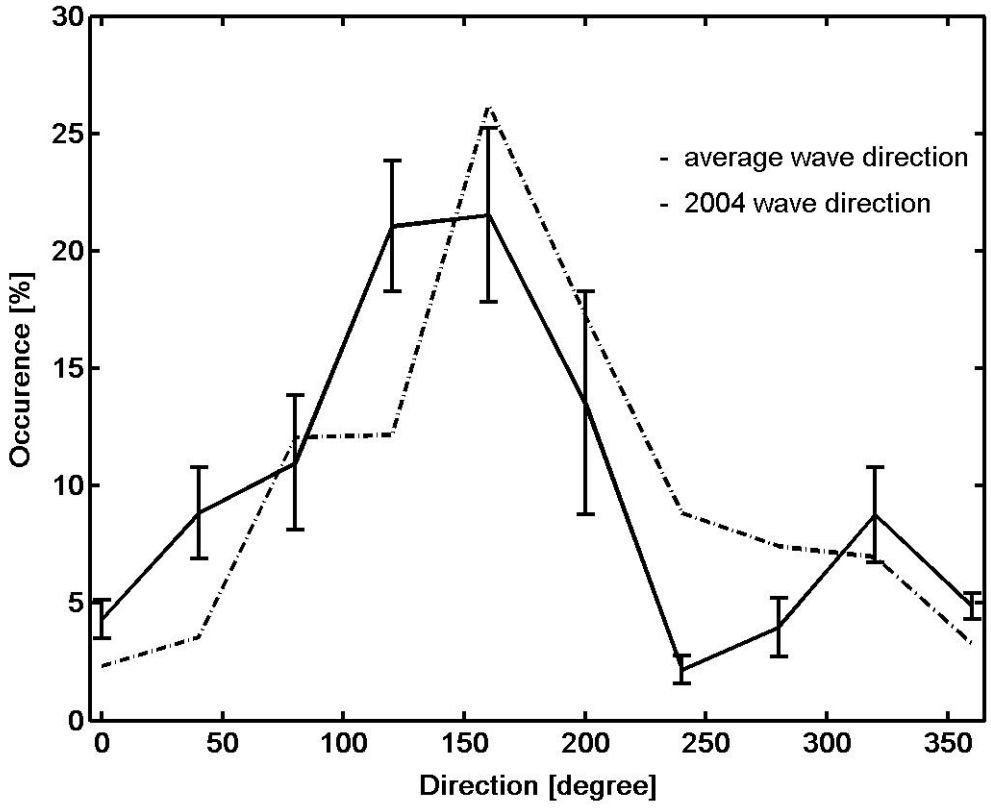

Figure 6. Wave direction comparison between 2004 and 1996-2001 average (buoy 42039, located at 28.80N-86.06W)

The monthly significant wave height (SWH) and wave peak period averages in figures 7 and 8 enhance the rather calm period between April and August. The yearly SWH mean is 1.1m but its median stands at 0.86m showing clearly the impact of hurricane and tropical storm period. The comparison between data collected in 2004 and 1996-2001 period averaged data do not depict any difference and present a 0.998 correlation coefficient.

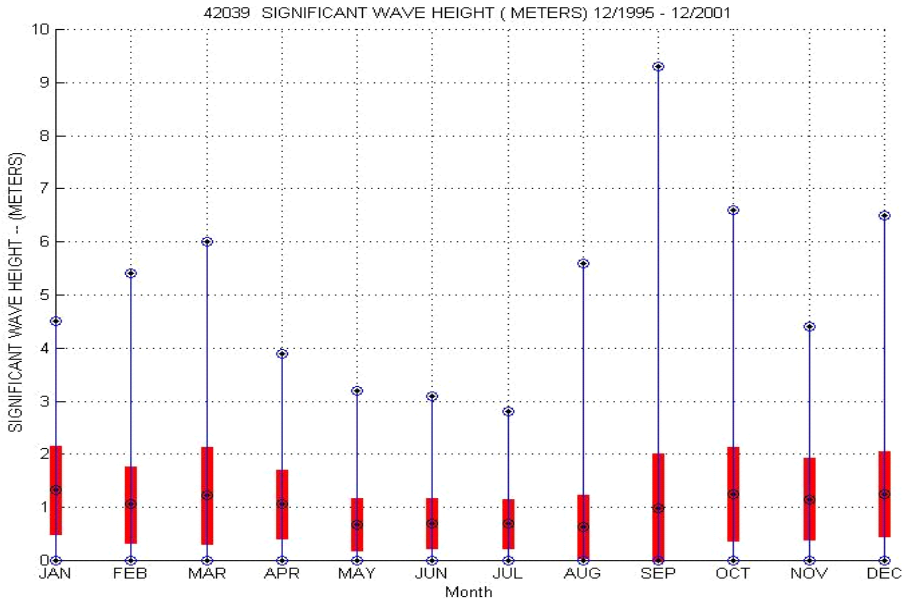

Figure 7. Average wave height between 1996 and 2001 (http://www.ndbc.noaa.gov/images/climplot/42039_wh.jpg) the 20-May-05

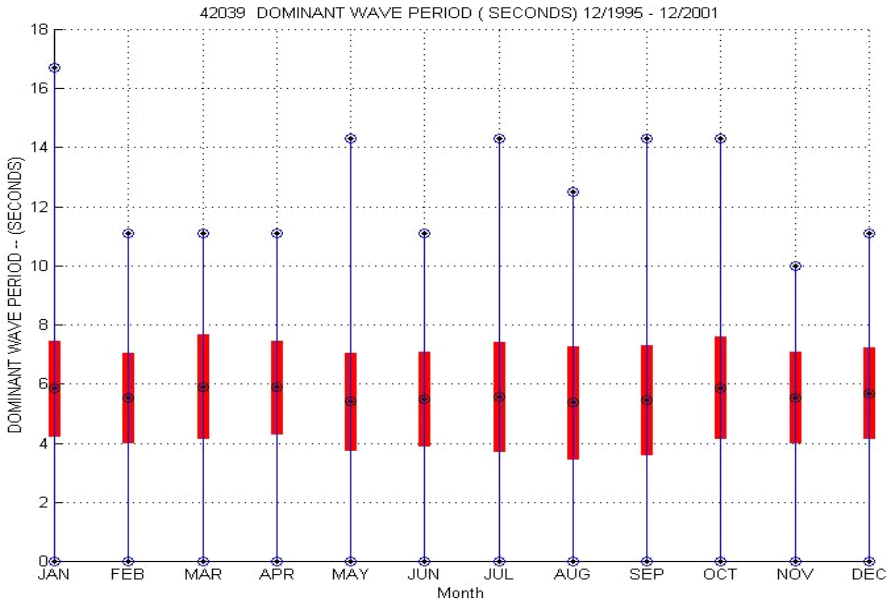

Figure 8. Dominant wave period between 1996 and 2001 (http://www.ndbc.noaa.gov/images/climplot/42039_wp.jpg) the 20-May-05

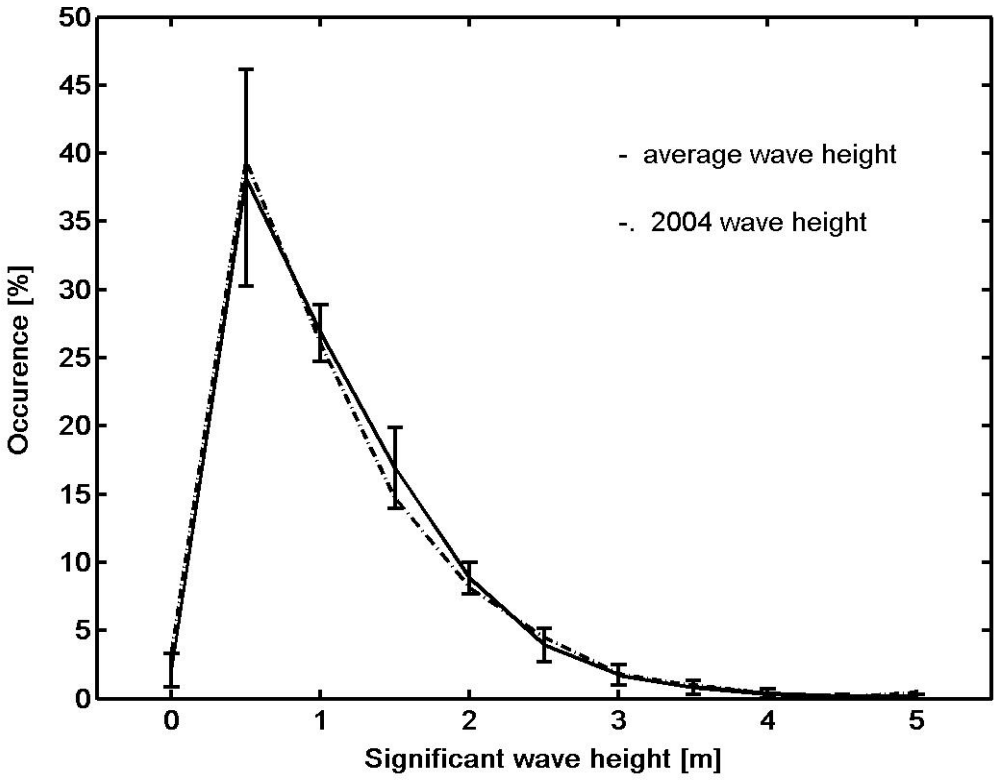

Figure 9. Significant wave height comparison between 1996-2001 and 2004 data sets (buoy 42039, located at 28.80N-86.06W)

However, wave generation in St. Andrew Bay is limited by fetch. Local harbor authorities state that wave height at Dyers Point is approximately 1.5 to 2.1 m during southeasterly hurricane force (≥33m/s) winds. Winds from other directions would result in lower wave heights. Wave heights may reach 6 m in the outer portion of the entrance channel, but do not reach the inner part of St. Andrew Bay.

D. ALONGSHORE CURRENT AND LITTORAL TRANSPORT

The main current affecting the surf zone is the alongshore current created by waves breaking at an angle to the shore. The magnitude of the alongshore current depends on the breaking wave characteristics, breaking angle and local bottom and shore configurations.

The alongshore currents are responsible for sand transport along the coast. For the study area, the net littoral transport is generally westward as the predominant waves are from the east and is estimated to be about 65,000 cubic yards per year. This estimate seems to be in agreement with the field evidence as indicated by the lack of strong erosion and accretion at the west and east side of the gulf entrance to the St. Andrew Bay (U. S. Army Corps of Engineers, 1971). However, the accumulation of hurricane-induced waves during the 1990's is likely to be responsible for East Pass closure that happened in 1998. Van de Kreeke (1990) showed that a two-inlet system could not be stable for a one-bay system. Even without erosion evidence, one of the inlets has to close. Moreover, Jain and al (2004) showed that both inlets were actually unstable and hence will request continuous dredging maintenance unless St Andrew bay is enlarged.

Bay County, to which Panama City belongs, has been scouting the shoreline since 1971 when Florida State made each county responsible for providing data on erosion trends, vegetation line, bathymetry surveys. From 30 years of data, the erosion causes have been split into two main processes.

1. Long-term changes

All beaches are experiencing erosion, the more severe locating on the northern edge of main entrance channel with a rate of 2.44 m/yr. This process is associated with the construction of St Andrews Inlet in 1934. Similar rates occur along Shell Island and

vary from 0.53m/yr in its western part to 1.95 m/yr close to the secondary channel entrance. The lack of construction on Shell Island does not make the eroding process as critical. However, bypass placements of sand have been helping in the stabilization of the shoreline.

2. Short term changes

These changes are mainly due to extreme weather system hitting the area. Hurricane Eloise in September 1975 caused a 100,000 m^3 beach-dune erosion. Hurricane Opal in October 1995 impacted the area by dredging almost 100,000 m^3 from both beaches and dunes (Bureau of Beaches and Coastal Systems Division). Finally, during hurricane Ivan event in September 2004, beaches alongside Bay County suffered a vertical loss of sand between 1.2 and 1.5 m (Bureau of Beaches and Coastal Systems Division, 2004).

III. ATMOSPHERIC FORCING

A. WINDS

Located at average latitude of 30º10'N, the St Andrew Bay system is under the influence of rather weak winds. The climatology of wind forcing in the Gulf of Mexico exhibits a pattern of seasonal variation. During the fall and winter months (mid-September to mid-February), winds are primarily from the north. In the late spring and summer (from March to July), the northern Gulf of Mexico is dominated by tropical weather with winds mainly southerly. During summer, the influence of the subtropical high (Bermuda High) increases as the frontal zone between subtropical and mid-latitude air masses moves north and out of the Gulf. Weaker pressure gradients and, hence, calmer winds associated with high pressure produce less vigorous wind stress forcing of oceanic or, in particular, shelf circulation. During summer, warm fronts move generally from south to north. The average data collected throughout the last 60 years show very uniform winds.

	Jan	Feb	Mar	Apr	May	Jun	Jul	Aug	Sep	Oct	Nov	Dec
Dir.	N	N	SSE	S	S	WSW	WSW	E	ENE	N	N	N
Speed	3.5	3.5	4	3.5	3	3	3	2.5	3	3	3	3.5

Table 1. Average wind direction and speed (m/s)

B. RAINFALL

The precipitation records from the last 30 years at Panama city airport correlates the maximum rainfall with the northern (winter) and southern (summer) winds. However, because of their tropical influence, rainfalls are often made from showers which may vary between two locations inside the bay, this phenomenon being pinpointed in former study (Blumberg and Kim, 2000).

	Jan.	Feb	Mar	Apr	May	Jun	Jul	Aug	Sep	Oct	Nov	Dec
rain	2.18	1.89	2.42	1.46	1.48	2.51	3.35	2.90	2.52	1.39	1.76	1.53

Table 2. Average rainfall (cm) at Panama City Airport

C. STORMS

The low wind speed average values must not hide episodic storm events this region has to face. The outstanding feature of the U.S. Gulf Coast region is its location on the north shore of the Gulf of Mexico and its orientation perpendicular to normal tropical cyclone tracks as they move more or less northward out of the tropics. Also of importance is the region's position between 25 and 30 degrees north latitude. This is within the normal location of tropical cyclone curvature change, which oscillates between latitudes 25N and 35N during the tropical cyclone season. This latter factor is significant since it is the character of tropical cyclones to slow and intensify during this stage. As an example, last September, hurricane Ivan passed by within 50 km producing 50-mph winds, 5 tornadoes over the bay system with 70 mph gust winds and wave surf of 1.7 meters (NOAA data). This extreme example is not lonesome and monthly wind speed increase between June and September is mainly due to tropical storm systems hitting that region.

A study based on 110 year record (1886-1996) of tropical storm entering the 330 km threat radius around Panama City with specific interest on Hurricane Eloise in 1975 and Hurricane Opal in 1995 conducted by the Navy[1] shows that no location on St. Andrew Bay at Panama City is suitable as a haven for U.S. Navy ships in a hurricane threat scenario. The low-lying terrain of coastal Florida offers no protection from hurricane effects and the bathymetry of the Gulf of Mexico coast adjacent to Panama City is favorable for storm surge generation (vertical rise in the motionless water level near the coast caused by reduction of atmospheric pressure and wind stresses on the water surface) whenever strong on-shore winds, such as might occur with a tropical cyclone passage, are present. Furthermore, the wave setup (superelevation of the water surface above storm surge level due to onshore mass transport of the water by wave action alone) is enhanced by exceptional high waves occurring in such a particular period. A further complication results from the relatively slow speed capability of the Navy vessels (usually belonging to Mine Warfare Fleet) visiting Panama City, and their intolerance for

[1] available online at https://www.cnmoc.navy.mil/nmosw/tr8203nc/panamac/text/frame.htm the 20-May-05

seas in excess of 4 to 5 meters. During the largest events that hit Panama City, all these phenomena summed up to reach 3.5 to 4 meters and worst case scenario predicts more than 6 m. Figure 10 (Fig. XXVIII-6 of the aforementionned study) presents how these events are distributed within the year.

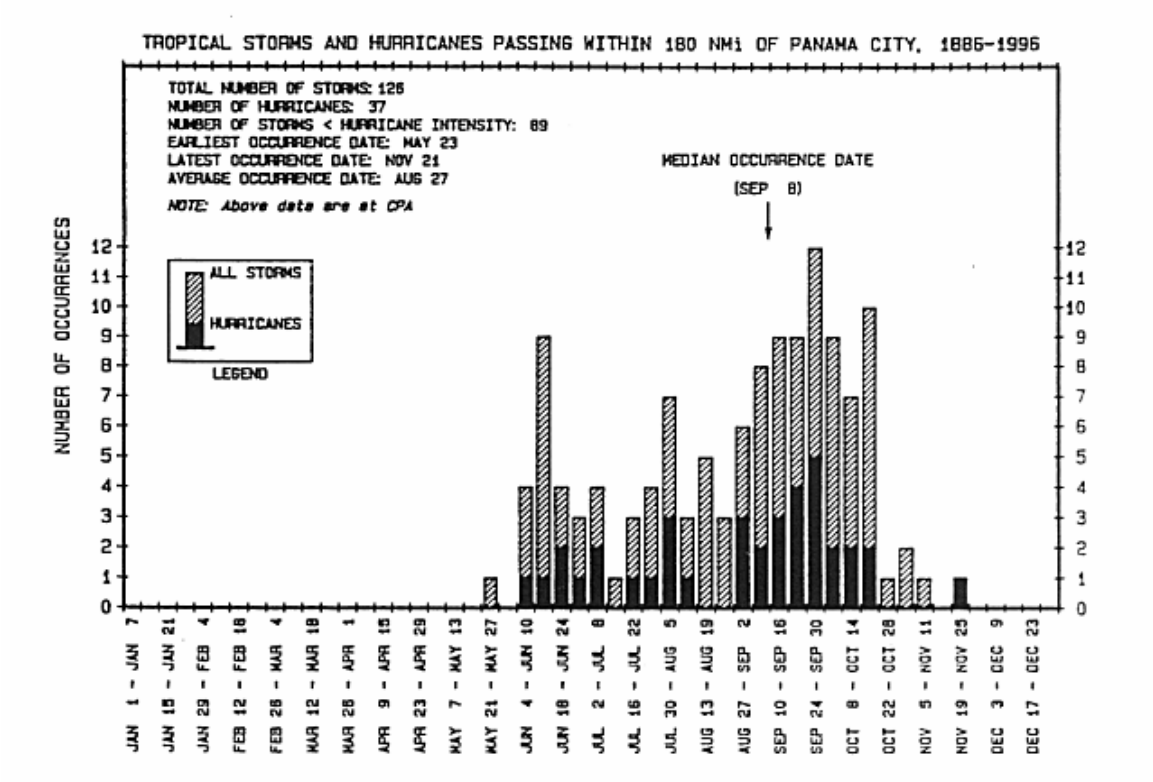

Figure 10. Annual distribution of the 126 tropical storms and hurricanes pissing within 330km of Panama City between 1886 and 1996

THIS PAGE INTENTIONALLY LEFT BLANK

IV. HYDRODYNAMIC MODEL

A. OVERVIEWS

The model used in this study is a three-dimensional, time dependent hydrodynamic model, the Water Quality Mapping and Analysis Package (WQMAP) developed by Applied Science Associate, Inc. out of Narragansett, Rhode Island. It is already being used by many institutions as NAVO, oil companies or coast guards (Ireland, Spain and USA). Continuity, momentum, salt and temperature transport equations are solved after applying a generalized orthogonal coordinate transformation on the horizontal and a sigma coordinate transformation on the vertical. These resultant equations are then decomposed into an exterior mode (barotropic or vertical averaged equations) solved implicitly and an interior mode (baroclinic or vertically structured equations), solved semi-implicitly. Some approximations are made in the model formulation such as the hydrostatic balance, and Boussinesq approximation.

This model solves the three dimensional conservation of mass, momentum, and energy equations with boundary conforming grid system and can be applied to both estuarine and littoral regions. The eddy viscosities can be both specified by the user or by turbulence closure using the turbulent kinetic energy (TKE) model. Output of the TKE model can be used in conjunction with a prescribed mixing length to determine the vertical eddy viscosities. The model outputs timeframe fields of surface elevations and velocities. The model can be forced with freshwater inflow, surface elevations, and wind fields.

In the exterior mode, the Helmholtz equation, given in terms of the sea surface elevation, is solved to ease the time step restrictions normally imposed by the aforementioned gravity wave propagation. In the interior mode the flow is predicted by an explicit finite difference method, except that the vertical diffusion term is treated implicitly (Madala and Piaczek, 1977). The time step generally remains the same for both exterior and interior modes (Spaulding et al, 1999). Hence, the user can specify the variable (currents, temperature, surface elevation and salinity) over a certain simulation period and then the results/ predictions are presented in either color contours or vectors.

B. COORDINATE SYSTEM

The basic foundation of the approach is to construct grids such that all domain boundaries are coincident with coordinate lines. This can be done using tensors which permit the model to transform the boundary fitted grid to a numerical grid employed for spatial discretization utilized in an Arakawa *C* Grid (Chu et al, 2004). Even though the transformed set of governing equations is considerably more complex than the original set, the transformed boundary conditions are specified on straight lines and the coordinate spacing is uniform in the transformed space. Orthogonal and conformal curvilinear grids, as well as simple stretched rectangular grids, are special cases of the generalized boundary conforming grid system (Spaulding et al, 1999).

The two metric tensors to transform orthogonal position (φ,θ) into conformal grid position (ξ,ψ) are defined by the following equations:

$$g_{11} = \left(\frac{\partial \varphi}{\partial \xi}\right)^2 \cos^2\theta + \left(\frac{\partial \theta}{\partial \xi}\right)^2 \qquad \textbf{(1)}$$

$$g_{22} = \left(\frac{\partial \varphi}{\partial \psi}\right)^2 \cos^2\theta + \left(\frac{\partial \theta}{\partial \psi}\right)^2 \qquad \textbf{(2)}$$

The user defines every single boundary point and then WQMAP numerically solves the coupled, elliptic coordinate transformation equations to determine the interior grid points within the model domain.

C. GOVERNING EQUATIONS

The hydrodynamic model included in the system solves the three dimensional, conservation of water mass, momentum, salt and energy equations on a spherical, non orthogonal, boundary conforming grid system and is applicable for estuarine and coastal areas (Muin, 1996). The two dimensional equations can also be predicted by vertically averaging the above over the water column.

A sigma stretching system (number of layers constant whatever the depth is) is used to map the free surface and bottom to resolve bathymetric variations. The basic dynamical system is represented by Kantha and Clayson (2000) with the following governing equations.

The momentum equations in the ξ- and η-directions are given by

$$\frac{\partial uD}{\partial t}+\frac{1}{\sqrt{g_{11}g_{22}}}\left[\frac{\partial\left(u^2D\sqrt{g_{22}}\right)}{\partial\xi}+\frac{\partial\left(uvD\sqrt{g_{11}}\right)}{\partial\psi}+uvD\frac{\partial\left(\sqrt{g_{11}}\right)}{\partial\psi}-v^2\frac{\partial\left(\sqrt{g_{22}}\right)}{\partial\xi}\right]+\frac{\partial u\omega}{\partial\sigma}-fDv$$
$$=-\frac{gD}{R\sqrt{g_{11}}}\left[\frac{\partial\eta}{\partial\xi}+\frac{D}{\rho_0}\int_\sigma^0\left(\frac{\partial\rho}{\partial\xi}-\frac{\sigma}{D}\frac{\partial D}{\partial\xi}\frac{\partial\rho}{\partial\sigma}\right)d\sigma\right]+\frac{1}{D}\frac{\partial}{\partial\sigma}\left(A_v\frac{\partial u}{\partial\sigma}\right) \qquad \textbf{(3)}$$

$$\frac{\partial vD}{\partial t}+\frac{1}{\sqrt{g_{11}g_{22}}}\left[\frac{\partial\left(uvD\sqrt{g_{22}}\right)}{\partial\xi}+\frac{\partial\left(v^2D\sqrt{g_{11}}\right)}{\partial\psi}+uvD\frac{\partial\left(\sqrt{g_{22}}\right)}{\partial\xi}-u^2\frac{\partial\left(\sqrt{g_{11}}\right)}{\partial\psi}\right]+\frac{\partial v\omega}{\partial\sigma}+fDu$$
$$=-\frac{gD}{R\sqrt{g_{22}}}\left[\frac{\partial\eta}{\partial\psi}+\frac{D}{\rho_0}\int_\sigma^0\left(\frac{\partial\rho}{\partial\psi}-\frac{\sigma}{D}\frac{\partial D}{\partial\psi}\frac{\partial\rho}{\partial\sigma}\right)d\sigma\right]+\frac{1}{D}\frac{\partial}{\partial\sigma}\left(A_v\frac{\partial v}{\partial\sigma}\right) \qquad \textbf{(4)}$$

where η, σ, f, R, ρ_0 and A_v successively represent the surface elevation, the vertical stretching coefficient ($\sigma=\frac{z-\eta}{H+\eta}$), the Coriolis parameter ($f = 2\Omega\sin\theta$), the Earth radius, the mean water density (1025 kg/m^3) and the vertical eddy viscosity. The vertical averaging of the afore equation leads to

$$\frac{\partial UD}{\partial t}+\frac{1}{\sqrt{g_{11}g_{22}}}\left[\partial\frac{\left(U^2D\sqrt{g_{22}}\right)}{\partial\xi}+\partial\frac{\left(UVD\sqrt{g_{11}}\right)}{\partial\psi}+UVD\frac{\partial\left(\sqrt{g_{11}}\right)}{\partial\psi}-V^2\frac{\partial\left(\sqrt{g_{22}}\right)}{\partial\xi}\right]-fDV=$$
$$-\frac{gD}{R\sqrt{g_{11}}}\left[\frac{\partial\eta}{\partial\xi}+\frac{D}{\rho_o}\int_{-1}^0\int_\sigma^0\left(\frac{\partial\rho}{\partial\xi}-\frac{\sigma}{D}\frac{\partial D}{\partial\xi}\frac{\partial\rho}{\partial\sigma}\right)d\sigma d\sigma\right]+\frac{1}{\rho_o}\left(\tau_\xi^w-\tau_\xi^b\right)+A_hD\nabla^2U \qquad \textbf{(5)}$$

$$\frac{\partial UD}{\partial t}+\frac{1}{\sqrt{g_{11}g_{22}}}\left[\partial\frac{\left(U^2D\sqrt{g_{22}}\right)}{\partial\xi}+\partial\frac{\left(UVD\sqrt{g_{11}}\right)}{\partial\psi}+UVD\frac{\partial\left(\sqrt{g_{11}}\right)}{\partial\psi}-V^2\frac{\partial\left(\sqrt{g_{22}}\right)}{\partial\xi}\right]-fDV=$$
$$-\frac{gD}{R\sqrt{g_{11}}}\left[\frac{\partial\eta}{\partial\xi}+\frac{D}{\rho_o}\int_{-1}^{0}\int_{\sigma}^{0}\left(\frac{\partial\rho}{\partial\xi}-\frac{\sigma}{D}\frac{\partial D}{\partial\xi}\frac{\partial\rho}{\partial\sigma}\right)d\sigma d\sigma\right]+\frac{1}{\rho_o}\left(\tau_\xi^w-\tau_\xi^b\right)+A_hD\nabla^2U \quad \textbf{(6)}$$

where $A_{h,}$ τ^w and τ^b successively represent the horizontal eddy viscosity, the wind stress and the bottom stress.

The continuity equation is given by

$$R\sqrt{g_{11}g_{12}}\frac{\partial\eta}{\partial t}+\frac{\partial\left(uD\sqrt{g_{22}}\right)}{\partial\xi}+\frac{\partial\left(vD\sqrt{g_{11}}\right)}{\partial\psi}+R\sqrt{g_{11}g_{12}}\frac{\partial\omega}{\partial\sigma}=0 \qquad \textbf{(7)}$$

where ω represents the vertical velocity normal to the sigma level. Finally, the transport equation for any substance S is given by

$$\frac{\partial S}{\partial t}+\frac{u}{R\sqrt{g_{11}}}\frac{\partial S}{\partial\xi}+\frac{v}{R\sqrt{g_{22}}}\frac{\partial S}{\partial\psi}+w\frac{\partial S}{\partial\sigma}=\frac{1}{R^2g_{11}}\left(D_h\frac{\partial^2S}{\partial\xi^2}\right)+\frac{1}{R^2g_{22}}\left(D_h\frac{\partial^2S}{\partial\psi^2}\right)+\frac{1}{D^2}\frac{\partial}{\partial\sigma}\left(D_v\frac{\partial S}{\partial\sigma}\right) \textbf{(8)}$$

where D_h and D_v stand for horizontal and vertical diffusivities.

D. STABILITY CONDITIONS

The salt and temperature transport equations are solved by a simple explicit technique, except for the vertical diffusion term that is solved by an implicit scheme to ease the time step restriction due to the small vertical length scale. The advection term is solved using an upwind scheme (first-order accurate) that introduces artificial diffusivity. The horizontal diffusion term is solved by a centered in space explicit technique. The time step limitation satisfying the stability criteria is given by:

$$\Delta t \le \frac{1}{\frac{2D_h}{\left(R^2 g_{11}\right)^2} + \frac{2D_h}{\left(R^2 g_{22}\right)^2} + \frac{u}{R\sqrt{g_{11}}} + \frac{v}{R\sqrt{g_{22}}}} \qquad \textbf{(9)}$$

E. BOUNDARY CONDITIONS

The flow normal to the shoreline is set to zero and there is no flow through the water surface or the bottom where the momentum equations successively reduces to:

$$\frac{A_v}{D}\left(\frac{\partial u}{\partial \sigma}, \frac{\partial v}{\partial \sigma}\right) = C_d \rho_a \left(\sqrt{W_\xi^2 + W_\psi^2}\right)\left(W_\xi, W_\psi\right) \qquad \textbf{(10)}$$

$$\frac{A_v}{D}\left(\frac{\partial u}{\partial \sigma}, \frac{\partial v}{\partial \sigma}\right) = C_d \rho_0 \left(\sqrt{u^2 + v^2}\right)(u, v) \qquad \textbf{(11)}$$

where C_d, ρ_a and W respectively being the drag coefficient, the density of air and the friction velocity.

There is no transport of salt at closed boundaries as the shoreline is supposed impermeable. At the open boundaries, the concentration is specified during the inflow, using the characteristic values for Gulf of Mexico (temperature was set at 21º C and salinity at 35 psu). The same temperature was used at the intracoastal open boundaries and the salinity was set to 22 and 20 psu at West and East Bay respectively according to Blumberg and Kim (2000).

F. CONFIGURATION

The results from Blumberg and Kim (2000) being considered, in this particular study, we ran the model with a rectangular grid in its baroclinic mode. The number of layers was set to 10, every layer representing one tenth of the averaged water column depth within every cell. The model is sensitive to bathymetry changes occurring between two nearby cells. To avoid it blowing up, smoothing passes were applied on top of the grid averaging and each cell was assigned a minimum 2m-depth to avoid a large computational flux increase. This process led to significant depth changes over the whole bay. As the model conserves the total mass, the resulting speeds computed in the different

cases correspond to the smoothed depths. Careful attention must be taken if these values have to be used for operational applications.

Since the temperature is well mixed through the water column, we considered it as being constant in order to ease the computational effort. The 3-D choice is obvious and will not be discussed; the choice of a rectangular grid was driven by computational time restriction. For satisfying the CFL condition, the time step had to be set to 0.1 minute, and hence each run was requesting 17 hours.

V. DATA

A. RIVERS

Overall, there are 15 sources of freshwater that are used as part of the model forcing. They are identified in Fig. 11 and tabulated in Table 3. The major source of freshwater to the bay is Deer Point Lake. Daily-based flow rates were calculated using measured weir heights at the dam itself. The long-term average flow is 27m^3/s (Musgrove et al., 1965). Freshwater also enters the bay at many other locations. Unfortunately, these sources are largely ungauged even through the flows are often substantial, especially during times of intense precipitation. Table 2 represents the flow rate estimation computed by Blumberg (2000).

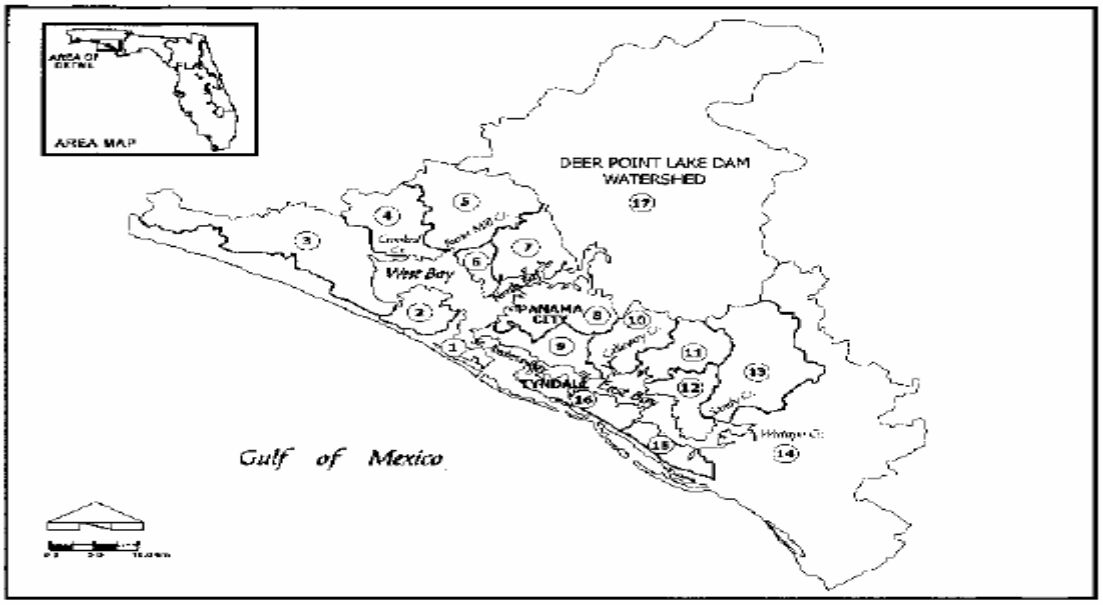

Figure 11. St Andrew Bay drainage sub-basins (30˚ N - 85˚ 30' W)

sub-basin	1	2	3	4	5	6	7	8	9	10	11	12	13	14	15	16	17
m^3/s	0.5	0.8	-	1.3	1.4	0.4	1.4	1.7	1	1.2	1.2	1	3.8	-	0.7	0.9	38.1

Table 3. Calculated mean flow (Blumberg and Kim, 2000)

Nevertheless these data are not as crucial, and thereby as accurate as they would have been for mass transfer computation. The effect of their fluctuation is, in this study, what is sought.

B. BAY ENTRANCES

1. Sea elevation

a. Tides

In this case also, the accuracy was not a key request for running this model. Data were collected at Panama City Beach where NOAA's National Ocean Service maintains a station providing among others water elevation in m above MLLW (Mean Lower Low Water) every 6 (or 60) minutes. As we considered the flow entered the bay through two passes, the evolution of each tidal constituent was examined as they propagate from East Pass onto West Pass on the continental shelf. The distance separating the two channels is 11.5 km. As a result, the phase shifts were of the order of the degree (1.1º for diurnal constituents and 2.5º for semi-diurnal constituents) and corresponded to a 5 minute-time lag. Moreover, the slight difference on the bathymetry in front of both entrances did not involve a large magnitude difference (0.1% for semi-diurnal constituents - K1 or O1- up to 2% for shallow water constituent – M4 – which only contributes little (1.1cm). At the end, these modifications were ignored. At last, even if the time series used at both locations were issued from Panama City Beach, 30km north of East Pass, we would not have had to correct them because the results from these series had not to be compared with any measured data set.

However, NOAA/NOS does not maintain gauge at the three open boundary locations and therefore the elevation time series were got using Wxtide32 software[2] (also called Tides and Currents) which is a free tool providing pure tidal elevation all around the world. The following table represents from left to right the Fourier decomposition of elevation gauge time series collected at NOAA station on Panama City Beach, the tidal constituents used by NOAA for predicting tides at Panama City Beach and the Fourier decomposition of tide predictions from Wxtide32 software. Numbers in parenthesis represents the 95% confidence interval for the computed values.

[2] Available online at www.wxtide32.com the 20-May-05

	Panama City Beach					
	collected data study		NOAA prediction data		Tide and current software	
	amplitude [cm]	phase [deg]	amplitude	phase	amplitude	phase
K1	15.89 (0.3)	296.2 (1)	14.5	286.7	15.53 (0.1)	313.9 (1)
O1	15.84 (0.3)	284.8 (1)	14.1	284.5	15.95 (0.1)	302.3 (1)
Q1	3.4 (0.3)	270.7 (5.5)	3.1	273.4	3.5 (0.1)	295 (4)
M2	3.4 (0.1)	287.4 (1.5)	3.4	277.1	2.3 (0.1)	329.5 (1)
S2	2 (0.1)	303.1 (2.5)	2	274.5	0.7 (0.1)	325.2 (3)
form ratio	5.90	---	5.30	---	10.50	---

Table 4. Main tidal constituents comparison

The major difference between the data from Tides and Current software and NOAA data lies in the semi-diurnal constituents which seem to be underweighted. However the resulting error remains low, being considered the low amplitudes of both M2 and S2. A comparison of both NOAA gauge and Wxtide32 software time series presented on the subsequent figure shows that differences are larger during spring tides.

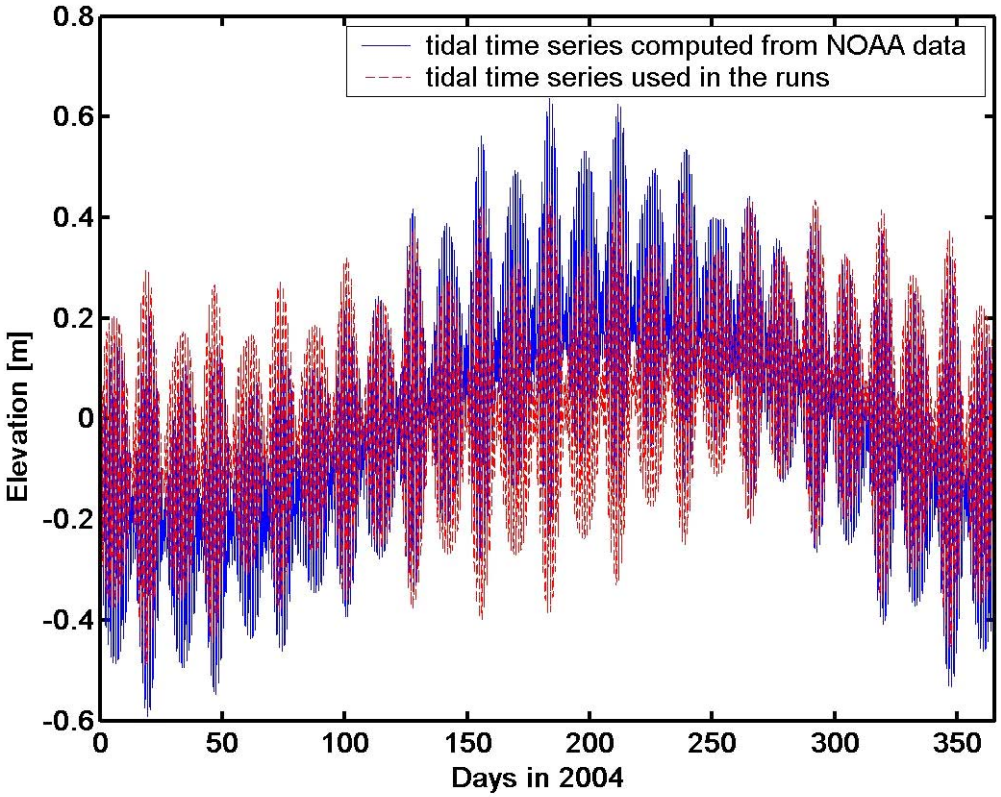

Figure 12. Time series comparison between NOAA and Wxtide32 data set

Finally, as NOAA could not provide time series for the lateral open boundaries, they were forced with Tides and Currents data. To be consistent, we also decided to force the Gulf open boundaries with time series provided by this software

b. Residuals

The residual elevation composed from storm surge, wind-induced waves and wave setup was obtained from the NOAA gauge measurements after filtering the tidal elevation out. The times series depicts a rather uniform shape, except during the hurricane event in September.

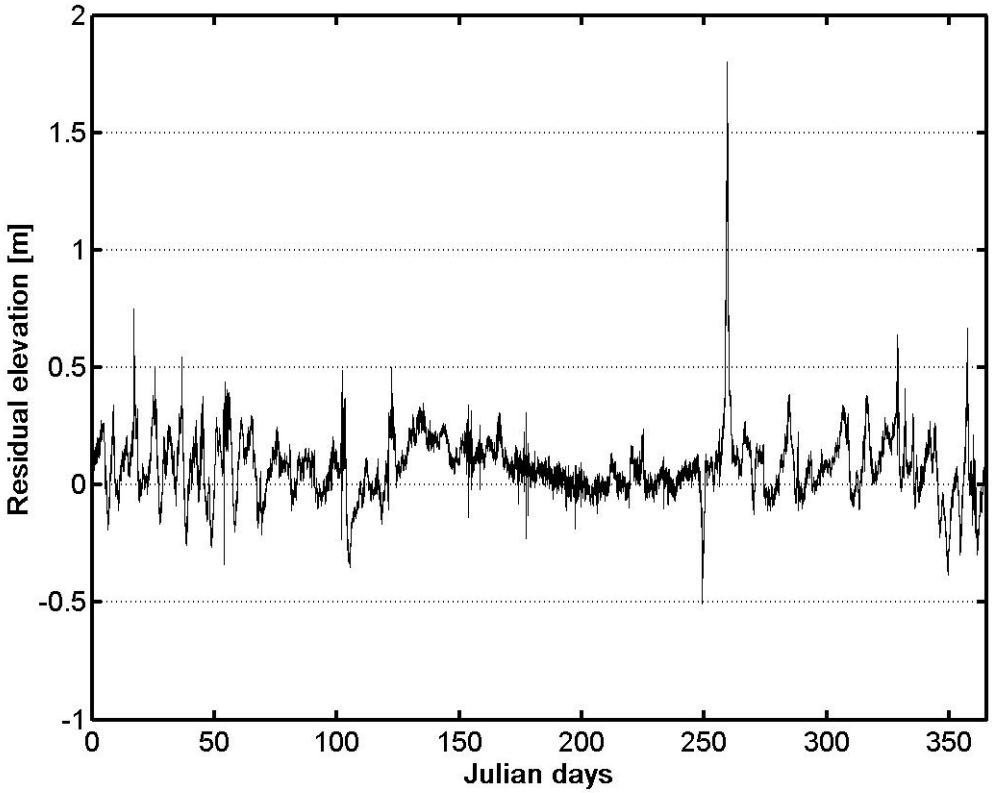

Figure 13. Residual time series

The residuals provide an average 7.7 cm setup, its standard deviation being 13.6 cm. It is to notice that the hurricane event does not impact much the statistics. When disregarding it, the mean drops to 7.3 cm and the standard deviation to 11.8 cm.

These residuals were put on top of the tidal elevation when forcing the last run Gulf open boundaries.

2. Wind

The wind files were also collected at Panama City Beach and have been applied unmodified and uniformly over the whole domain. The station provides data hourly in standard weather conditions and increases the sampling to every 6 minutes when extreme weather does occur. WQMAP automatically manages the sampling differences.

3. Temperature

Despite the seasonal fluctuation of temperature, we ran the different configuration setting a constant 21˚C temperature value. As the temperature is uniform over the water column, its influence on density distribution is negligible. Forcing the fresh water temperature to the same value has probably introduced the larger error.

4. Salinity

The different boundaries -West Bay, Gulf entrances and East Bay- were given salinity values -22, 35, 20 psu respectively- in agreement with measurements collected by Blumberg and Kim (2000). Finally, the rivers cells were forced with pure fresh water which remains questionable as water enters the system through seepage.

THIS PAGE INTENTIONALLY LEFT BLANK

VI. NUMERICAL EXPERIMENTS WITH WQMAP

Different cases were featured with separate forcing to examine the special impacts caused by each of them. Three of them are described in this chapter occulting the run where the open boundaries were forced with residual elevation. It is enough to say that the results practically matched the ones observed in the case where open boundaries were forced by wind only. This being set, the following cases describe no forcing, tidal forcing and wind forcing situations.

A. RUN 1: NO FORCING

1. Initial conditions

This case is featured with no wind and tidal forcing. The salinity is taken its climatological values at the open boundaries of the bay. The average values of runoff are assigned at all the river entries with pure fresh water. The salinity initial conditions for the basins were not crucial and several runs made from different values (32, 25, 15) ended up with the same final equilibrium state. The temperature was set to 21˚C and surface elevation is automatically given a 0-value.

2. Numerical results

a. Salinity profiles

The model is integrated from 01/01/2004 with no wind and tidal forcing. After one month, the model reaches its steady state with different zonal features. Fed by Deer Point Lake Dam, North Bay rapidly mixes and becomes fresh until it connects West Bay. St Andrew Bay presents a uniform 35 psu-salinity profile due to its connection to Gulf of Mexico. The salinity profiles of both East and West Bay are driven by the bathymetry contour. Being very shallow East Bay does not permit a lot of saline water to enter from St Andrew Bay and therefore, we end up with a rather fresh well-mixed profile of 4.8 psu. On the other hand, because West Bay is much wider and deeper, most of the salty water entering the system finishes its course westward and mixes the fresh input from Deer Point Lake Dam. The resulting feature depicts a uniform salinity profile of 17.5 psu.

A cross section view between West and East Bay points (Fig. 14) shows how salinity is distributed over the water column (Fig.15). Two spots gather the conditions for a baroclinic circulation to take place and locate at marks A and B. They obviously stand into a transition zone between the salty inflow from the Gulf and the fresh runoff occurring farer inward. The resulting profiles (Fig. 16) portray a large stratification process.

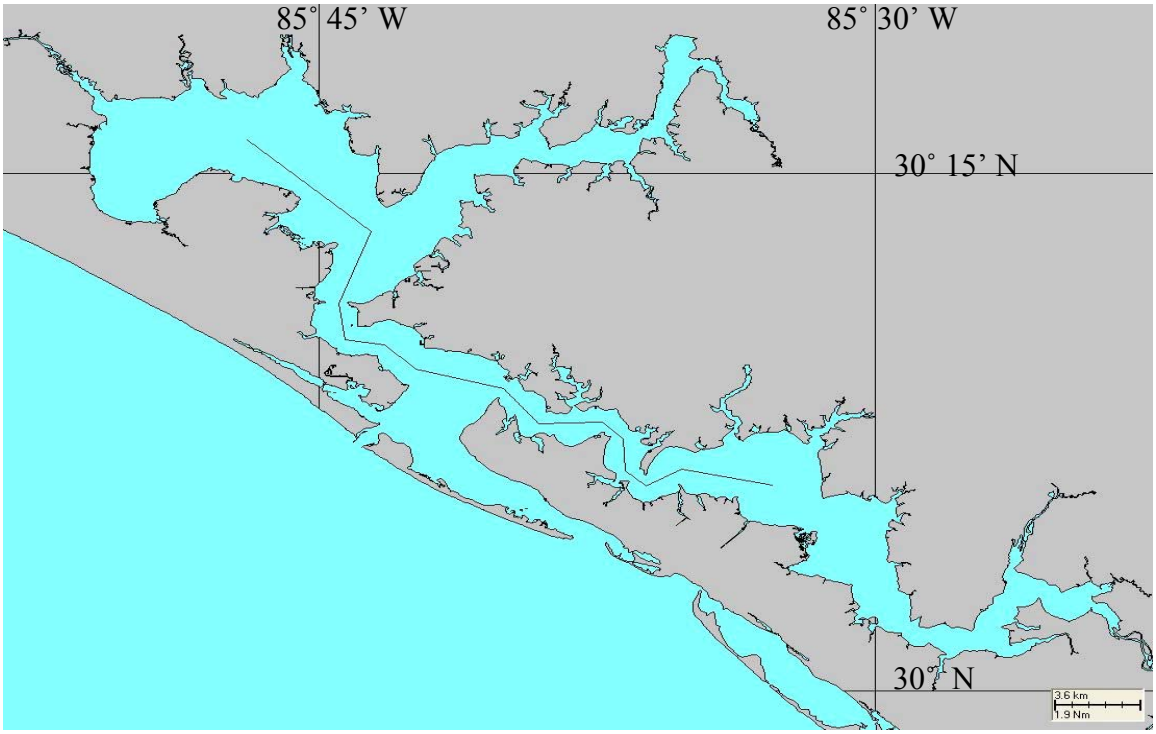

Figure 14. Cross-section between West Bay and East Bay

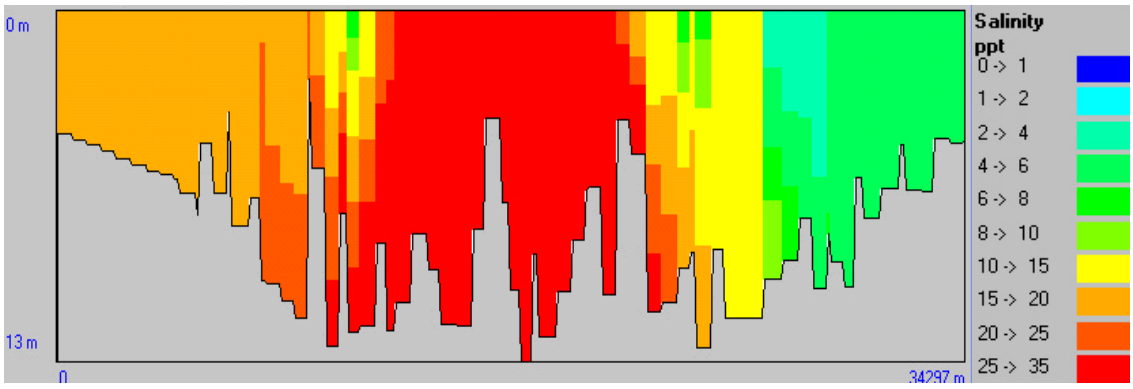

Figure 15. Salinity cross-section view between West Bay and East Bay

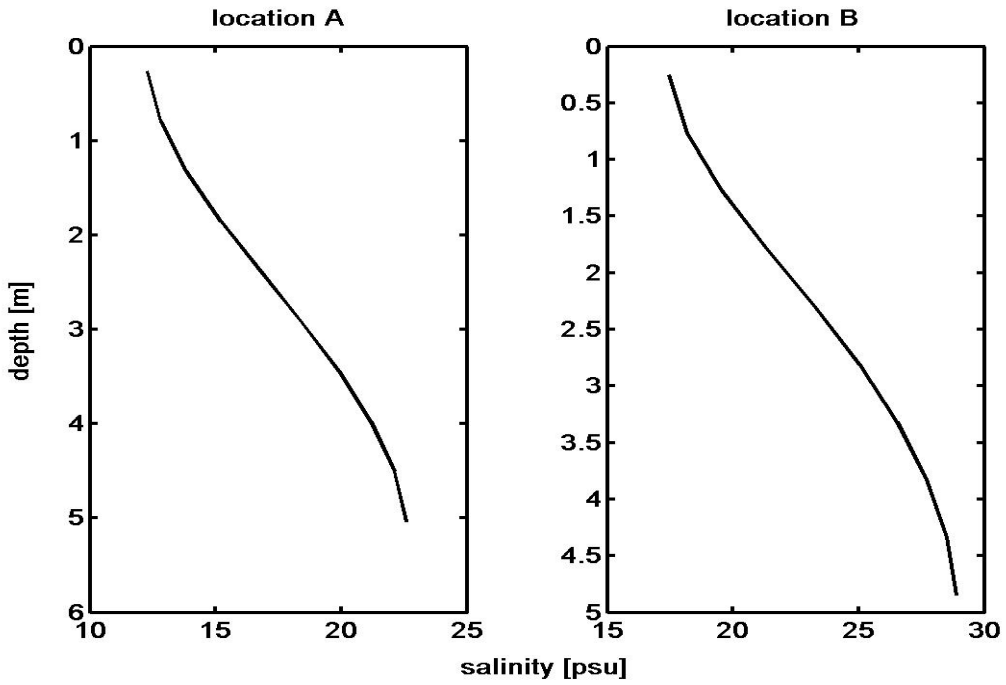

Figure 16. Salinity profile at locations A and B (see Fig. 2)

b. Velocity profiles

The speed profiles only depend upon the salinity distribution as this run has no other forcing. Therefore, the speed is uniform over the water column at all open boundaries but presents large change at locations A and B according with the salinity profiles described above. The velocity fields at surface and bottom (Fig.17) clearly picture the baroclinic circulation at locations A and B. The velocity profiles at both locations are plotted in Fig.18.

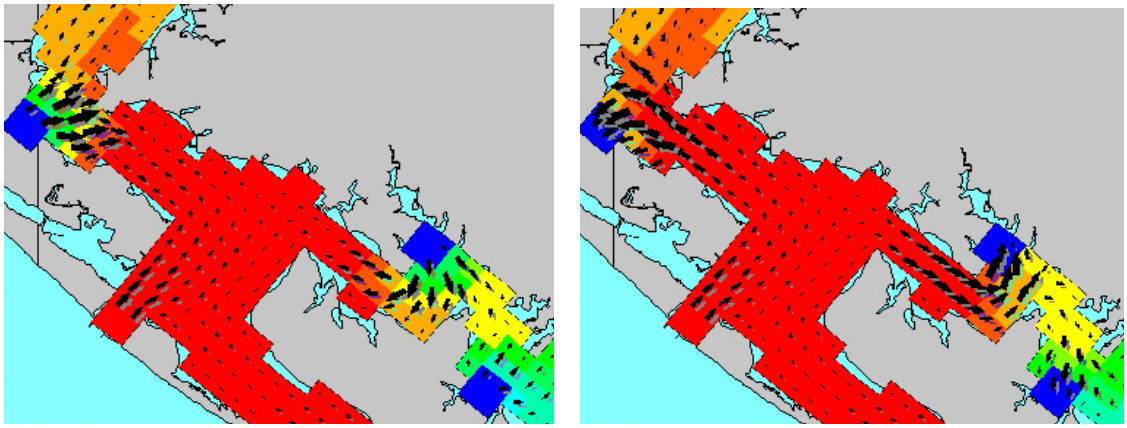

Figure 17. Velocity at (a) surface and (b) bottom (30˚ 09’ N - 85˚ 42’ W)

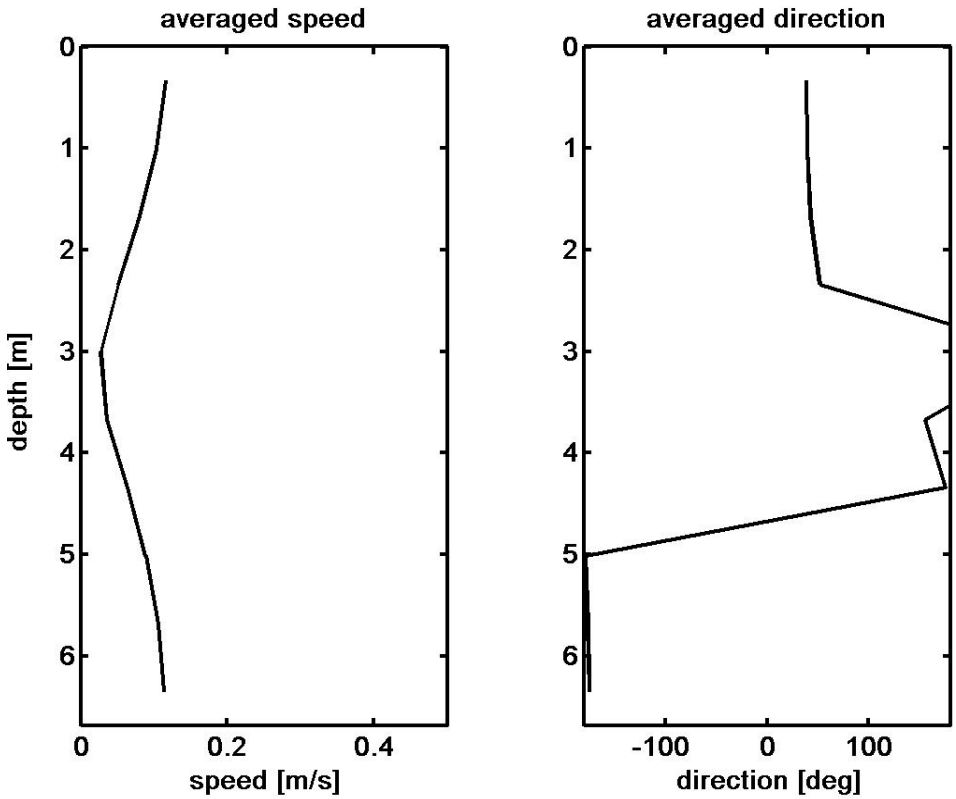

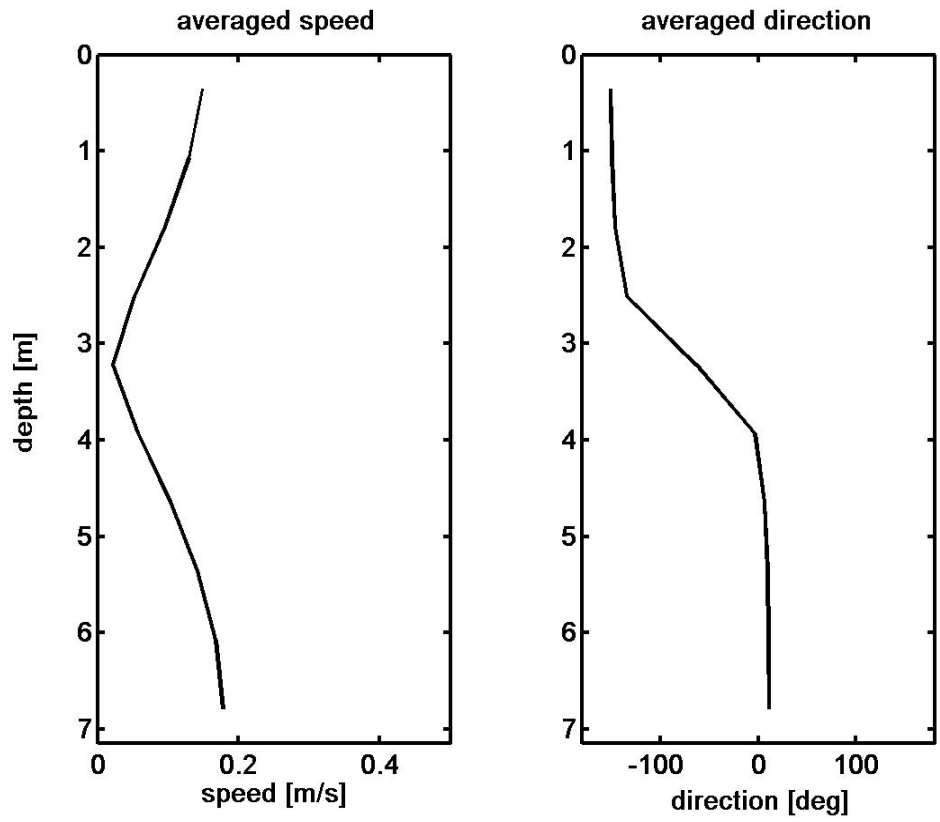

Figure 18. Vertical variation of horizontal velocity: (a) speed at location A, (b) direction at location A, (c) speed at location B, and (d) direction at location B. (see Fig.2)

c. Fluxes

The computation of the flows at each open boundary describes how the water is flowing over the whole system. The total inflow represents 879 m^3/s (622, 202 m^3/s at West and East Pass respectively and 55 m^3/s river runoff) roughly balanced by the water out-flowing at West and East Bay (538 and 334 m^3/s respectively).

Accordingly with Figure 18, the flow at locations A and B is two-layered and the system can be summarized as in Figure 19. At locations A and B, dashed arrows represent the flow in the lower layer and the plain ones the flow in the upper layer. Notice that, despite the shear occurring at location A, the water always flows northwestward. The upper arrow symbolizes the fresh water input being aware that no location is associated with this arrow. It helps, however, the system to be in balance. All values are

in m^3/s and are not associated to standard deviation as the system is in steady state at the end of the run. By running the model in several river salinity values, we observed that increasing the river salinity by 1psu reduced the inflow by 15 m^3/s.

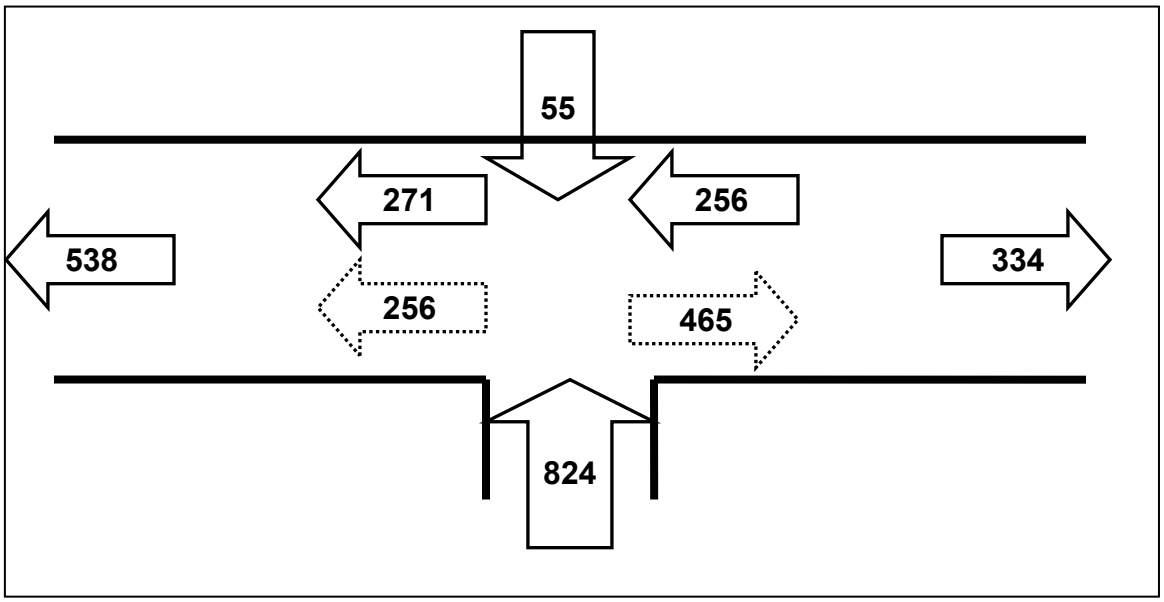

Figure 19. Synthesized fluxes (m^3/s) in steady state over St Andrew Bay system

B. RUN 2: TIDAL FORCING

1. Initial conditions

This case is featured with purely tidal forcing at all open boundaries. They were initialized with different sets from Tides and Currents software. Both salinity and temperature were given similar values from the ones used in the first case.

2. Numerical results

a. Salinity profiles

By driving the system with tidal forcing, we induced large fluctuations in speed and salinity profiles. The general features described in run 1 are still valid but the transition parts have been extended dramatically. On these spatial variations overlay temporal ones which are of the nature of tides.

First of all, the boundaries do not behave identically. Because East Pass is too shallow, most of the water outgoing the system flows through West Pass. As a result, the salinity remains constant at 35 psu. West Pass, on the other hand, can see its salinity varying from 35 down to 21 psu, the larger fluctuation occurring in spring tides. Moreover, the water column remains well homogenized and a slight difference is perceptible during spring tides ebb (1 psu between surface and bottom).

The two lateral boundaries portray two very different situations. East Bay, shallow and narrow, can hardly oppose the natural outward fresh flow. Hence, salinity is entering the system during small episodes with spring tides flows (Fig.20).

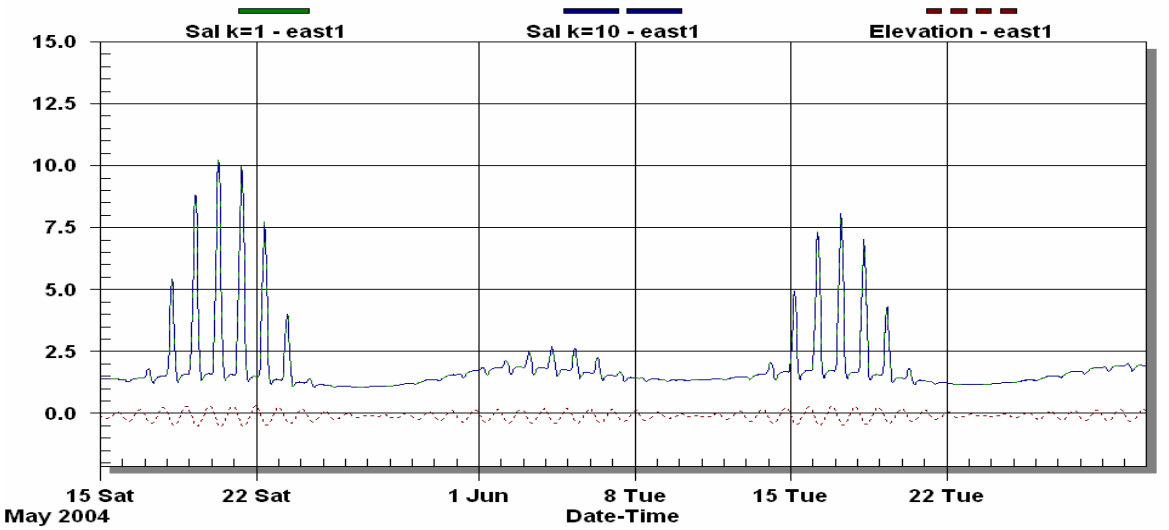

Figure 20. Salinity time series at East boundary

West Bay entrance exhibits much larger exchanges between the Intracoastal Waterway and the bay. In that case again, the water column appears to be well-mixed which emphasized run 1 observations that described the flow at boundaries to be barotropic. We can also notice how salt gradually diffuses inward during neap tides (less than 20 cm elevation fluctuations) (Fig.21).

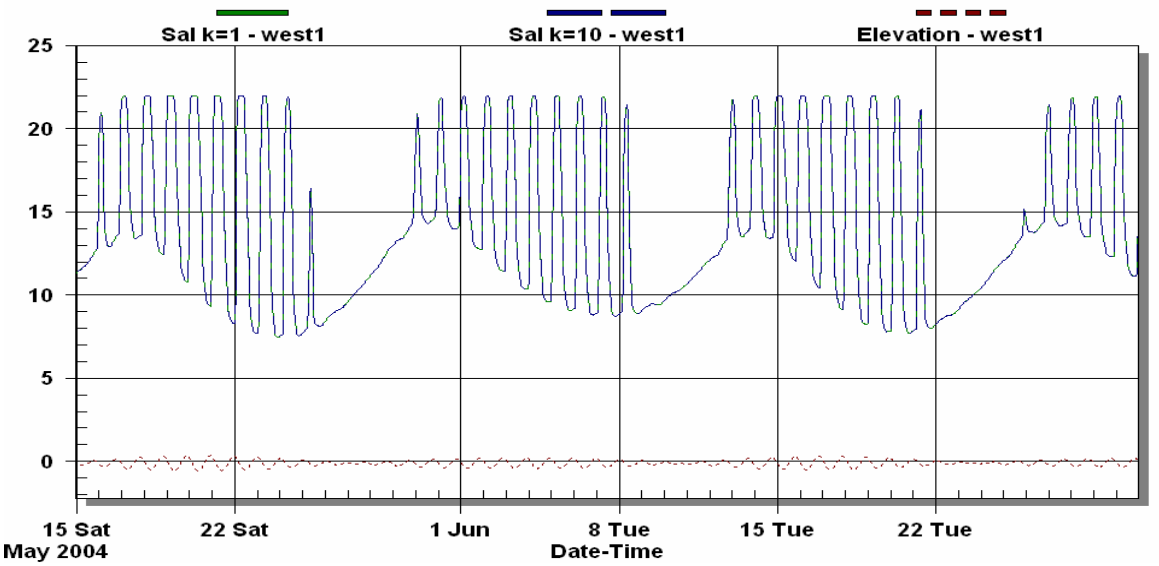

Figure 21. Salinity time series at West boundary

The following plots utterly illustrate the tidal pumping process due to tidal forcing. These two shots have been captured from two successive low and high tides during spring tides (Fig.22). The tidal pumping also results in large salinity changes in West Bay. During spring tides, the tidal pumping makes the water flow in the same direction over the water column even at locations A and B where the flow was initially baroclinic. So, the constant supply of West Bay with salt from St Andrew Bay stops during ebb flows and the water freshens, the salinity reaching its stable value during the subsequent neap tide.

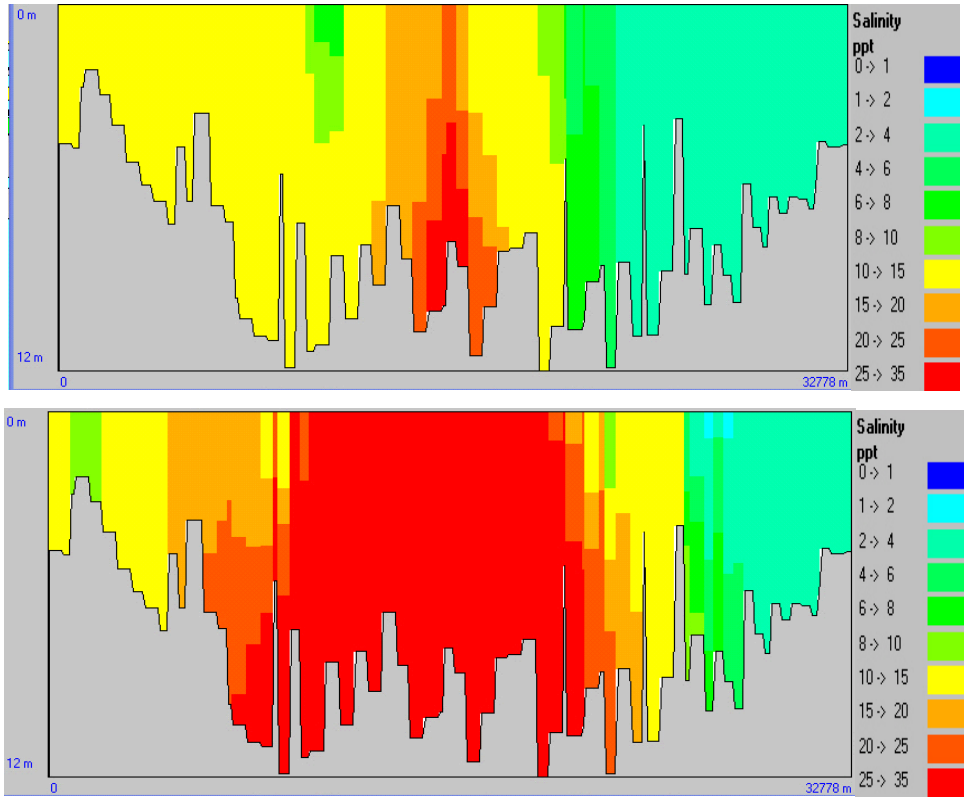

Figure 22. Salinity cross-section view during (a) ebb and (b) flood period

The conditions observed at both West Bay and St Andrew open boundaries perfectly correlate these remarks (Fig.23). The salinity remains constant throughout the water column and varies from 35 to 32 psu at St Andrew opening and from 22 to 7 at West Bay boundary. Both panels represent salinity profiles at low and high tides measured at St Andrew boundary which explains why the salinity increases during ebb tide at West Bay boundary.

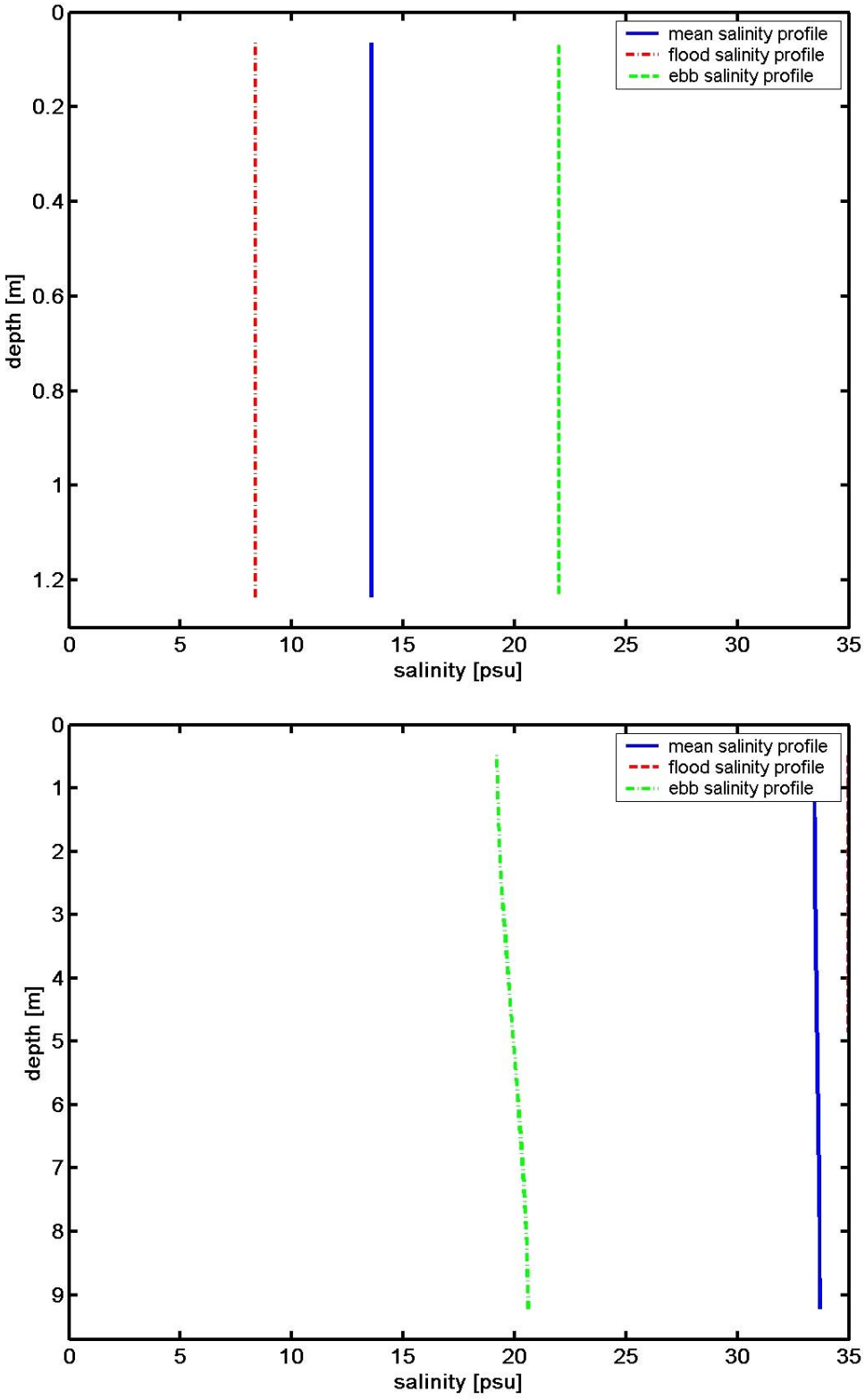

Figure 23. Salinity profiles at (a) West and (b) Gulf entrances

b. Velocity profiles

The flow at the Gulf boundary controls the flow at the lateral boundaries. Nevertheless, the inward flow in never very important because of its natural tendency to go out of the system. The same observation prevails for the Gulf entrance with an inverse tendency. Finally, the mean flow over a year-long run almost equals the flow during flood periods (Fig.24). At these locations the standard deviation of the flow is almost one order of magnitude greater than the flow itself. The last feature to notice is that the vertical speed shear observed at Gulf entrance (Fig.24c) is not due to a vertical stratification but is likely to result from bottom interactions.

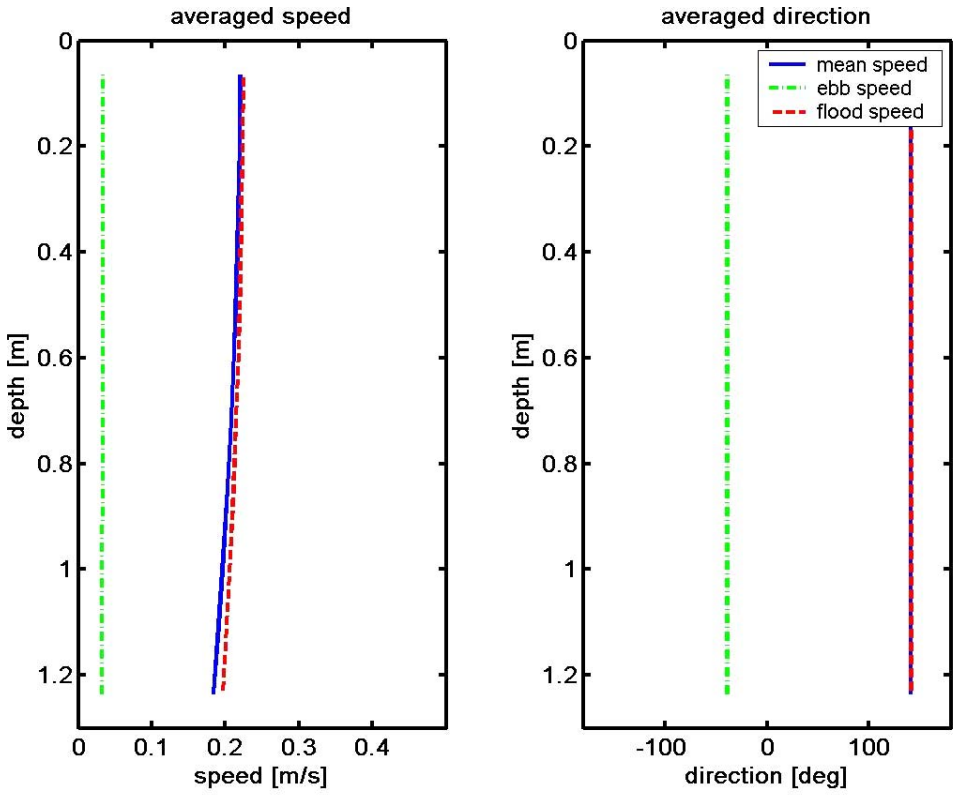

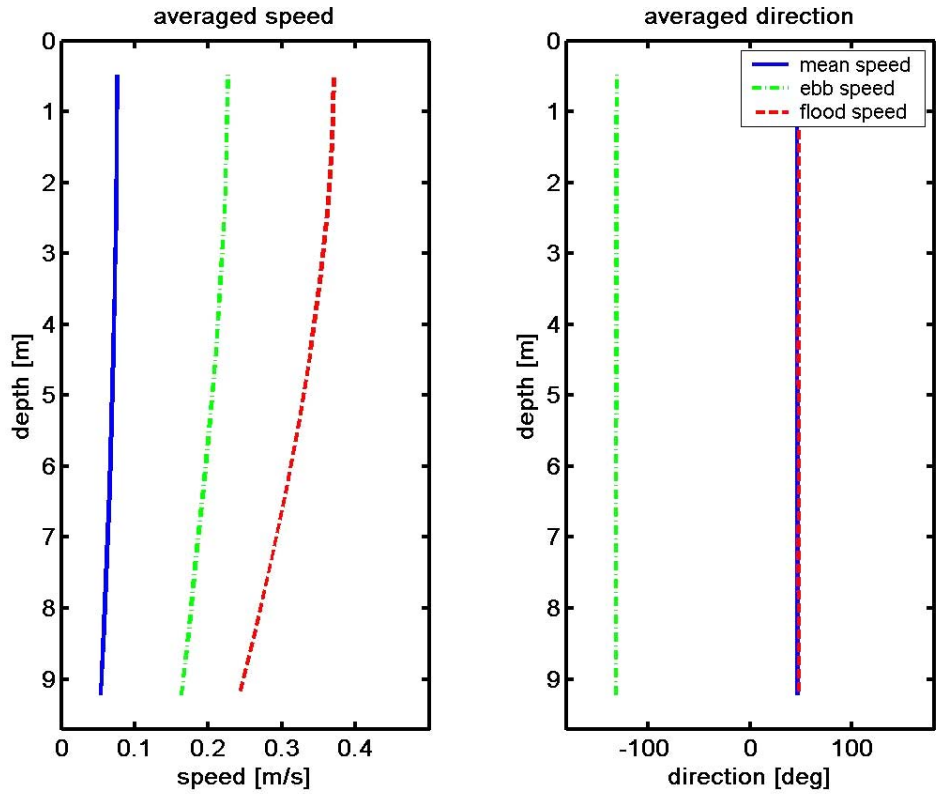

Figure 24. Vertical variation of horizontal velocity: (a) speed at West open boundary, (b) direction at West open boundary, (c) speed at West Pass, and (d) direction at West Pass.

Hence, the general conditions described during run 1 at both locations A and B are no more valid. The subsequent plots (Fig. 25) describe how extreme can be the changes over a tidal period. On these schemes, the tidal pumping effects are obvious at both locations. Location A exhibits a particular feature in the sense that the mean surface salinity is greater than its value measured during high and low tides.

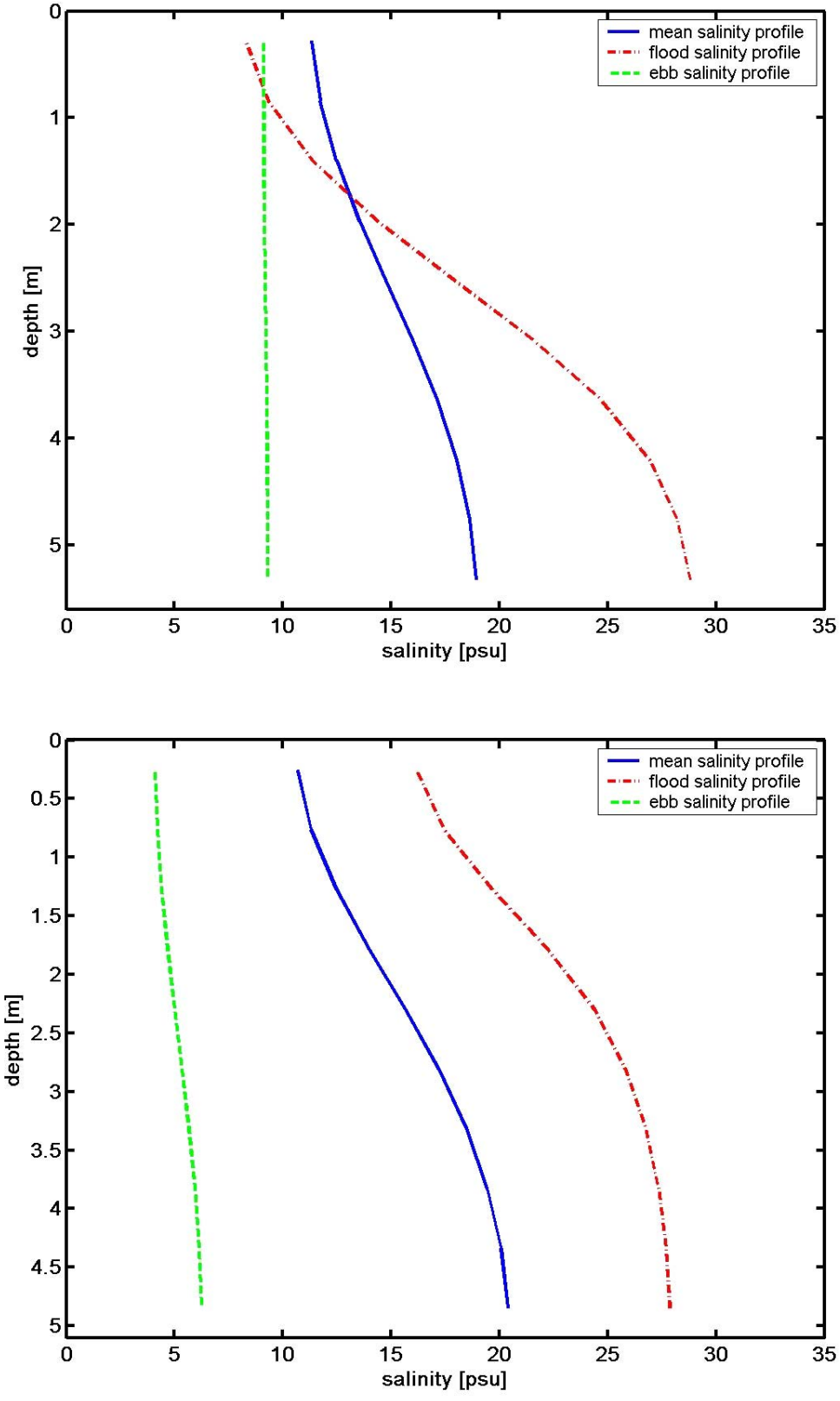

Figure 25. Salinity profiles at locations A and B (see Fig. 2)

Notice that the flow is no more baroclinic during ebb flows at location A (Fig.26 b). The standard deviation of the flux can be tenfold greater than the flow itself, which is mainly visible at location A. In that case again, most of the salty water originating at West Pass flows towards West Bay which is much deeper and so make location A conditions fluctuate over a wider range. At location B, the tidal pumping influence results in a 90˚ shift of the flow in both the upper and lower layers but the shear remains (Fig.26d). Its lighter influence finally outcomes in a standard deviation of the order of magnitude of the flow itself.

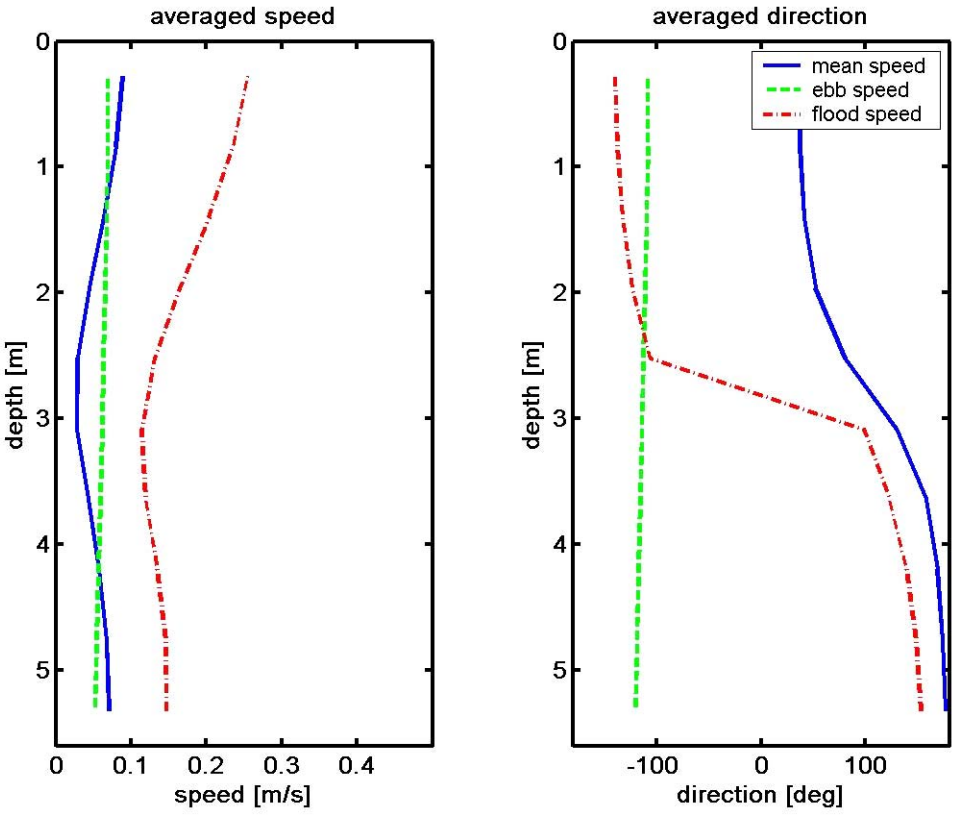

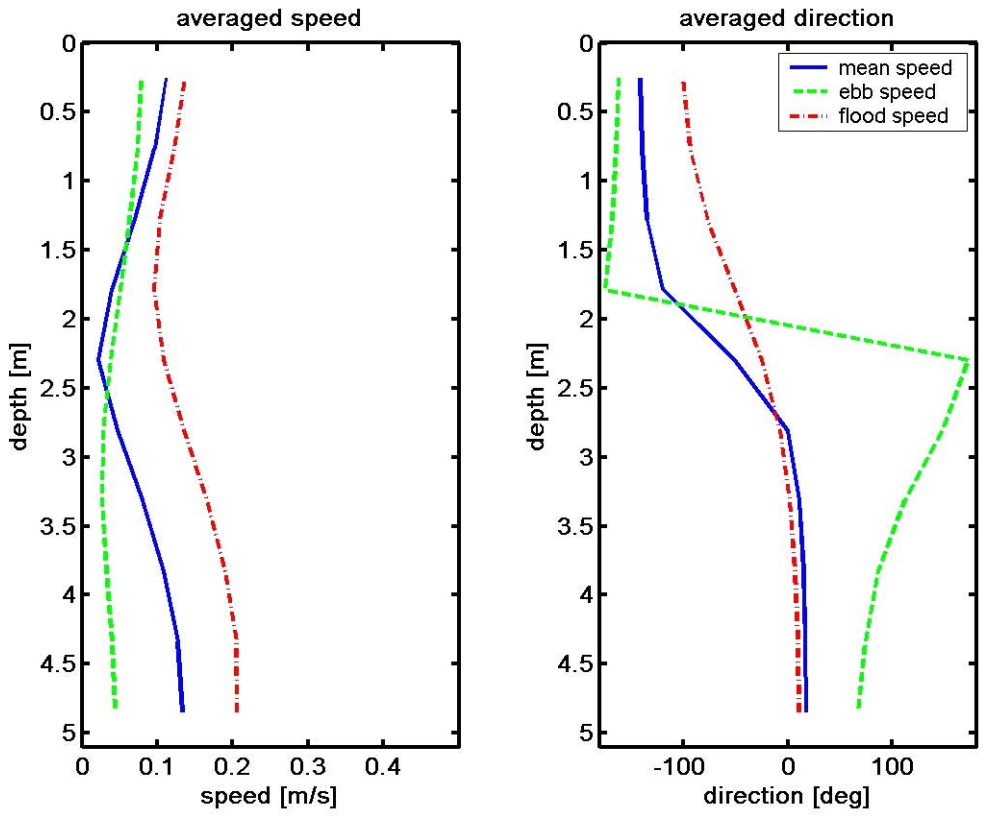

Figure 26. Vertical variation of horizontal velocity: (a) speed at location A, (b) direction at location A, (c) speed at location B, and (d) direction at location B (see Fig. 2)

The subsequent plots (Fig.27) show how the flow propagates between St Andrew Bay and West Bay. The starting profile of the left panel stands in the solid black line of its right. The tide is high and the water column starts to mix up before the global salinity decreases with the ebb flow. Starting from the dashed blue line on the left side of the right panel, the salinity increases significantly in the lower layers and the water column stratifies all through the flood tide (the last black line pictures the beginning of the next ebb flow). These two plots show why the surface salinity during both high and low tides is less than its average. During the ebb flow, the surface salinity first raises until the water column has mixed and then drops.

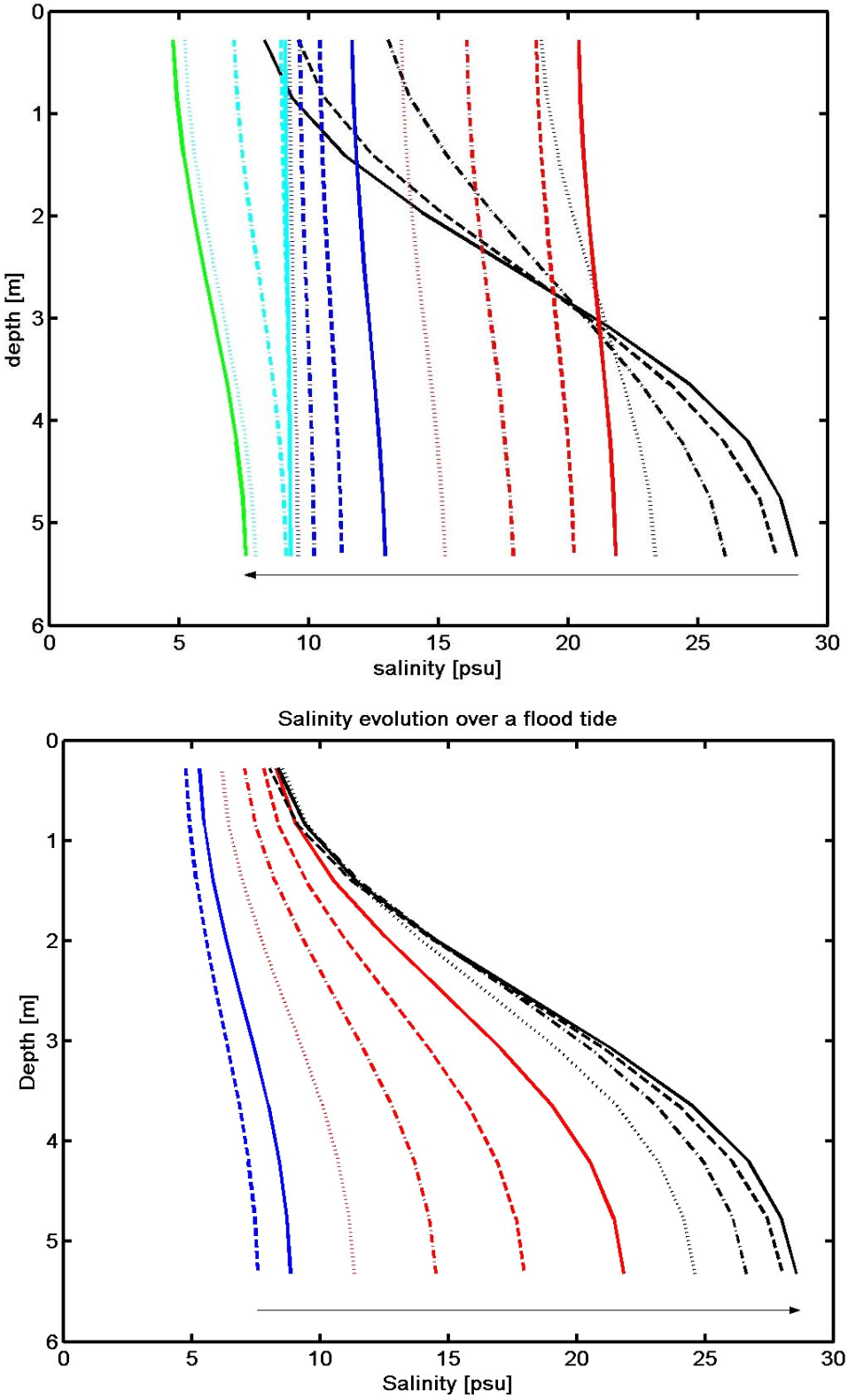

Figure 27. Salinity profile evolution over a tidal period

As the flow induced by the horizontal salinity gradient is weak, the tidal impact drastically increases its fluctuation. Figure 28 presents speed magnitude and direction at locations A and B (mean and mean plus/minus standard deviation).

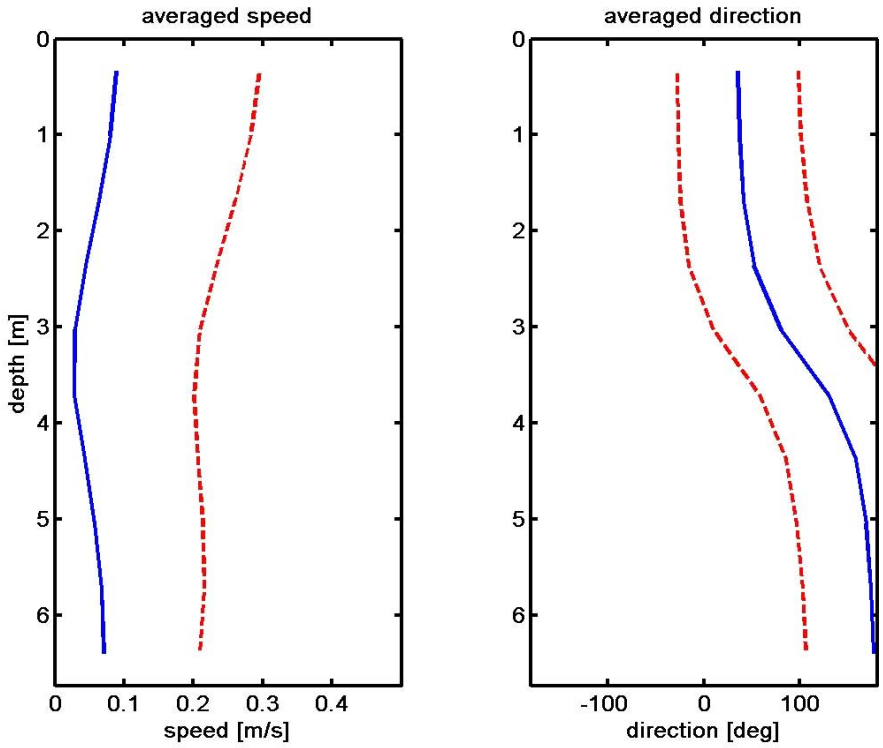

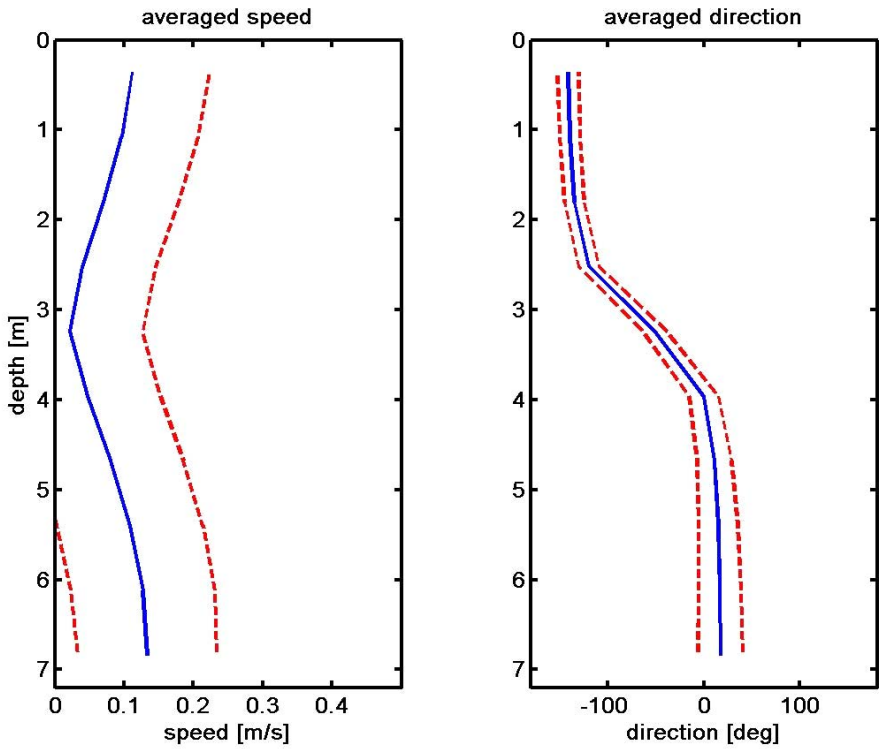

Figure 28. Vertical variation of horizontal velocity: (a) speed at location A, (b) direction at location A, (c) speed at location B, and (d) direction at location B. (see Fig.2)

c. Fluxes

In terms of fluxes, we obtained very similar averaged values to the ones computed in the run 1; this result was expected as tides should cancel out over a large period of time. If the resultant flow is still directed towards the same direction at all locations, it may vary significantly with tides. As a result, the standard deviation of the flow can be as large as 6 times the flow itself (at Gulf entrance).

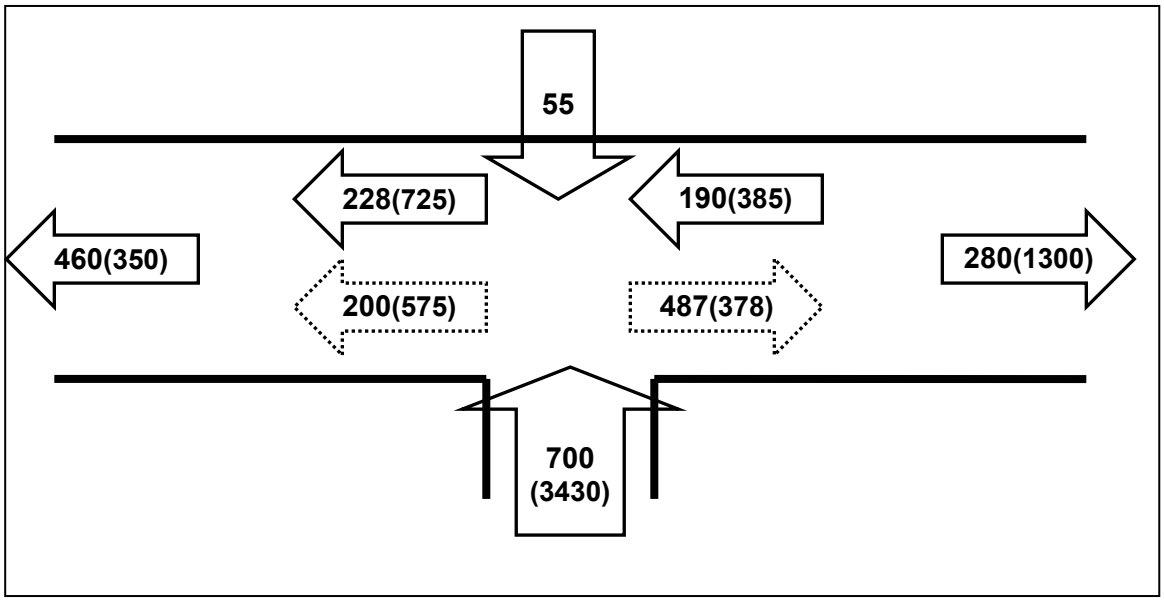

Figure 29. Synthesized fluxes due to tidal forcing

C. RUN 3: WIND FORCING

1. Initial conditions

This case is featured with the wind forcing. Hourly wind data are collected at Panama City Beach from the NOAA gauge. The wind field has been applied over the whole area. This run should provide specific features due to wind forcing. Moreover, we paid specific interest over the hurricane period (15-17 Sep.) when winds were blowing at 25 m/s. The open boundaries were forced by salinity only with no elevation.

2. Results

As the resulting wind obtained from NOAA records is rather weak and oriented outward (averaged speed and direction are 0.12m/s from NW), the global situation has not dramatically changed from the steady situation described in run 1. However, temporal variability can be large in the occurrence of severe weather systems or singular wind regimes.

a. West Bay boundary

When westerlies are blowing, the force faces the natural outward flow at West open boundary which reverses when the speed exceeds 6 m/s. As a result, the whole flux is directed towards East Bay

b. East Bay and Gulf of Mexico boundaries

Surprisingly, both East Bay and Gulf entrances open boundaries behave simultaneously and have opposite responses to wind forcing. Despite the orientation of the bay, the flow at East Bay boundary does not reverse when easterlies are blowing because they feed the system through East Pass. But when winds are blowing from north-east at a speed above 8 m/s, the flow overturns in St Andrew channel acting as a tidal pumping process. However, this was not detectable during the days forced by Hurricane Ivan winds. When over 20 m/s winds from south-east forced the system, the entire flow directed towards West Bay.

c. Hurricane Ivan

We focused on the period when Hurricane Ivan hit the north Florida Panhandle. We considered this period to begin when winds reached a steady 5 m/s speed on the 15th of September at 8 PM and to end 2 days later after wind has felt under 5m/s. Meanwhile, the average speed was 15 m/s and its peak achieved 25 m/s in the morning of September the 16th during 4 consecutive hours (Fig.30). Even though strong winds all come from the same direction, a rather slight change can largely impact the whole circulation in the bay.

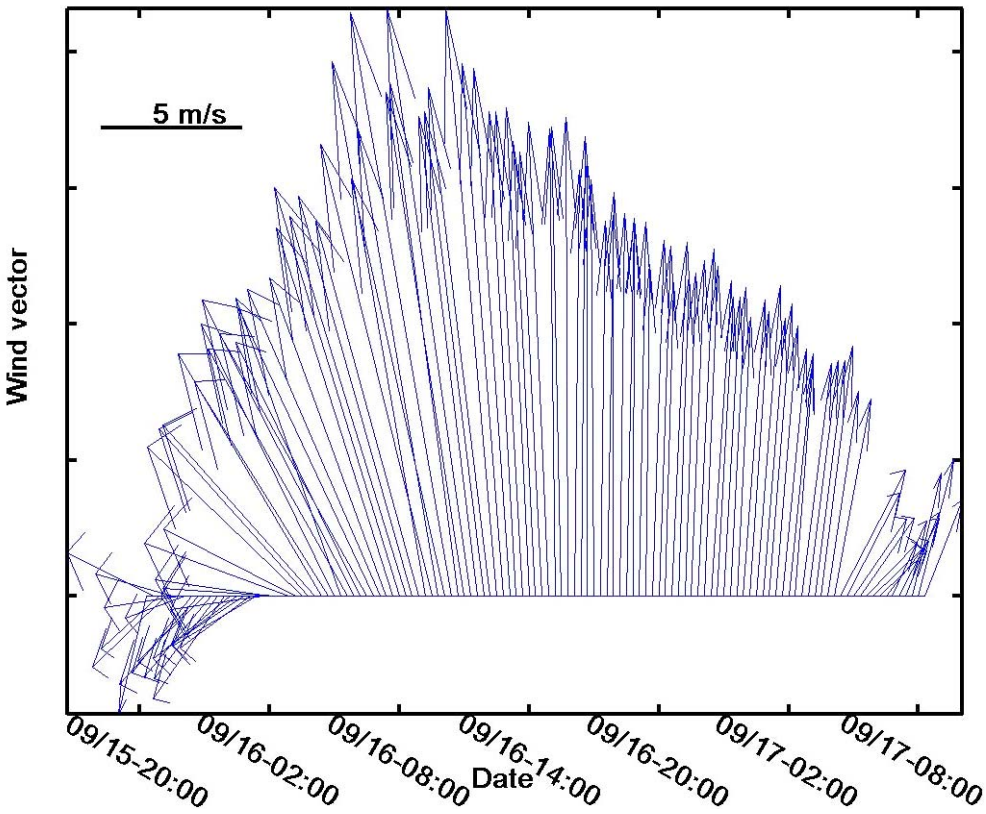

Figure 30. Wind field during Hurricane Ivan

If we noticed that East Bay reacted to wind forcing as it would have done to tidal pumping, West Bay response to strong wind forcing largely depends upon its direction. Fig.30 - 31 depict two dramatically different situations as the wind shifted from 105 to 150 between 05:00PM and 01:20AM. Oriented in the axis of East Pass, the wind drains the water westward. Because the current is so intense, the water enters North Bay avoiding the fresh water to flow from Deer Point dam. As noticed above, the water also enters the system through East Bay accordingly with the flow at East Pass (Fig.31).

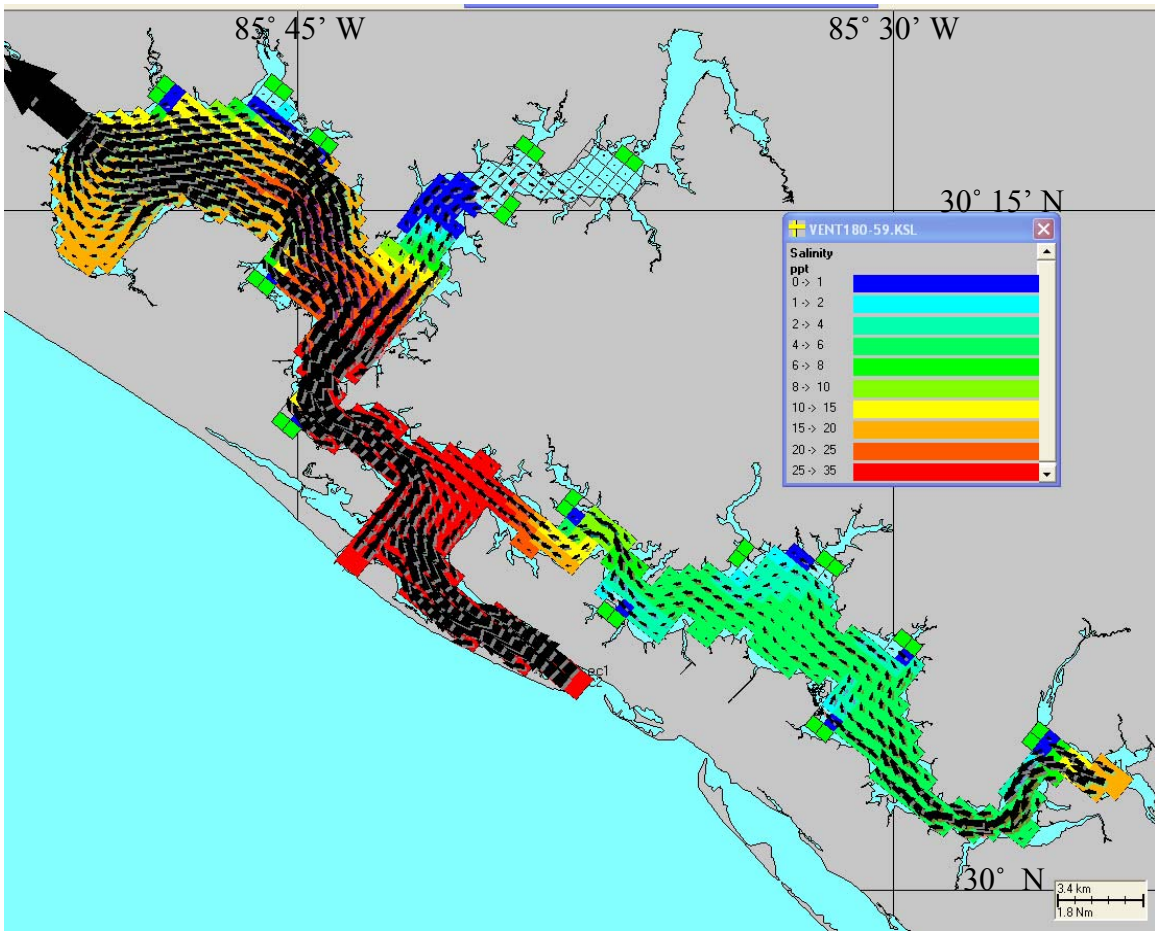

Figure 31. Surface current the 09/16 at 05:00 AM

Later on after the wind had shifted, the circulation pattern does not correlate anymore the previous one. In Fig. 32, the wind is blowing from 150˚. Because the circulation reacts with West Pass flow increase, the water now exits the system through East Bay. The water, pilled up by the winds, still enters North Bay and hence there is a large deficit of water inside West Bay balanced by the western open boundary. A twisting motion then takes place for the surface current to balance the wind stress.

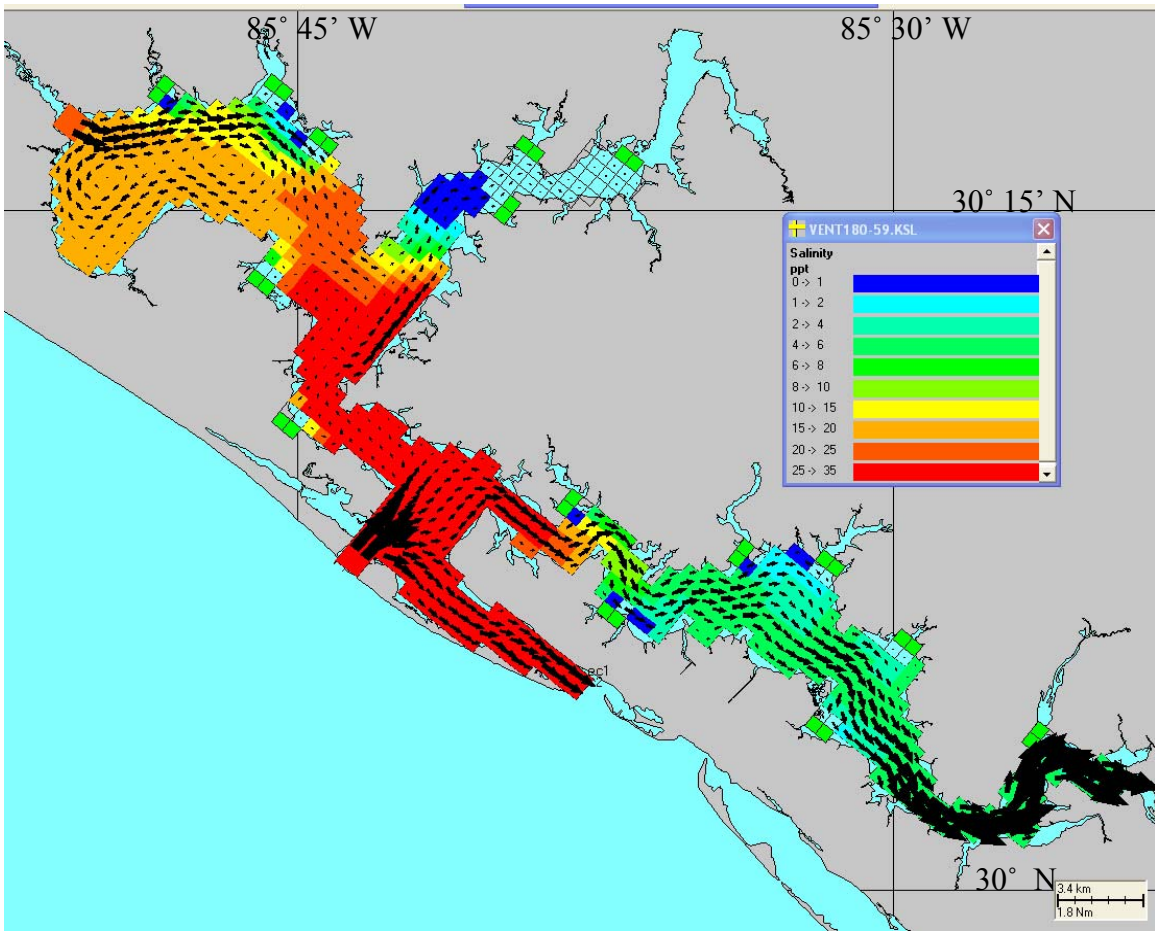

Figure 32. Surface current the 09/16 at 01:20 PM

The wind also impacted the system by increasing its salinity. The elevation in North Bay increased up to 50cm from a standard value of 6cm, containing most of the fresh water supply in the very northern end of the system. As Hurricane Ivan passed by, we could detect lumps of salty water alternatively diffusing into West Bay and East Bay from all three open boundaries.

d. Fluxes

As the mean wind blew from NW, the resulting impact is weak and decreased the fluxes a little. The standard deviation is not large because strong winds were always blowing in the same direction and hence the flow never really reversed.

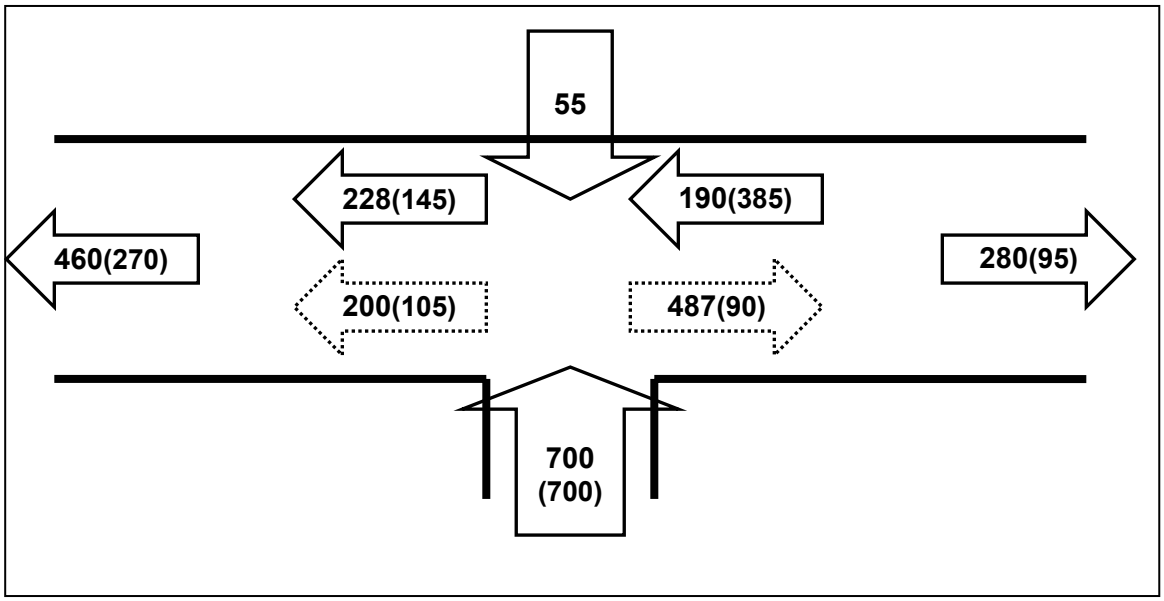

Figure 33. Synthesized fluxes due to wind forcing

VII. FORCING MECHANISMS FOR THE HYDRODYNAMIC SYSTEM

The control run, a case featured with all forcing mechanisms described in the previous chapter, is used as reference. We then disturbed the forcing conditions to assess their influence on the circulation and salinity distribution. The perturbations we applied have been chosen such as they are reasonably realistic. The results from the beginning of April and the end of September are compared applying error measurements between the control run and every single disturbed run.

A. STATISTICAL ANALYSIS

Forcing mechanisms are detected using three statistics applied on ψ representing (u, v, S) for both the surface and bottom layers: relative mean difference (RMD), root mean square difference (RMSD), and relative root mean square difference (RRMSD). Let (ψ_{ref}, ψ_{sen}) be the model outputs [i.e., (u, v, S)] for the reference and sensitivity runs. The three statistics are defined by

$$RMD(x,y) = \frac{\bar{\psi}_{sen} - \bar{\psi}_{ref}}{\sqrt{(\sum_n \psi_{ref}^2)/n}}, \qquad RMSD(x,y) = \sqrt{\frac{\sum_1^n \left(\psi_{sen} - \psi_{ref}\right)^2}{n}},$$

$$RRMSD(x,y) = \sqrt{\sum_1^n \left(\psi_{sen} - \psi_{ref}\right)^2 / (\sum_n \psi_{ref}^2)}. \qquad \textbf{(12)}$$

B. CONTROL RUN

This case is featured with all forcing at all open boundaries. The model is initialized from zero velocity, 25 psu salinity and 21˚C temperature throughout the whole domain. The model is integrated with the previously described elevation time series sets and the wind field. The boundaries are given the standard salinity and temperature values used in the preceding cases. The river cells took their averaged runoff values.

The next figure gives a synthetic vision of the fluxes at open boundaries and locations A and B. The fresh water input has been represented with a single arrow which does not match the reality but was necessary for the mass conservation balance. All the

values are in m^3/s. The flux at location A and B has been split into an upper flow (plain line) and lower one (dashed line).

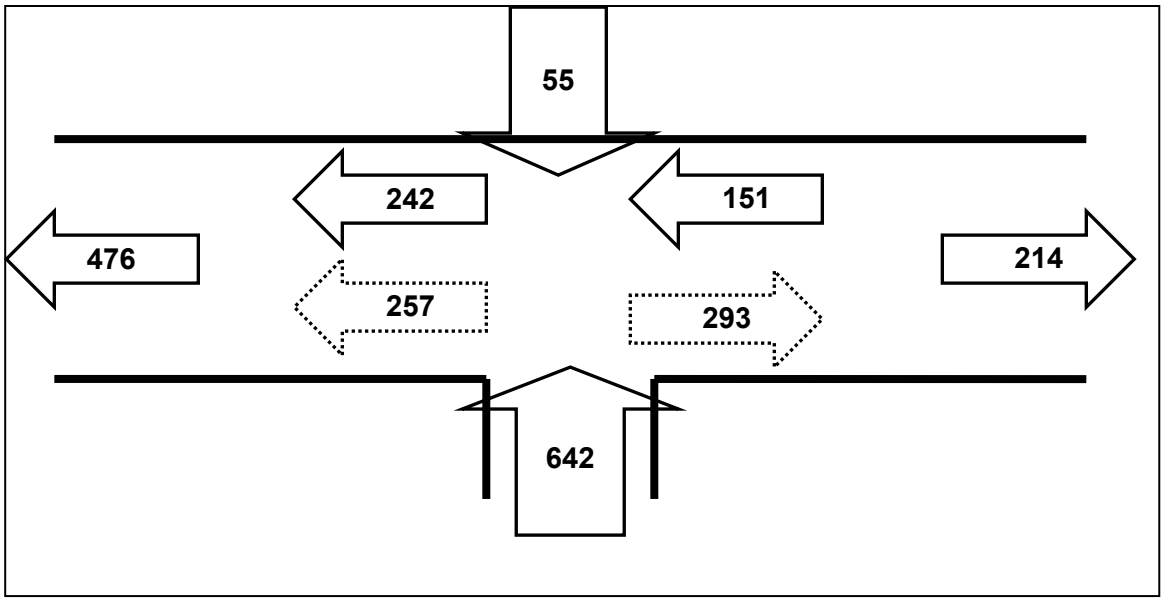

Figure 34. Synthesized fluxes for control run

C. FRESH WATER INFLUENCE

In this case, the river cells are featured with a doubled total flux. All the remaining conditions remain unchanged. The increase (100%) can appear very large but only represent a 55 m^3/s extra input.

The extra fresh water input slightly impacted the dynamics in St Andrew Bay system. As a matter of fact, this 100% increase only represents 8% of the total amount of water flowing inward the bay and as $20m^3/s$ out of the initial $55m^3/s$ of fresh water input originate in North Bay, the impact in terms of velocity or salinity are negligible at the Gulf entrances (RMSD values of $3.10^{-3}m/s$ for both u and v components and RMSD of 0.16psu for the salinity) and East Bay (RMSD of $2.10^{-3}m/s$ for u- and v-components and RMSD of 0.17psu for salinity). The values of the RRMSD average 5% clearly describing a weak impact. It is clear from Fig. 35 and 36, that the water column remains well mixed and that the influence is much greater at West Bay open boundary than at St Andrew Bay's. At West Pass, the salinity disturbance only occurs during spring ebb tides whereas

the influence at West Bay exit can be sensed during the whole period. The impact on East Bay was insignificant and will not be further discussed.

As the initial disturbance constantly applies by increasing the inflow, the resulting errors for u, v and salinity always have the same sign for a given location.

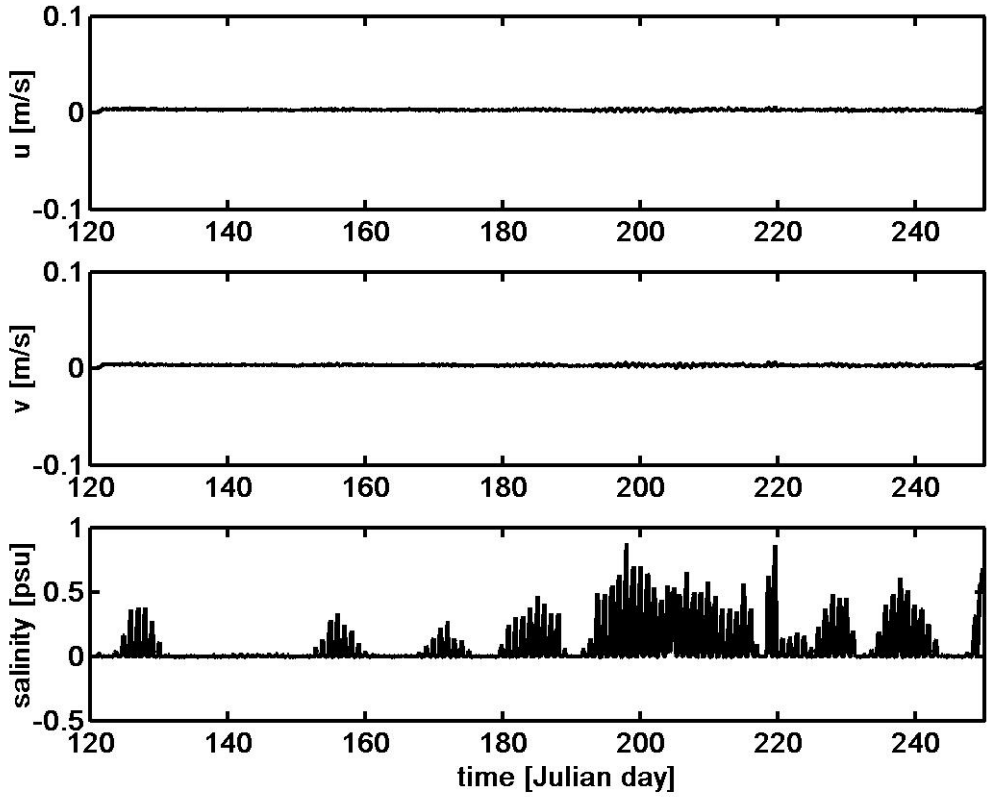

Figure 35. Time series of (u, v, S) differences between the control and river disturbed runs valid for both surface and bottom layers at West Pass.

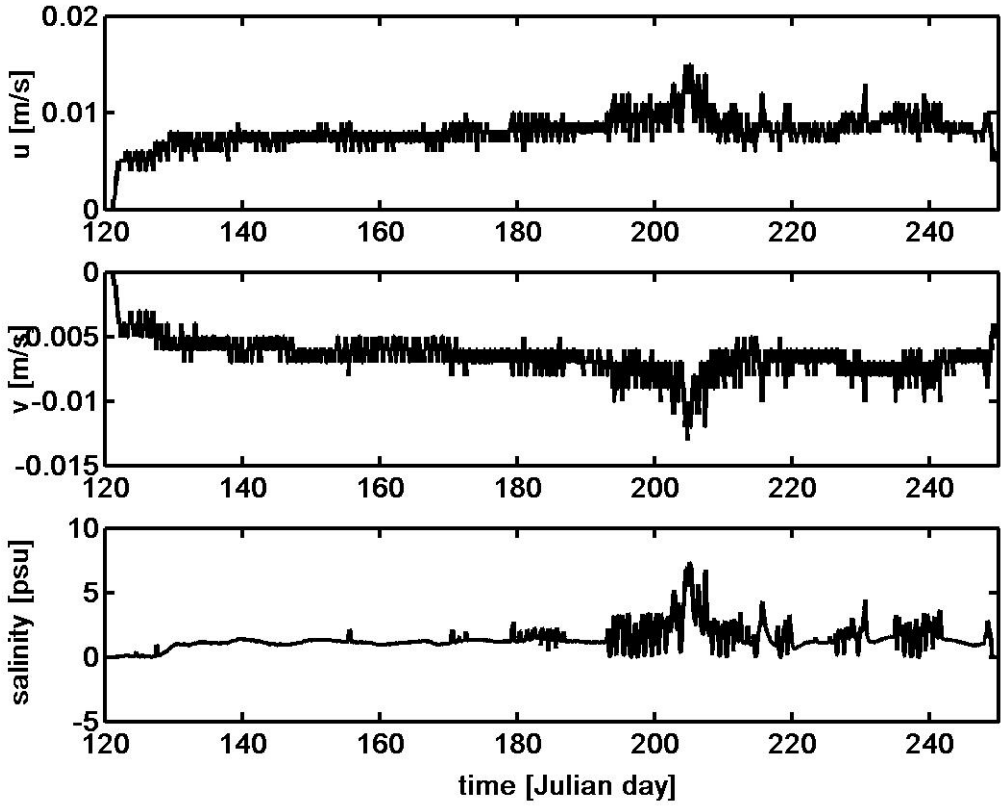

Figure 36. Time series of (u, v, S) differences between the control and river disturbed runs valid for both surface and bottom layers at West Bay open boundary.

The values, all in m^3/s, represent the flux computed at each time series location and the difference between this run and the control run is indicated in parenthesis. The differences observed at open boundaries correlate with the extra fresh water input. The highest values locate between West Bay and St Andrew Bay where most of the water flows and where the greatest fresh water sources stand.

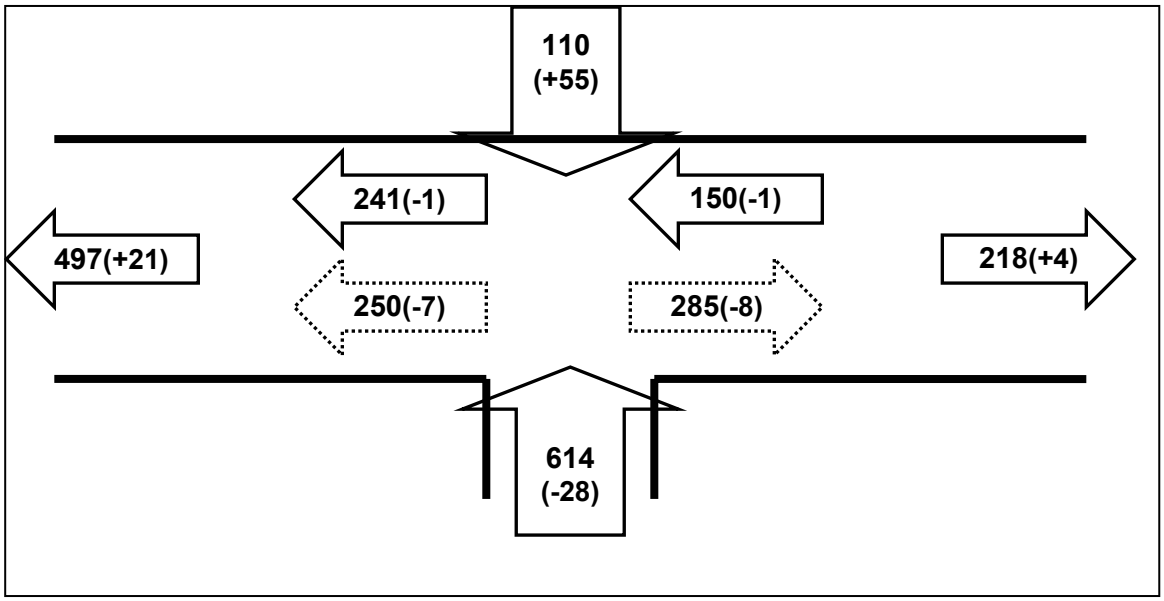

Figure 37. Synthesized fluxes for fresh water fluctuation run

D. WIND IMPACT

This case was featured without wind forcing, therefore the system was forced by river inflow and surface elevation. During the studied period, the averaged wind was blowing from 155 at a 4m/s speed.

This run shows clear features happening at all open boundaries. It is clear that the lack of wind has few not to say any impact on speed in the bottom layer even at East and West Bay open boundaries where depths average 2m. The bottom layer salinity is only influenced at west Bay for which the presence of high fresh water supply in North Bay is likely responsible. In this case, we can notice that the impact can either be positive or negative depending on the direction the wind was blowing from. The RMSD values for the speed are of the order of 10^{-2}m/s and the RRMSD ranges around 15%. The influence on salinity however is significantly different at lateral boundaries and at West Pass. West Pass is characterized by a 0.24psu-RMSD corresponding to a 0.7%-RRMSD whereas West Bay open boundary time series show a 2.4psu-RMSD and a 20%-RRMSD. The RRMSD is even higher at East Bay and reaches 30% with a 0.7psu-RMSD. The lower salinity observed in East Bay enhances the weight of the relative error.

In the surface layer, the impact is obvious from East Bay to West Bay. The lack of wind enlightens both tidal and residual signals which can be easily identified. The speed-errors induced by the absence of wind are often greater than the speed itself and are tenfold higher than the errors computed in the bottom layer. The RMSD of the speed u-component fluctuates around 0.25m/s at West Pass and West Bay which correspond to RRMSD being 460 and -150% respectively (the negative sign portrays an outflow). At East Bay open boundary, RMSD and RRMSD values are respectively 0.08m/s and 117%. These errors do not weight identically when scouting the salinity. At West Pass, the RMSD has a value of 2.8psu which stands for a RRMSD of 8%; at West Bay open boundary, RMSD and RRMSD have values of 7.6psu and 60%; at East Bay open boundary, these values are 5.2psu and 200%. At last, one must notice that the fluctuations can achieve values as high as 2m/s for the speed and 25psu for the salinity depending on the location.

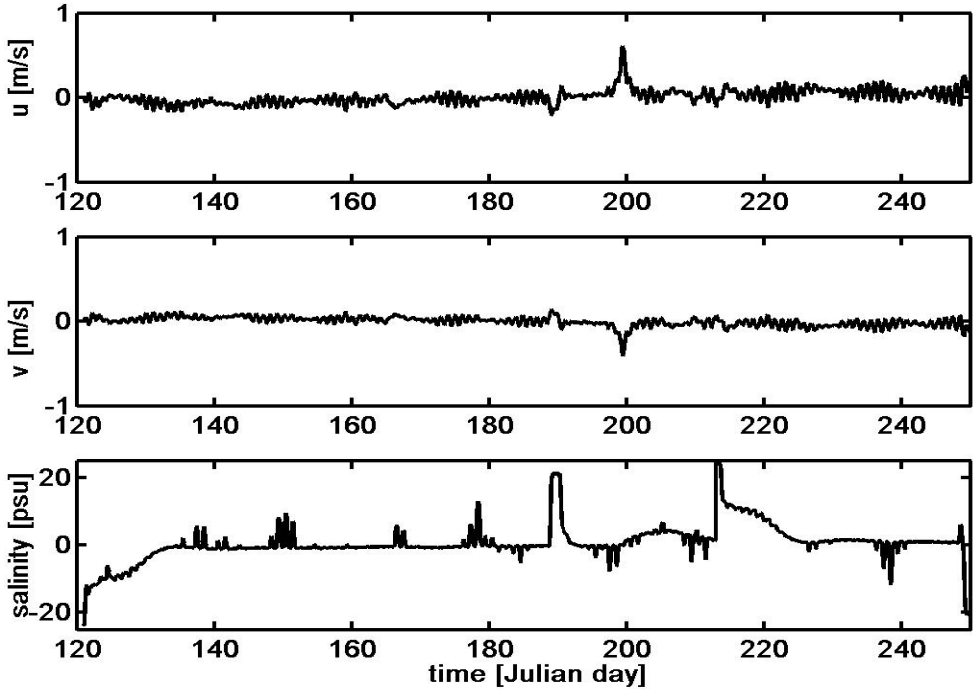

Figure 38. Time series of (u, v, S) differences between the control and no wind forcing runs for the surface layer at East Bay open boundary.

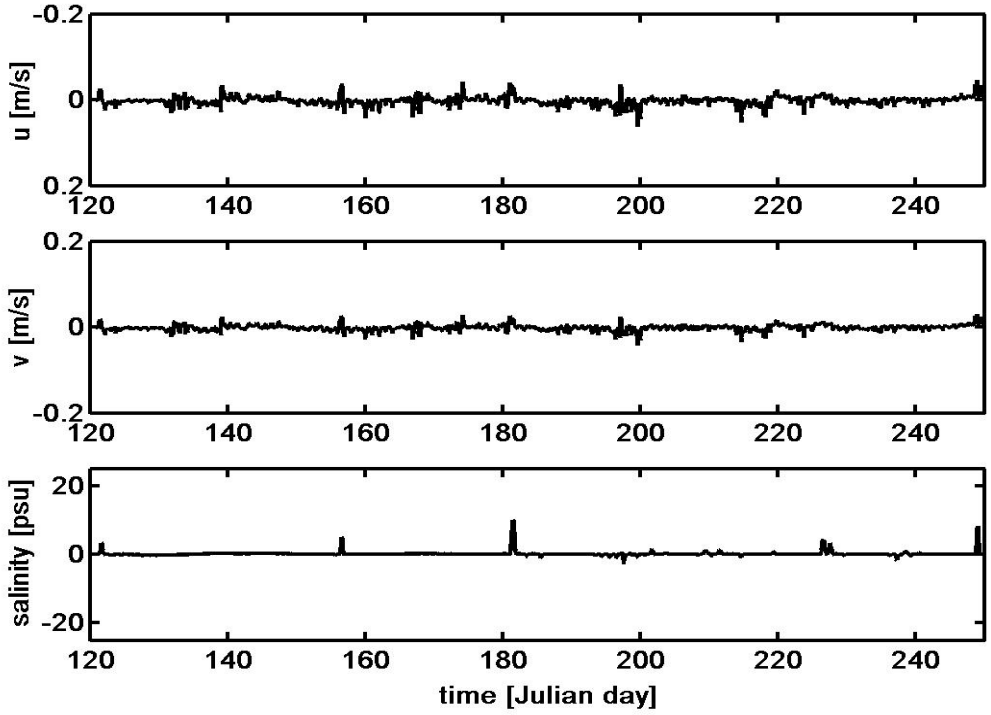

Figure 39. Time series of (u, v, S) differences between the control and no wind forcing runs for the bottom layer at East Bay open boundary.

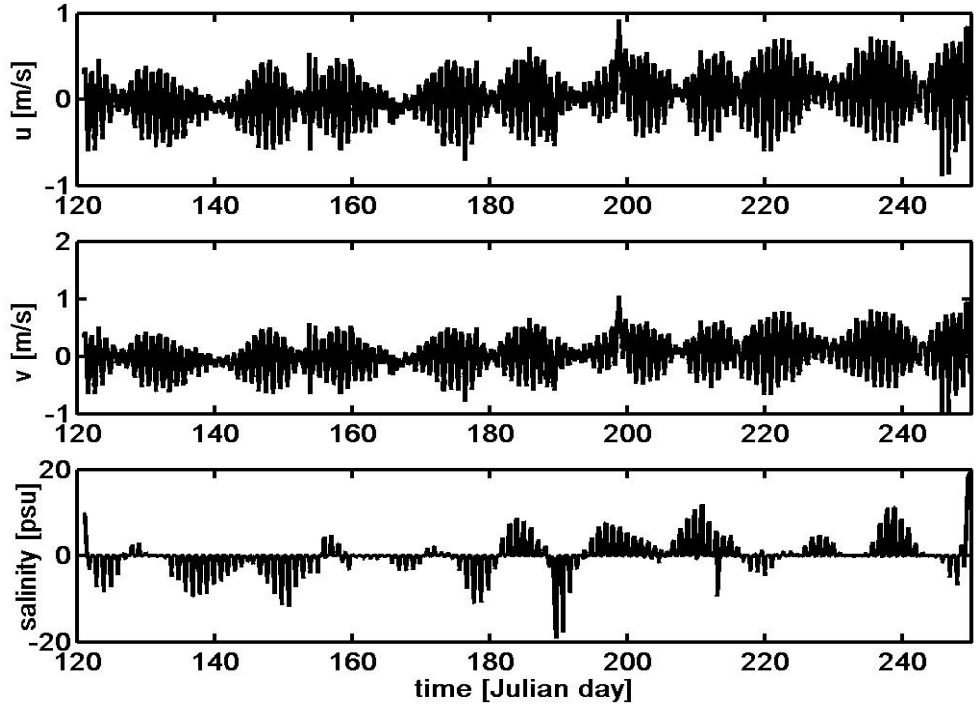

Figure 40. Time series of (u, v, S) differences between the control and no wind forcing runs for the surface layer at West Pass.

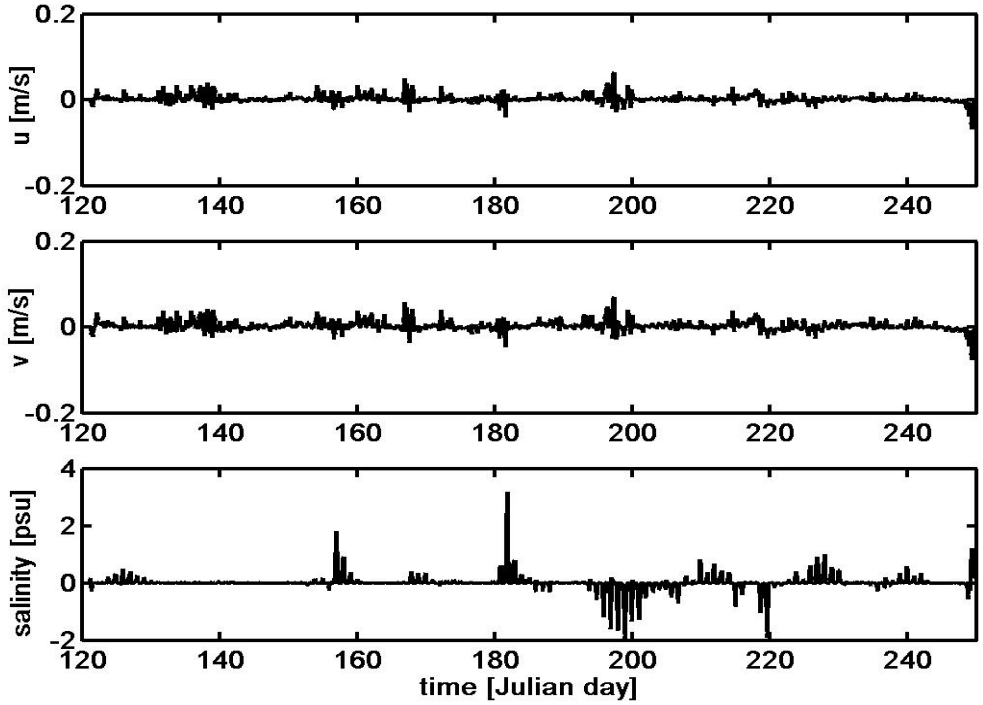

Figure 41. Time series of (u, v, S) differences between the control and no wind forcing runs for the bottom layer at West Pass.

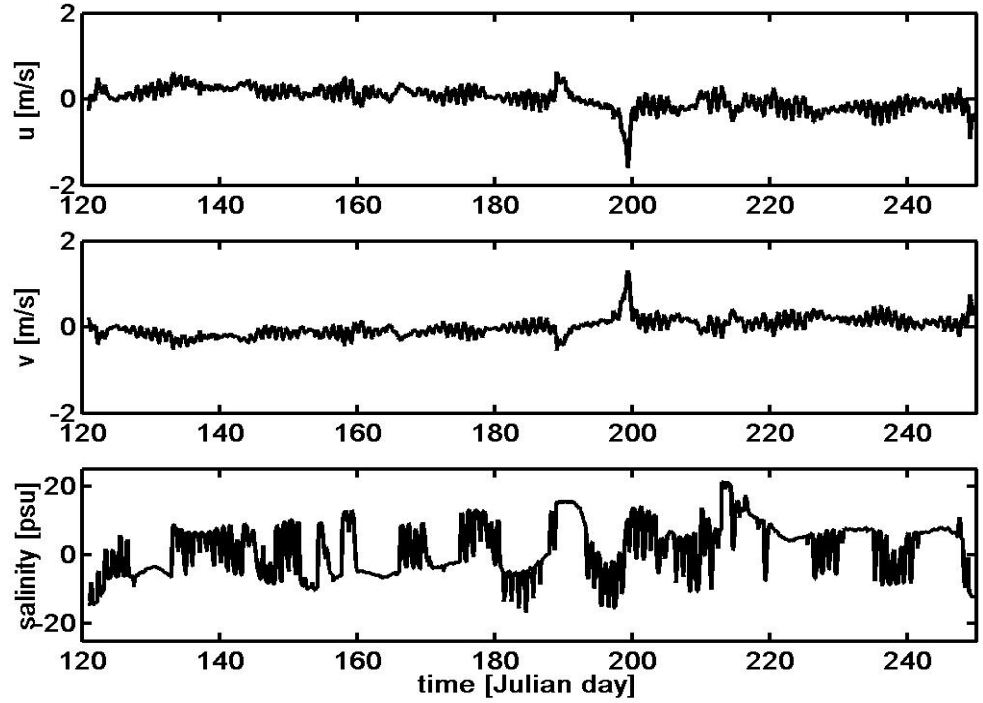

Figure 42. Time series of (u, v, S) differences between the control and no wind forcing runs for the surface layer at West Bay open boundary.

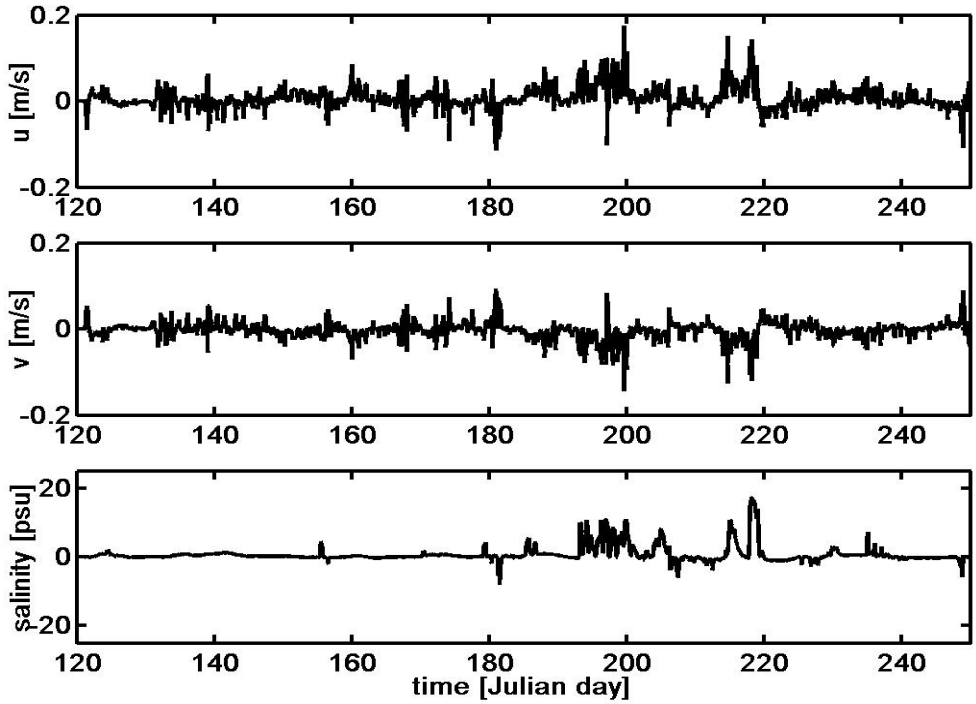

Figure 43. Time series of (u, v, S) differences between the control and no wind forcing runs for the bottom layer at West Bay open boundary.

Figure 44 plainly depicts the surface influence of the wind. It is interesting to notice that despite the lower outward flux occurring in East Bay, the absolute difference equals the one observed in West Bay, clearly pointing the shallow waters wind driven circulation.

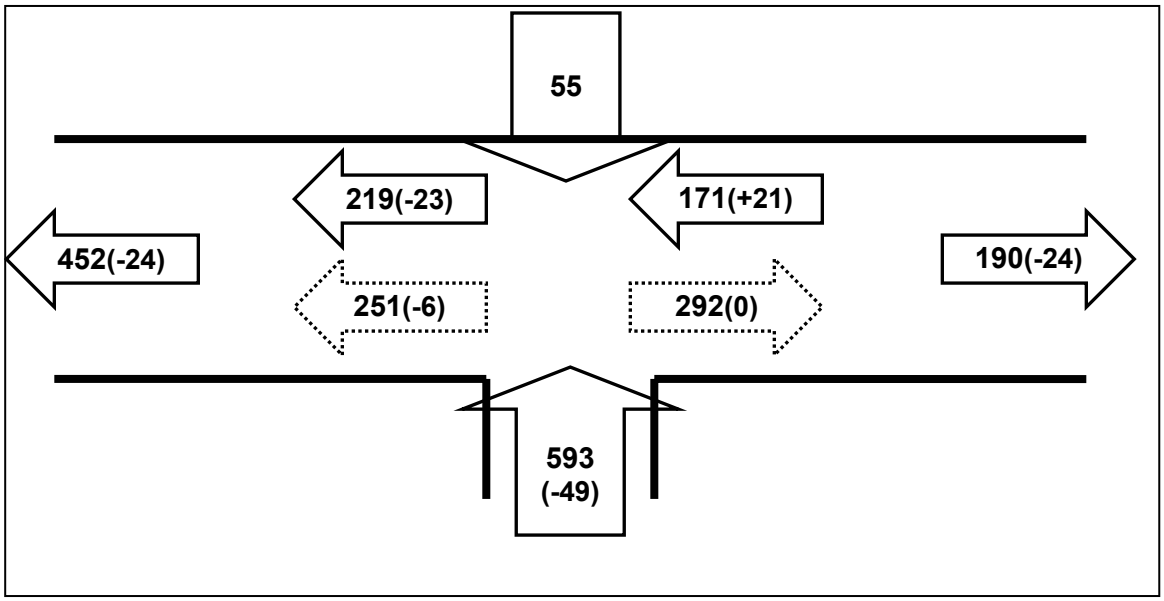

Figure 44. Synthesized fluxes for run without wind forcing

E. WIND FLUCTUATION

This case was features with a modified wind time series. We applied on each component of the original wind time series a normally distributed random perturbation which mean is 0 and standard deviation 1 m/s. All the remaining conditions stayed unchanged when compared with the control run.

Because, in that case, the disturbance was randomly applied, the comparison between the control run and this one gives results far different from the ones obtained when the wind had been removed. First of all, the surface RMSD values are very weak for both speed and salinity being 0.6cm/s and 0.04psu at West Pass, 0.4cm/s and 0.14psu at East Bay and 1cm/s and 0.4psu at West Bay. These values are approximately 25 times lower than the ones observed in the previous comparison. The difference between the surface and the bottom layers is, however, insignificant as shown by Fig. 45 to 50 and RMSD values remain practically unchanged in the deeper layer although slightly reduced.

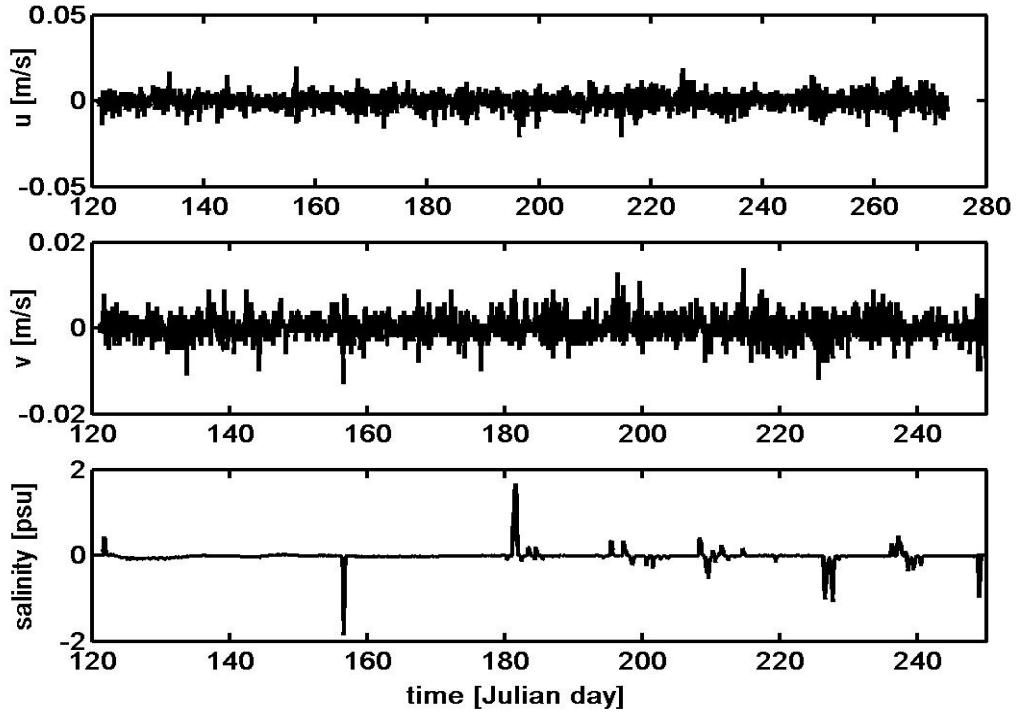

Figure 45. Time series of (u, v, S) differences between the control run and the wind disturbed forced run for the surface layer at East Bay open boundary.

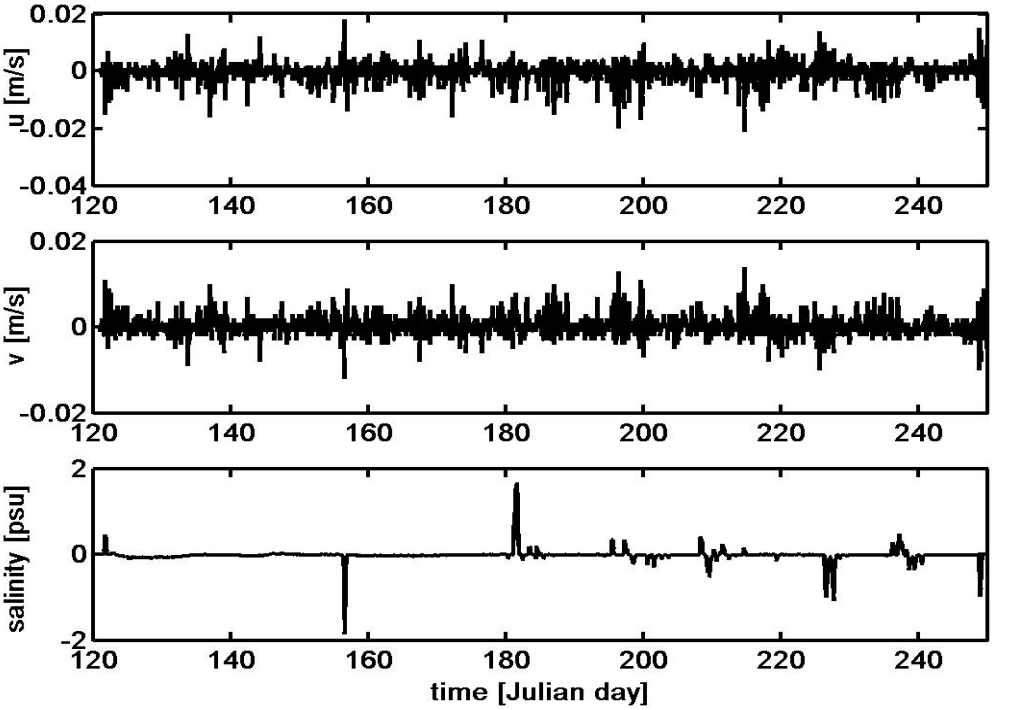

Figure 46. Time series of (u, v, S) differences between the control run and the wind disturbed forced run for the bottom layer at East Bay open boundary.

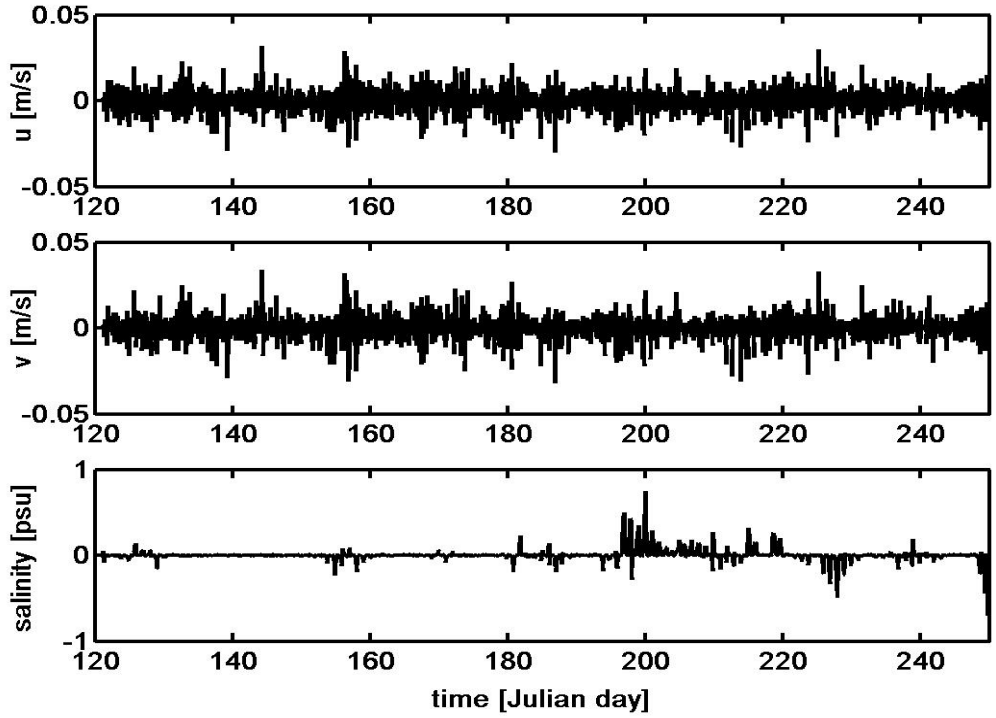

Figure 47. Time series of (u, v, S) differences between the control run and the wind disturbed forced run for the surface layer at West Pass.

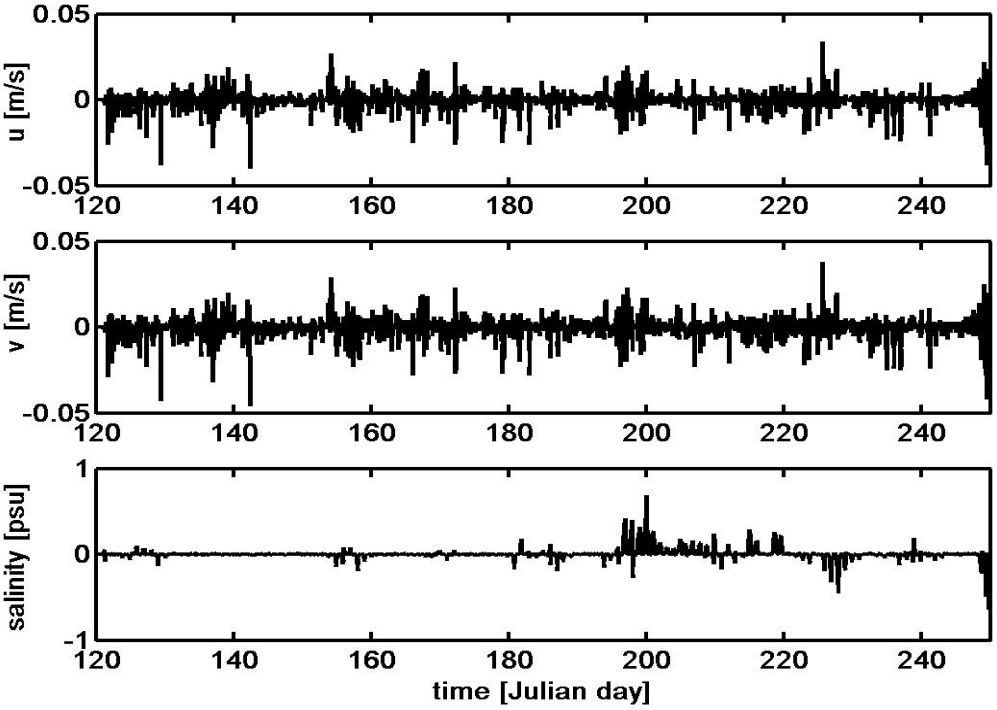

Figure 48. Time series of (u, v, S) differences between the control run and the wind disturbed forced run for the bottom layer at West Pass.

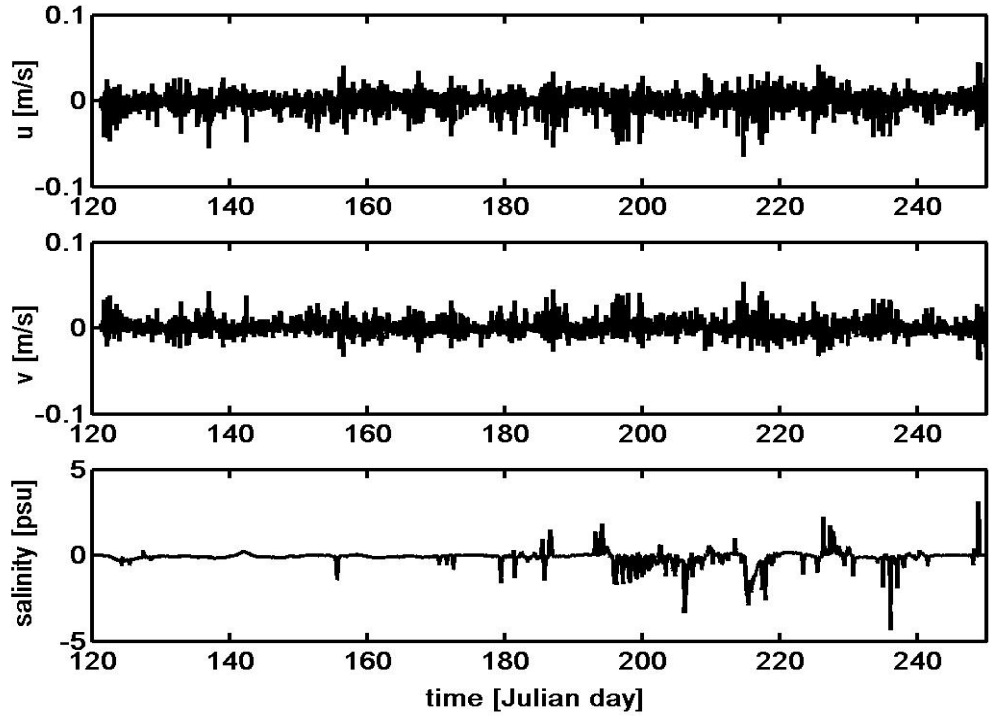

Figure 49. Time series of (u, v, S) differences between the control run and the wind disturbed forced run for the surface layer at West Bay open boundary.

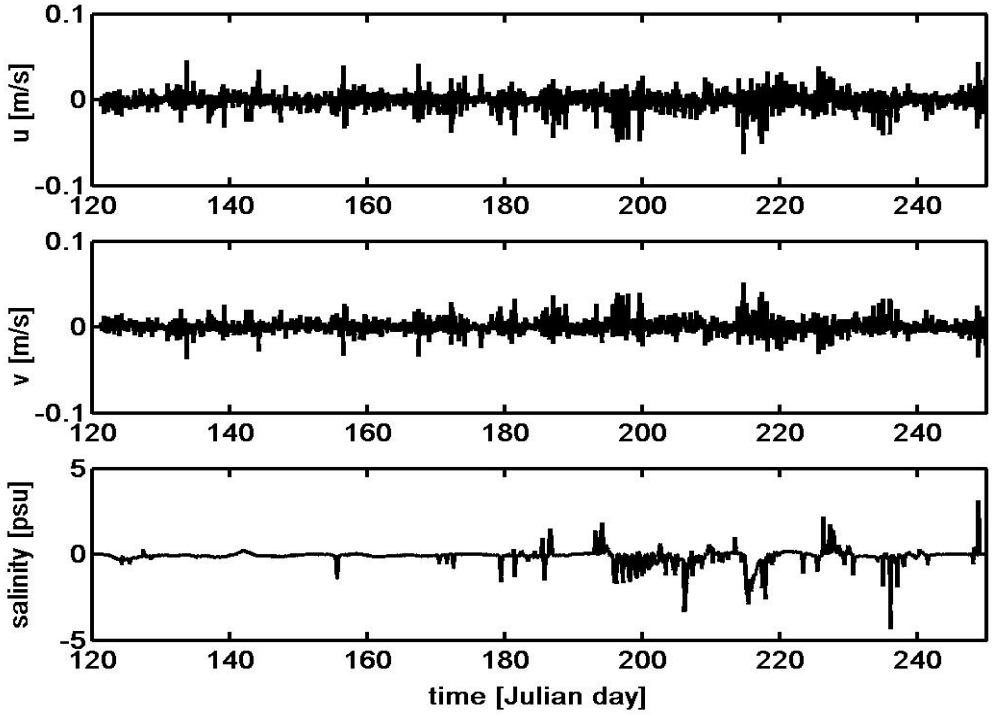

Figure 50. Time series of (u, v, S) differences between the control run and the wind disturbed forced run for the bottom layer at West Bay open boundary.

The lack of difference throughout the water column probably stands in the fact that the minor increase or decrease applied on the wind may not have induce a significant wind direction shift which impact is predominant as observed in the previous chapter. As a matter of fact, the highest differences observed in the previous plots occurred when the wind speed had its lowest values. The computation of the fluxes did not depict great changes as the perturbation respected a mean of 0 and Fig. 51 clearly shows that point.

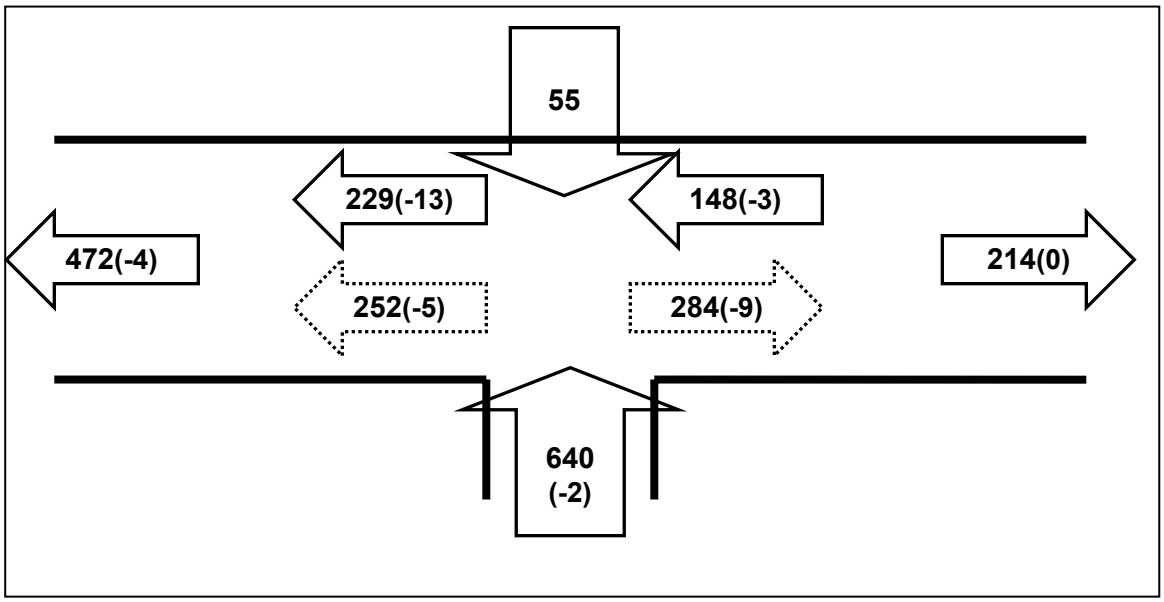

Figure 51. Synthesized fluxes for wind fluctuation run

F. TIDAL RESIDUAL

This case was featured in order to evaluate the impact of the tidal residuals. We then forced the model with tidal constituents only, getting rid of the residuals, and with the original wind data set, all remaining conditions staying unchanged. During this period, the residual averages 7.34 cm.

The first observation from Fig. 52, 53 and 54 is that the lack of residual impacts both the surface and the bottom layers the same way and the difference between both layers is slightly discernible. For u and v, the impact the absence of residual created is more evident at West Pass (Fig.53). We can observe that the remaining signal has not a 0-

mean value. Because the average residual was positive, its absence diminished the inward flux and hence the difference between the control run and the new one is positive. The RMSD at that location is 0.07m/s for an RRMSD of 126%.

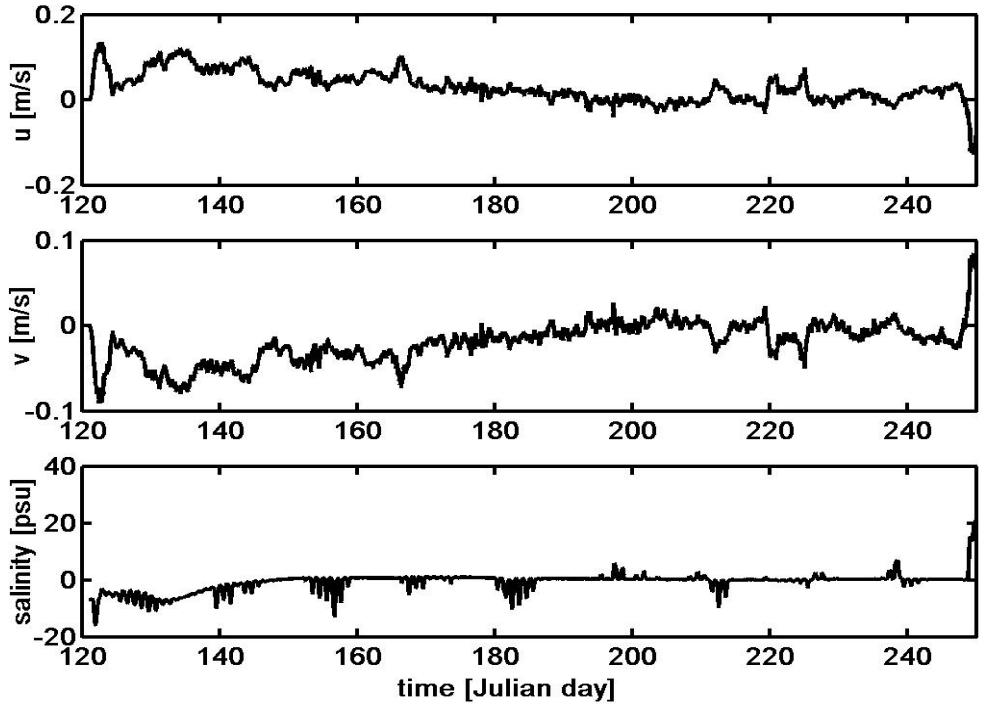

Figure 52. Time series of (u, v, S) differences between the control and no residual forcing runs valid for both surface and bottom layers at East Bay open boundary.

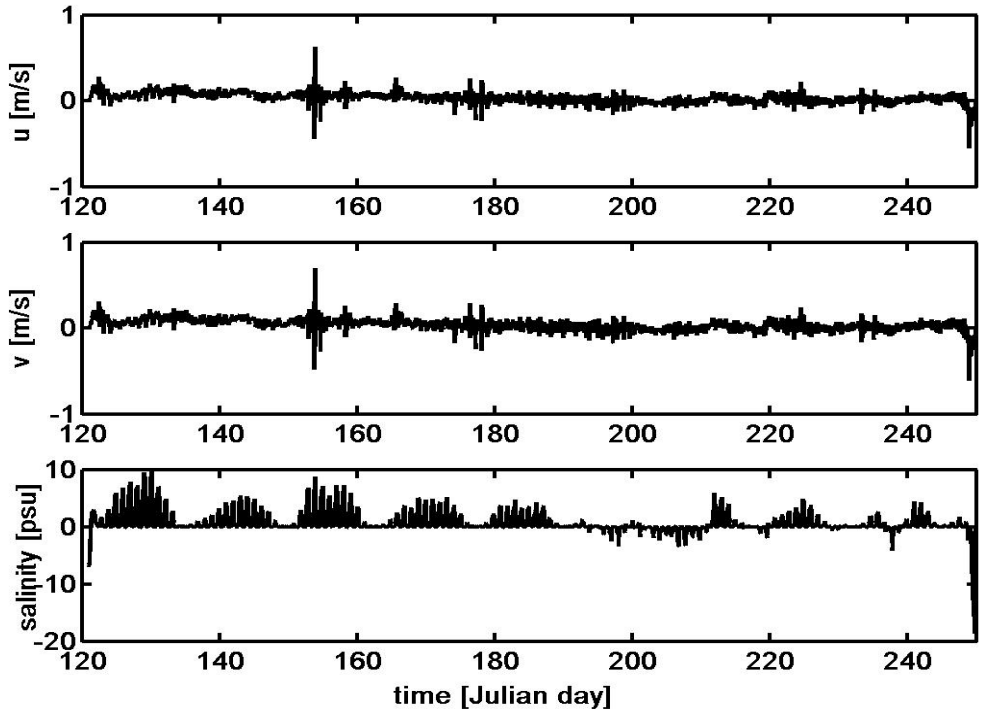

Figure 53. Time series of (u, v, S) differences between the control and no residual forcing runs valid for both surface and bottom layers at West Pass.

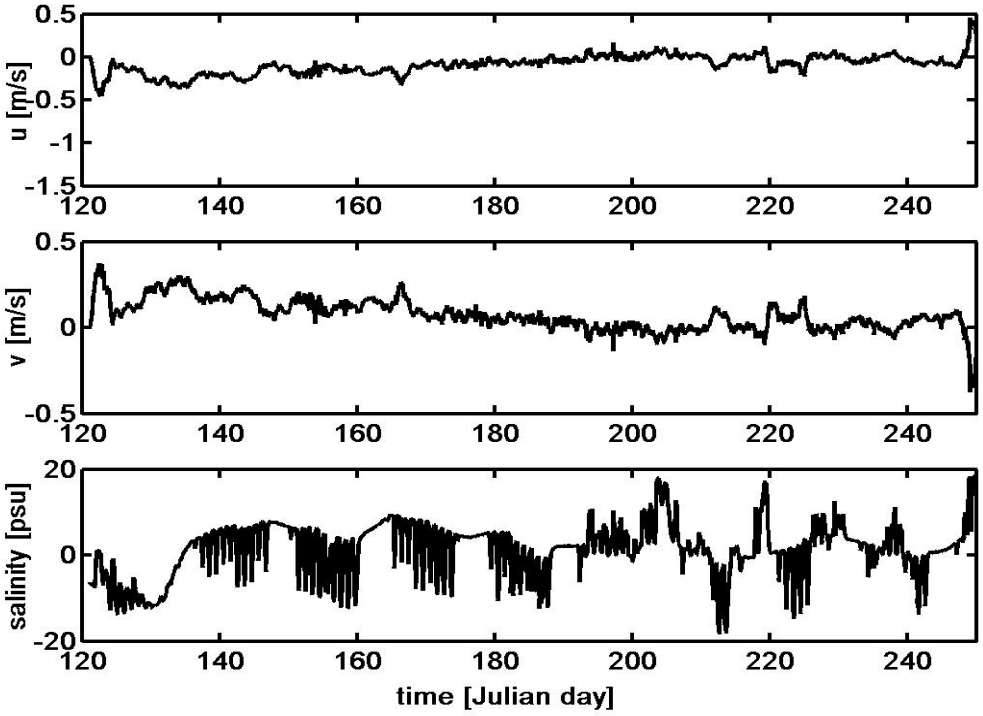

Figure 54. Time series of (u, v, S) differences between the control and no residual forcing runs valid for both surface and bottom layers at West Bay open boundary.

The error induced on the computed fluxes is huge. Because the residuals are fundamentally positive (wave surge, quasi permanent high pressure systems above this area), the pressure gradient has tremendously diminished when they have been removed. Notice that the impact is greater towards West Bay.

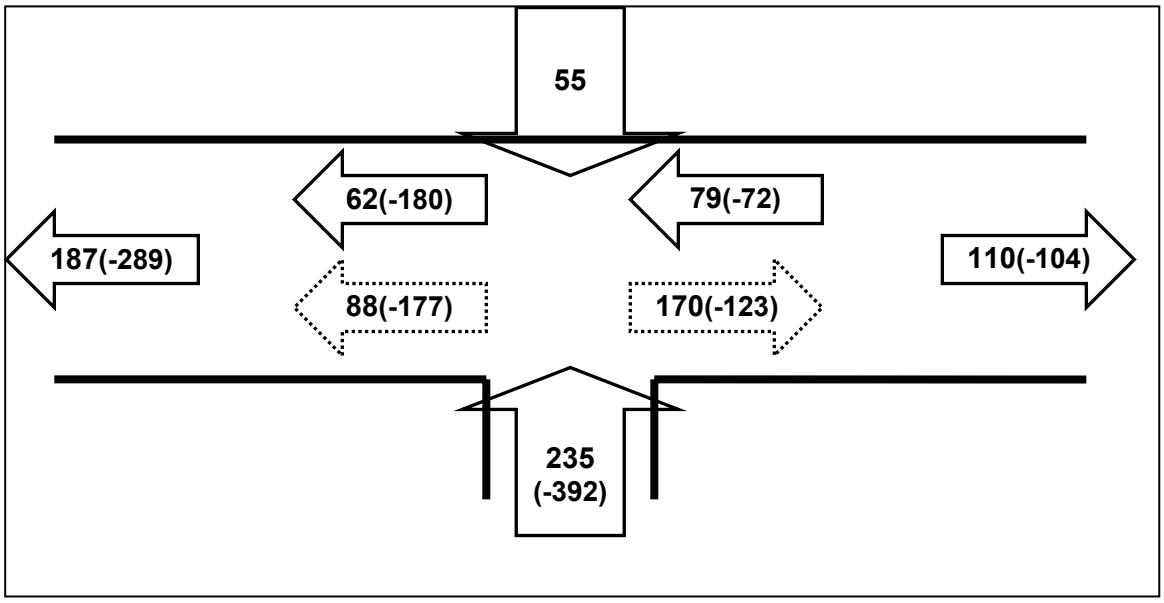

Figure 55. Synthesized fluxes for run without tidal residual forcing

G. TIDAL CONSTITUENT FLUCTUATION

This case was featured in order to analyze the accuracy weight of the tidal constituents of the time series. This case gathers three runs in which the Gulf open boundaries were successively forced with modified elevation time series. In the first case, we decreased the diurnal K1 amplitude from 15.53 down to 14.5cm and in the second one we increased the semi-diurnal M2 amplitude from 2.3 up to 3.4cm. These two new values correspond to the ones used by NOAA for predicting tides in Panama City Beach. The third run used the gauge elevation collected at the NOAA Panama City Beach station. All the remaining parameters remained unchanged when compared with the control run.

The first two cases did not produce great changes on the system. The small variation applied successively on the diurnal K1 and semi-diurnal M2 tidal constituents did not really impact the picture obtained with the initial conditions in the control run. As no shift was applied on the constituent phases, the perturbation obviously correlates the

tidal elevation. The speed RMSD values remain weak (1.2cm/s at West Pass, 0.5cm/s at East Bay and 1.5cm/s at West Bay) and so do the salinity RMSD values (0.1psu at West Pass, 0.15psu at East Bay and 1psu at West Bay). It is interesting to notice that, even if the disturbances were applied at Gulf entrance open boundaries only, the greatest errors were observed at West Bay open boundary. It emphasizes the fact that most of the inward flux flows towards West Bay where the shallowness enhances the speed shift. The speed-RMSD are constant at both West and East Bays through the water column and present at West Pass a 40% difference when comparing the surface layer to the bottom layer, salinity RMSD remaining unchanged. The RRMSD values however represent 20% in both layers, which tends to prove that the difference between the two layers is likely to be related to the bottom friction.

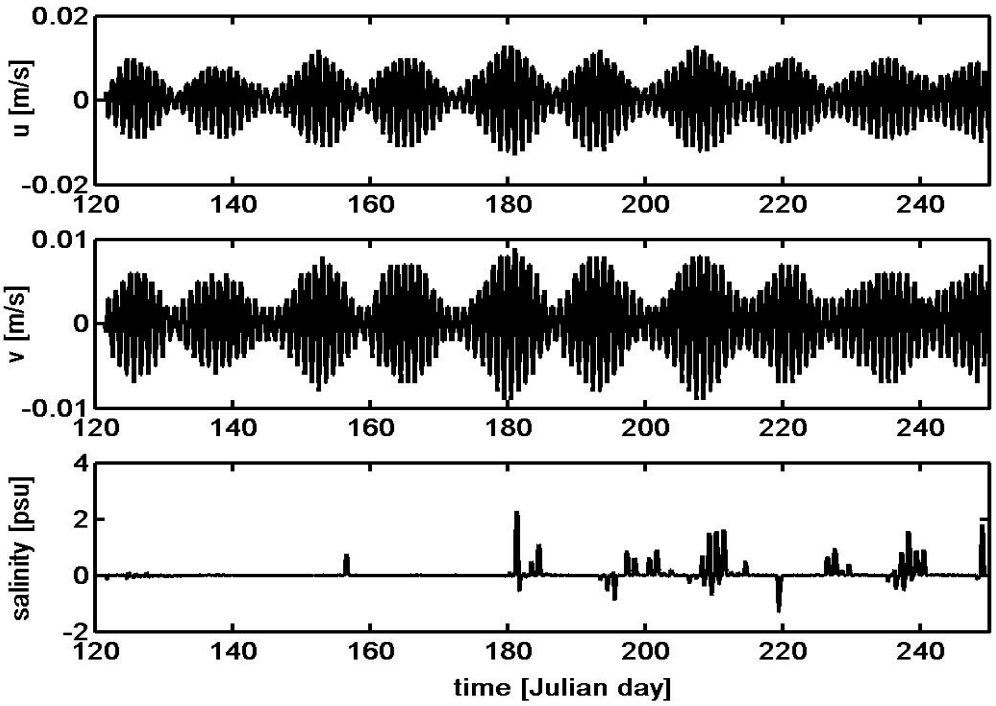

Figure 56. Time series of (u, v, S) differences between the control run and the tidal constituent disturbed run valid for both surface and bottom layers at East Bay open boundary.

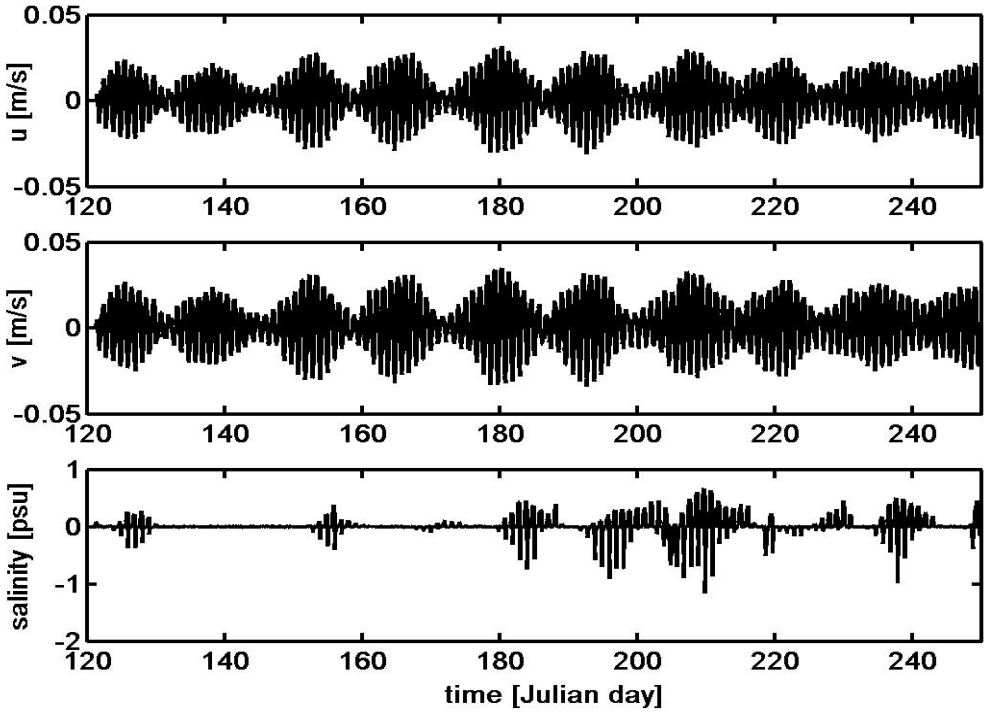

Figure 57. Time series of (u, v, S) differences between the control run and the tidal constituent disturbed run valid for surface and bottom layers at West Pass.

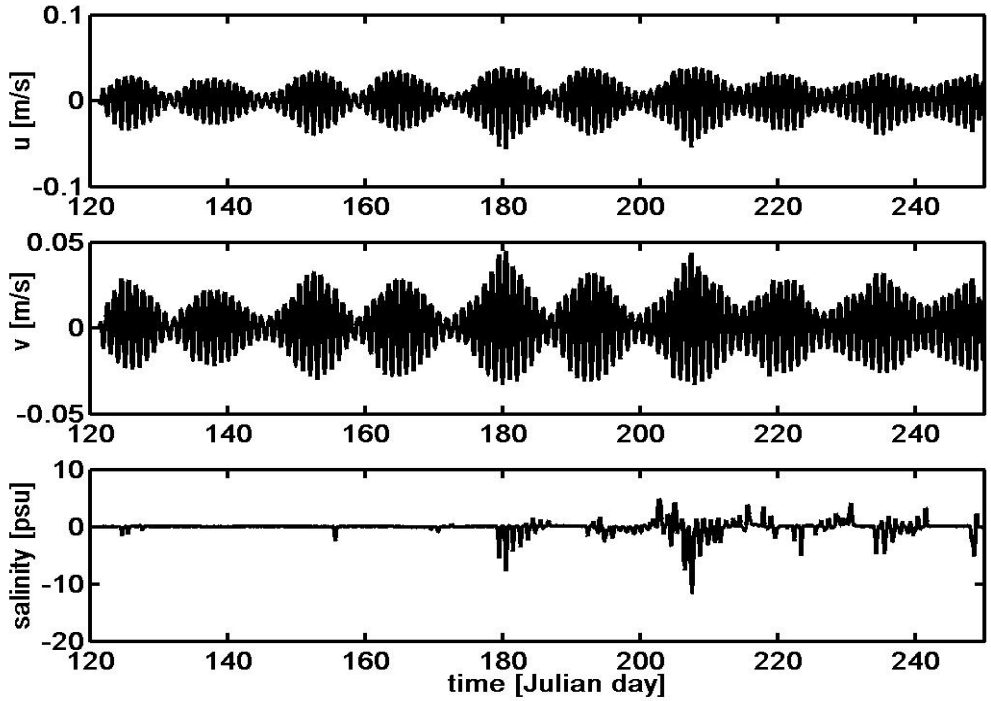

Figure 58. Time series of (u, v, S) differences between the control run and the tidal constituent disturbed run valid for both surface and bottom layers at West Bay open boundary.

Over the five month period, the flux fluctuation is everywhere less than 3 m^3/s. The next figure, representing fluxes, is by the way valid for both changes applied on K1 and M2 tidal constituents.

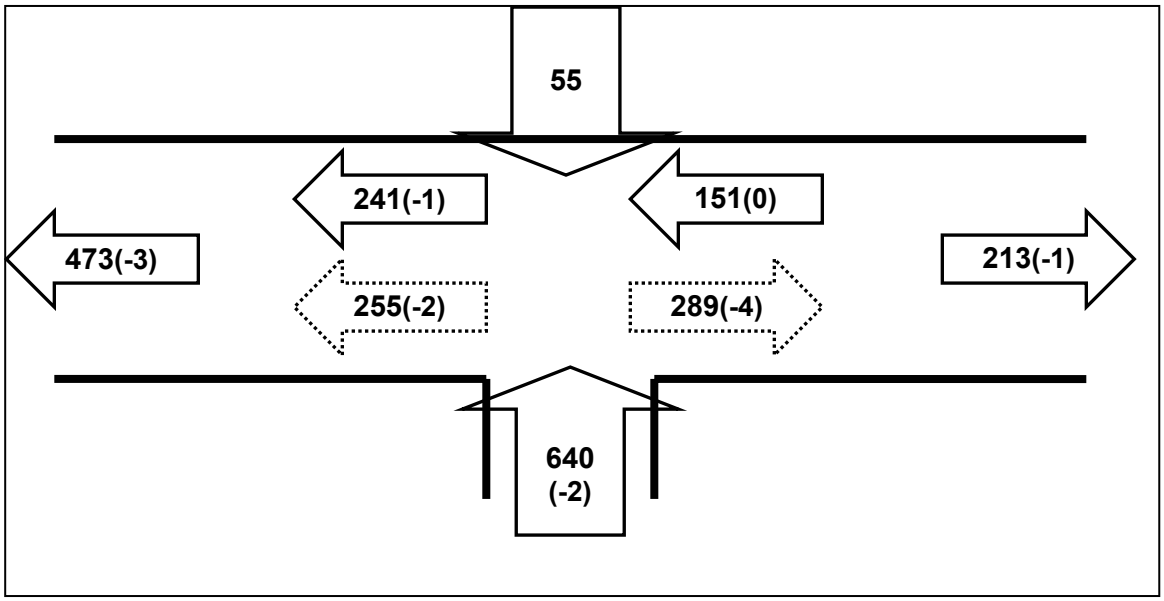

Figure 59. Synthesized fluxes for tidal fluctuation run

THIS PAGE INTENTIONALLY LEFT BLANK

VIII. HYDROCHEMICAL PROCESSES AND CHEMICAL THREAT

Besides WQMAP, ASA also built model applications used as rapid response models named OILMAP, SARMAP or CHEMMAP after Oil, Search and Rescue or Chemical Mapping and Analysis Program successively. We ran the three dimensional version of WQMAP which prompted us to use CHEMMAP in order to evaluate the baroclinic influence on accidental release. Each case will be featured with chemical compound being released at surface and near the bottom to estimate the effects on dispersion. We will also conduct the release at different period of time to assess the influence of forcing conditions on the dispersing process.

A. CHEMMAP

CHEMMAP is a chemical discharge model designed to predict the trajectory, fate, impacts and biological effects of a wide variety of chemical substances three-dimensionally in both marine and fresh water. The CHEMMAP model system is made up of several integrated components among which the chemical database, the chemical fate model are of outmost importance.

1. The chemical database

The database encloses all the physical/chemical properties required for simulating transport and fate of the spilled material. CHEMAP uses either the Chemical Abstract System (CAS) registry number or the UN number to reference each chemical. The chemical state can be defined as solid, liquid or gas, dissolved or not in aqueous solution or in solvent. As chemical properties do vary with temperature, there all referred to their value at 25˚C.

2. The chemical fate model

The spill model itself predicts the movement of chemicals on the water surface and the distribution of chemicals in the environment in the water column, in sediments and on the shoreline. The model simulates spreading, dispersion, evaporation, entrainment, dissolution, sedimentation and degradation processes. The model is initialized with the user-specified time, location and duration release of selected material. Its state and solubility are driven the initialization algorithm. In the case of a highly

soluble chemical, the chemical mass is initialized in the water column in the dissolved state. All the different cases are defined in McCay and Isaji (2004).

The mass is transported in three-dimentional space and time, relying on environmental data such as wind drift and currents. The vertical velocity of chemical components is computed with Stoke's law, which relates the terminal settling or rise velocity of a smooth, rigid sphere in a viscous fluid of known density and viscosity to the diameter of the sphere when subjected to a known force field (gravity). The equation is:

$$w = \frac{2}{9}\frac{\left[\left(\rho_{chem} - \rho_{water}\right) r_{chem}{}^{2} g\right]}{\nu_{water}} \qquad \textbf{(13)}$$

where ρ_{chem}, ρ_{water} are the densities (kg/m^3) of the chemical component and the water; r_{chem} is the radius (m) of the chemical component; ν_{water} is the water viscosity (Ns/m^2).

The currents in the surface water layer (surface drift currents) are calculated with hourly wind field. The surface drift currents have the magnitude ranging between 1 and 6% of the wind speed and are in a direction 0-30˚ to the right (in northern hemisphere) of the down-wind direction. In this study, the horizontal turbulent diffusion coefficient ranges between 1 and 10m^2/s and its value was set to 1 m^2/s in the different cases. The vertical turbulent diffusion coefficient ranges from 0.00001 (for stratified ocean) to 0.001 m^2/s (for well mixed ocean). It is set to be 0.00001 m^2/s in this study.

The chemical is modeled using a Lagrangian approach in which spillets are tracked in both space and time. All the phase transfer rates are computed at each time step. This type of model is frequently used to trace back harmful substances to their sources and constitutes a valuable tool in the identification of environmental polluters.

3. Environmental data and stochastic model

CHEMMAP also includes an embedded Geographic Information System (GIS). The GIS is used to store, display and analyze any type of geographically referenced data. GIS also includes data which are not necessarily used by the spill model, such as place names, critical habitats for fish and wildlife, spill response equipment, shipping lanes,

and real-time spill observations, but they are often helpful in analyzing and interpreting model results.

The stochastic model randomizes at a given location spill date and hence wind and current conditions. This model output consist in statistical maps defining, for example, the probability of exceeding a concentration threshold or the time when the concentration first exceeds the threshold.

B. CHEMICAL COMPONENTS

The choice of the chemical components used in the afterward scenarii ensued from our will to analyze the baroclinic impact on dilution and spill. Therefore, instead of focusing on the lethal power of the chosen component, we picked up components which tend not to evaporate promptly. Since this thesis is unclassified, we are not going to relate the results to any relevant threat scenario. However, our statements can be transposed to all similar chemical components which are in the field of interest in national security concerns.

1. Physical information

Ethylene glycol, $OH\text{-}CH_2\text{-}CH_2\text{-}OH$, is a non volatile, soluble sinker, its density being 1.1132×10^3 kg/m^3. It is referenced as CAS 107-21-1 or UN 8027. Ethylene glycol is a clear, colorless, slightly syrupy liquid at room temperature. It is odorless but has a sweet taste.

2. Industrial use

It is used to make antifreeze and de-icing solutions for cars, airplanes, and boats; to make polyester compounds; and as solvent in the paint and plastics industries. Ethylene glycol is also an ingredient in photographic developing solutions, hydraulic brake fluids and in inks used in stamp pads, ballpoint pens, and print shops.

3. Exposure effects

Eating or drinking very large amounts of ethylene glycol can result in death, while large amounts can result in nausea, convulsions, slurred speech, disorientation, and heart and kidney problems. Female animals that ate large amounts of ethylene glycol had babies with birth defects, while male animals had reduced sperm counts. However, these effects were seen at very high levels and would not be expected in people exposed to

lower levels at hazardous waste sites. Ethylene glycol affects the body's chemistry by increasing the amount of acid, resulting in metabolic problems. Similar to ethylene glycol, propylene glycol increases the amount of acid in the body. However, larger amounts of propylene glycol are needed to cause this effect.

Its primary hazard is the threat to the environment. Immediate steps should be taken to limit its spread to the environment. Since it is a liquid it can easily penetrate the soil and contaminate groundwater and nearby streams.

4. Safety recommendations

The EPA has set a drinking water guideline for ethylene glycol of 7,000 µg in a liter of water for an adult. The American Conference of Governmental Industrial Hygienists (ACGIH) recommends a maximum level of 127 milligrams of ethylene glycol per cubic meter of air (127 mg/m³) for a 15-minute exposure.

C. TRANSPORT PATTERN

In all cases, 10 tons of the aforementioned chemical constituent are released within 10 hours with an original plume thickness of 0.5m. The choice of the date did not respond to any particular need. The release locations, however, were selected in order to maximize the tidal pumping effect and minimize the vertical mixing process.

1. Release at (30° 08' 45.5"N, 85° 40' 46.8"W) on June 1st at 12am.

The chemicals are released at (30° 08' 45.5"N, 85° 40' 46.8"W) 12 am on June 1st. We analyze differences between surface and bottom release. As ethylene glycol is not volatile, the evaporation process is weak. Because of the tidal pumping, the chemical dilutes far away from its source in both West Bay and East Bay directions (Fig.61). Even if this location is closer to East Bay, it essentially diffuses westward accordingly with the mean winds (from 155° at 4m/s) whereas flow tends to push the water eastward. The maximum dissolved concentration rarely exceeds 1mg/m^3 beyond 85°35' toward East Bay and occurs between 4 and 10 days after the release. The same peak reaches a position as far as 8.5km south west of West Pass on the inner shelf 4 days after the release. A maximum concentration of 32000 mg/m^3 is obtained 1 hour after the release started (Fig.62). Figure 63 shows that the ethylene glycol is immediately mixed into the

water column. Its decreasing rate is 0.3024 per day at 25˚C and after 3 weeks ethylene glycol has disappeared from the bay.

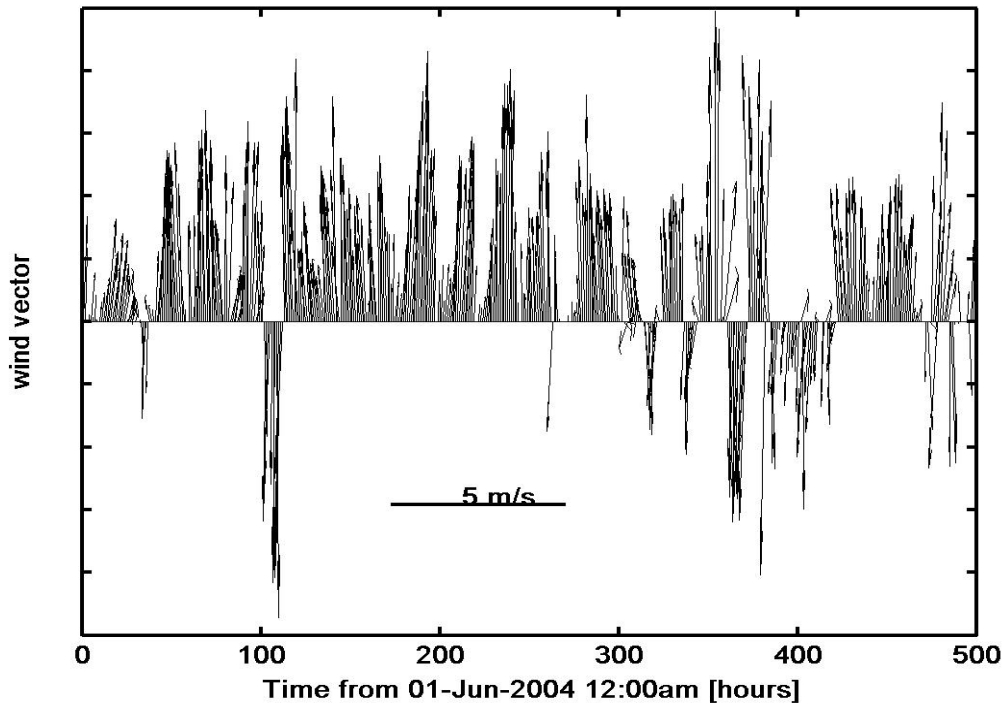

Figure 60. Wind field over the domain between the 01-Jun-2004 12:00am and the 21-Jun-2004 11:00pm

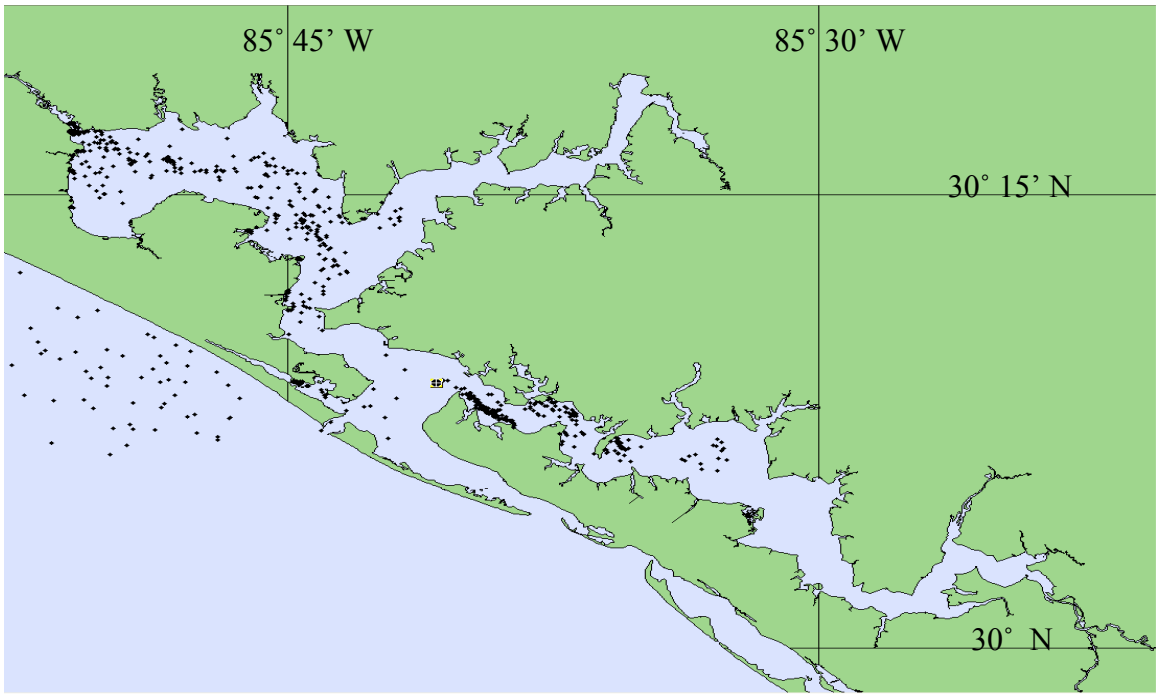

Figure 61. Spillet dispersion after 3 weeks

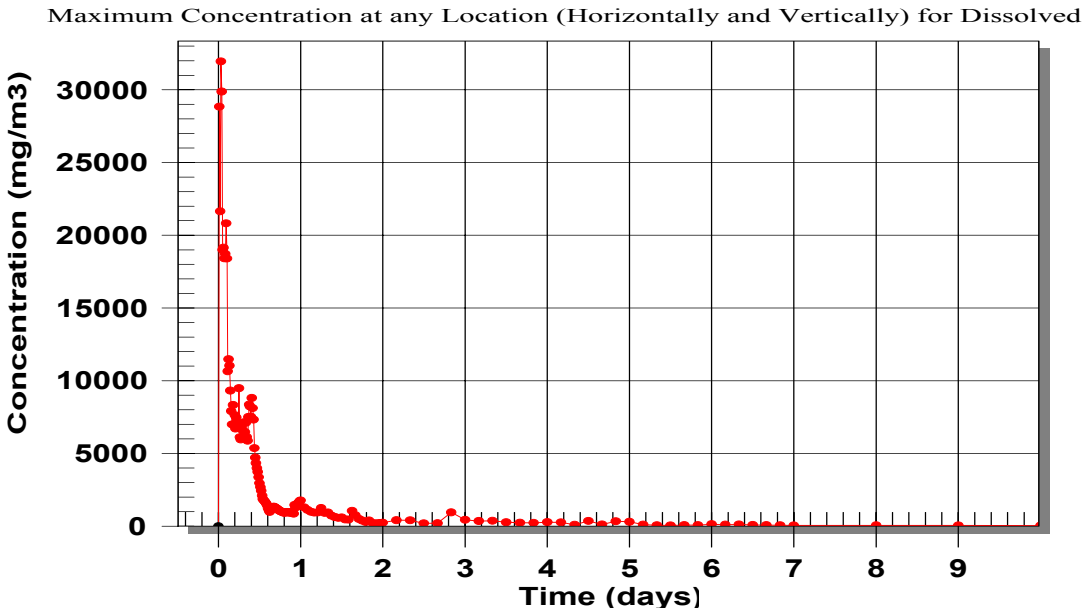

Figure 62. Maximum concentration for dissolved ethylene glycol

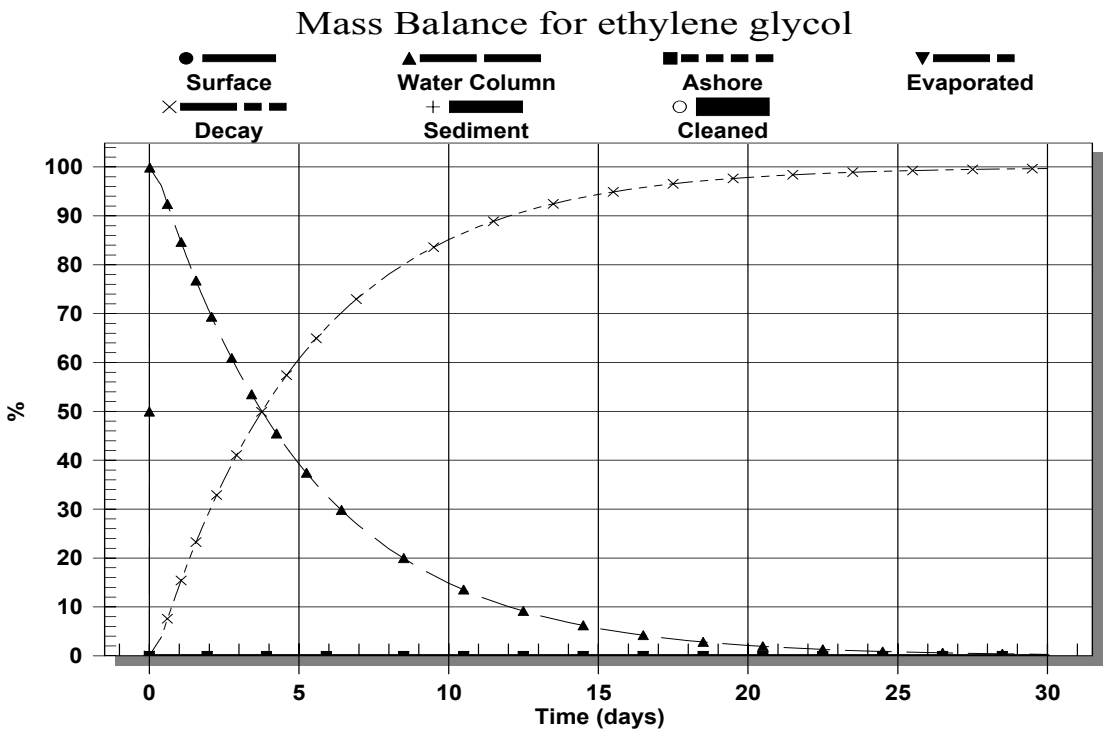

Figure 63. Mass balance for phenol release at location φ = 30° 08' 45.5N -G = 85° 40' 46.8W

It is difficult to correlate the signal between two different locations as the plume goes back and forth with tides and as the concentration depends upon the depth at each location. As it propagates westward from the release point to the end of West Bay, the shape of the signal varies significantly as shown in Fig. 64, 65 and 66. We can also notice that, the shape smoothes with time (only the largest peak can be tracked) but when the depth is shallow enough, we detect again higher peaks which were present nearby the release location. It is clear from these plots that the water depth influences the dissolved concentration between the last two locations (the depth decreases from 10 to 2m). The concentration naturally decreases as we move away from the source.

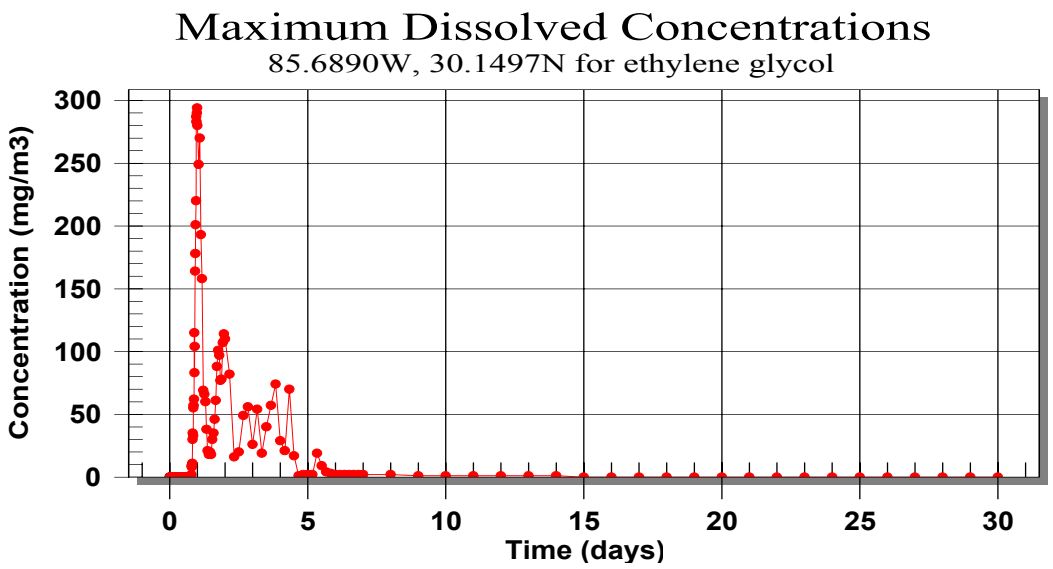

Figure 64. Signal in St Andrew Bay

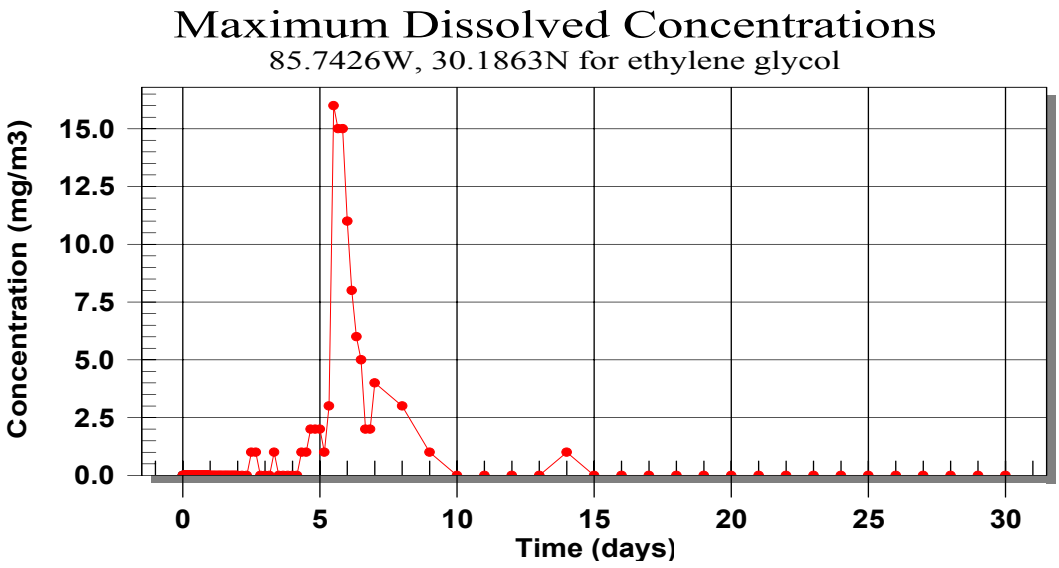

Figure 65. Signal at location A

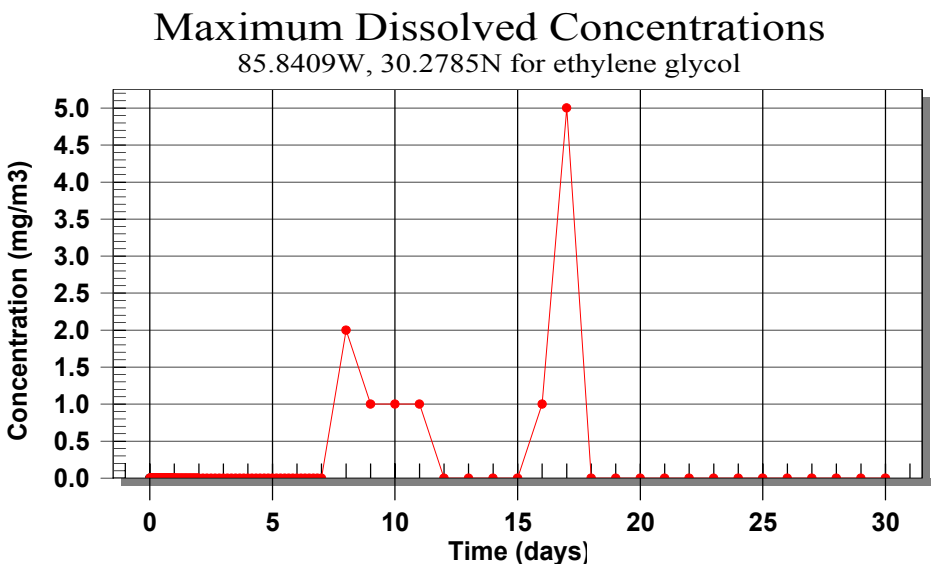

Figure 66. Signal at West Bay open boundary

Figure 67 enhances the effects a semi enclosed small creek can produce. With southeastern winds, the chemical piles up in the northern part of West Bay where it remains and accumulates until being diluted into West Bay by changing wind conditions. We can therefore find lumps of pollutant in very small areas which can more severely impact the environment.

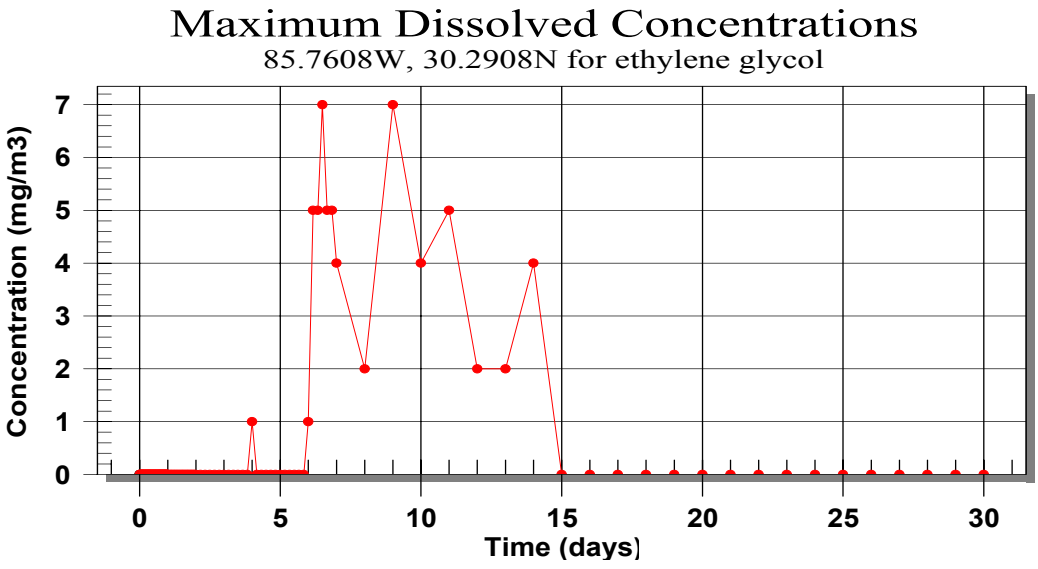

Figure 67. Signal in the north of West Bay

2. Wind influence study

If the tidal influence in the spreading of the plume can be viewed during the simulation, the impact of the wind is less obvious. Two cases are designed to show the wind effect: (1) reversing wind direction and (2) eliminating wind. When the simulation was done without wind, most of the pollution remained contained between points A and B defined in the previous chapters during the first two weeks (the 15th of June corresponds to the highest tidal range after the release). After that period, a large part of the chemical diffuses into West Bay. Figure 68 also shows the following features. As the pollutant transits within the mean flow in West Bay, it seems to pile up in different places in East Bay. This statement only characterizes that particular snapshot and does not reflect a steady state.

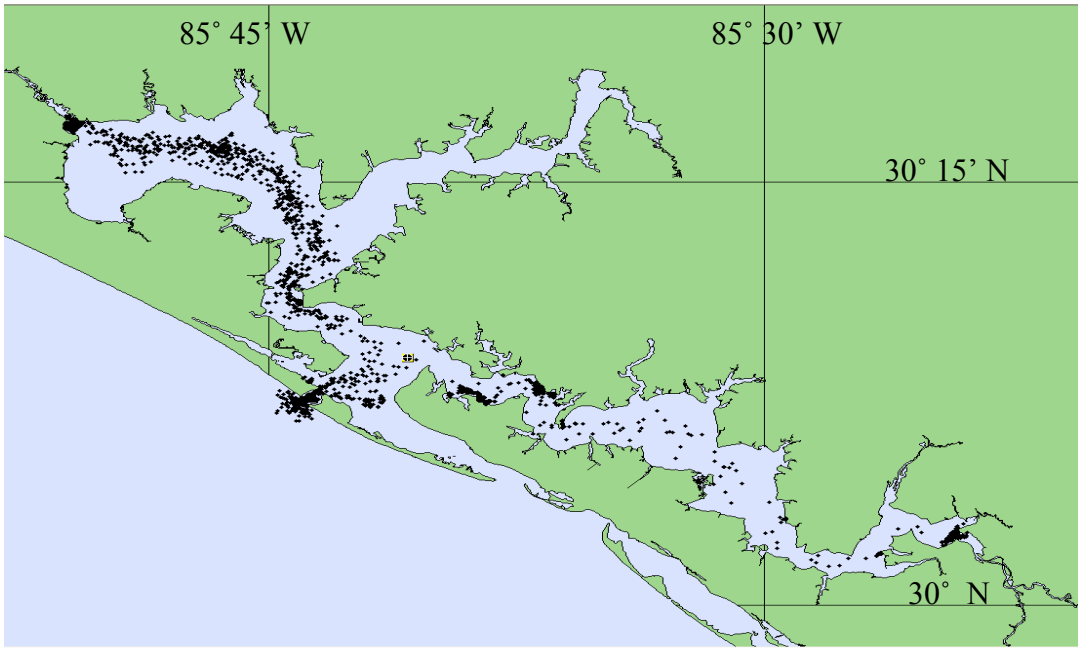

Figure 68. Spillet dispersion after 3 weeks without wind

When the wind field is reversed, it is not surprising that the pollutants mainly diffuse eastward (the average wind now blows from WNW at 4 m/s) and outward the bay system (Fig.69).

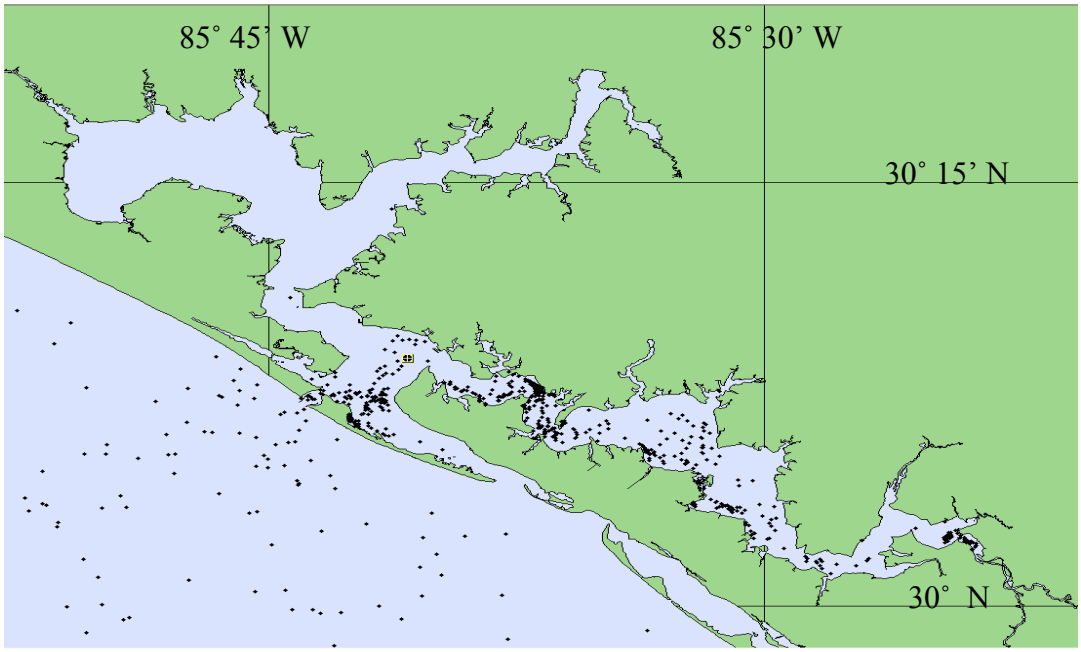

Figure 69. Spillet dispersion after 3 weeks with reversed wind

3. Release time influence using the stochastic model

The dependence on the wind field appears to be of importance. None of these cases, hence, is representative of the average impact a chemical release would have on the bay even though the release location remains unchanged. We then applied the stochastic model featured with 50 randomized dates of release taken between the 1st of June and 31st of August. Figure 70 represents the run number of the worst case scenario for each cell (each run is featured with different release date, then different wind and current data but same location and same amount of chemical). The worst case scenario is defined for giving the maximum value encountered at each cell during all the runs. Thus, the large discrepancies observed on figure 68 lights the importance of the chosen date of release. To each tone of grey correspond 5 consecutive runs (even if they are not related to each other).

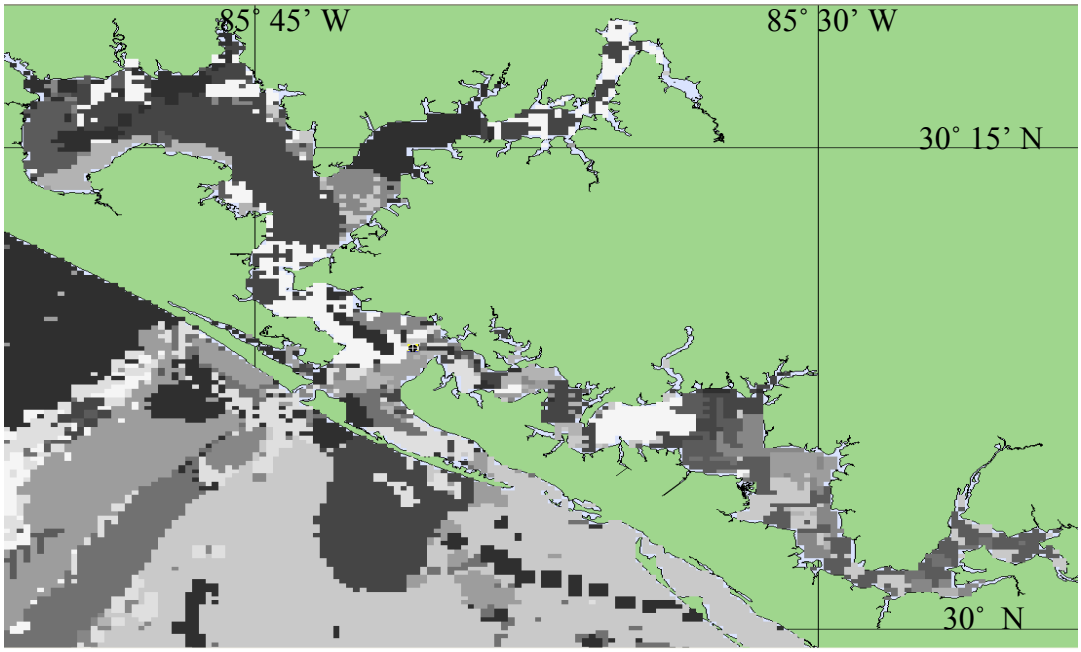

Figure 70. Run numbers for worst case scenario

Fig. 71 shows a severe case with a maximum dissolved concentration and two major features. First, the pollutant predominantly diffuses westward which correlates the averaged wind encountered during this period of the year. Second, the pollutant tends to concentrate in shallow motionless waters on the edges of West and East Bay. Note that the two patches of lower concentration in St Andrew Bay correspond to the deepest locations of the bay.

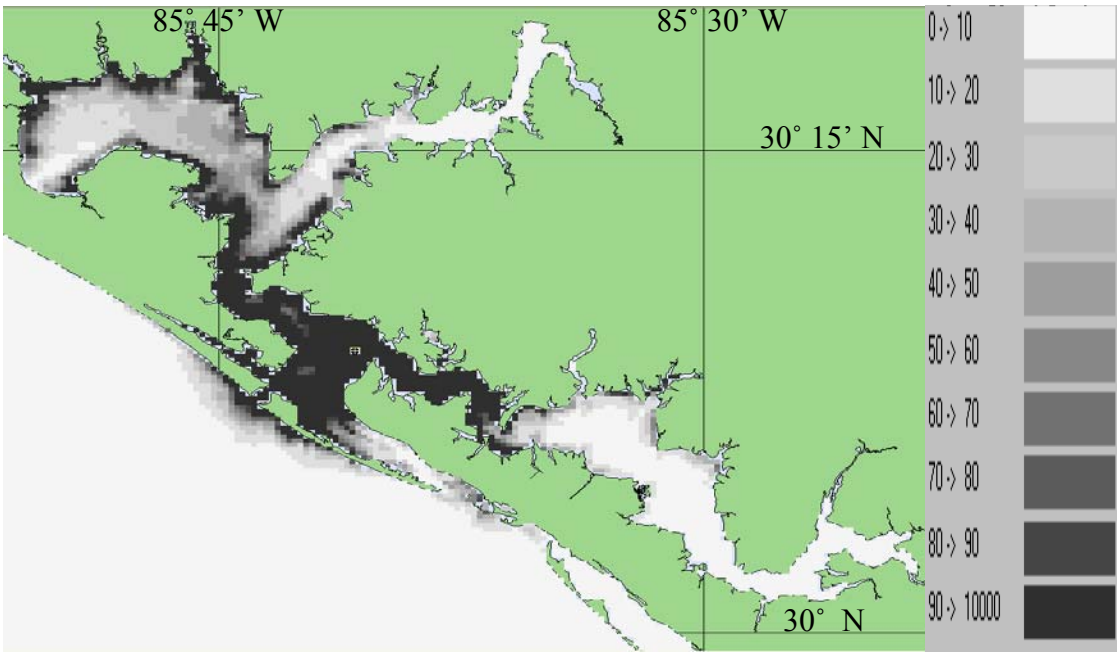

Figure 71. Worst case maximum dissolved concentration (mg/m^3) with spill released in St Andrew Bay

Therefore, defining the probability a threshold to be overshoot at each grid cell is important. This threshold represents a short term exposure limit (STEL) or an immediately dangerous for life or health (IDLH) limit. The model provides such a probability being given in percentage of runs during which this threshold has been exceeded. If we only consider the possibility of the bay system to be polluted (threshold is given a 0-value), then this percentage is 100% for the whole bay except in the northern part of North Bay and the eastern one of East Bay where probability never drops under 50%. The knowledge of such a probability is vital for deciding the deployment of antipollution devices. But of even furthest importance is the time given before this value can be reached. Fig. 72 then represents the minimum time requested for exceeding the threshold at each grid cell. Hence, for that particular release location, all St Andrew Bay will be polluted within 12 hours, within 24 hours the pollution will extend from point A to the first third of East Bay. It will last over 3 days for the pollutant to reach West Bay open boundary and 10 days for East Bay's.

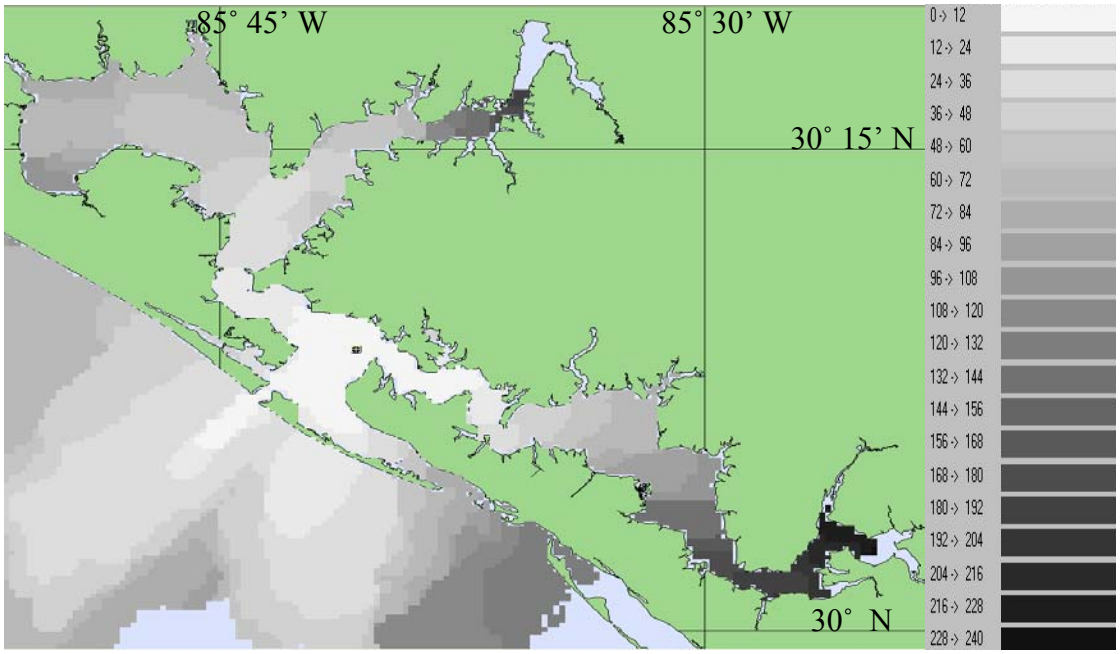

Figure 72. Minimum time (hours) to exceed threshold

4. Spill location influence study

It is obvious that the time for the pollutants transporting outward the bay mainly relies on the winds and source location. If the application of the stochastic model somehow handles the wind factor, the release location must be shifted to other places in order to evaluate the relative weight of this factor. We then applied the same concept to 4 different sites, point A, point B, the center of East Bay and the center of West bay which were supposed to depict different pollutant propagation features accordingly with the hydrodynamic model results.

Because the flux originating from Gulf of Mexico predominantly flows westward, a release point located between St Andrew Bay and West Bay or even more inside West Bay is likely not to deeply impact East Bay. The pollution will only reach the end of East Bay after 15 days if the pollutant is spilled at point A, which only stands 8km away from the previous spot. As this chemical is not volatile, it does not evaporate and its mass is roughly conserved into the system until its natural decay acts. West Bay is much shallower than St Andrew Bay, thus the small concentration decrease close to the Gulf entrance involves a large pollutant mass transfer into West Bay.

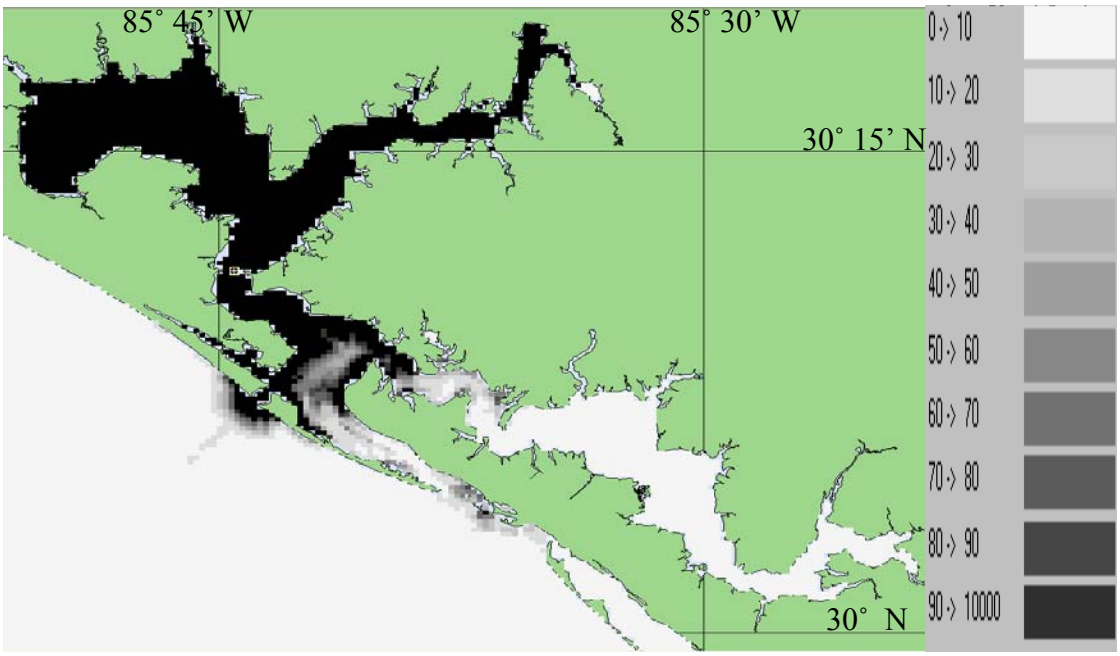

Figure 73. Worst case maximum dissolved concentration (mg/m^3) with spill released at point A

THIS PAGE INTENTIONALLY LEFT BLANK

IX. CONCLUSIONS

In this thesis, we first study the baroclinicity and forcing mechanism for a hydrodynamic model in St Andrew Bay, Florida. The un-nested trait of this model required the open boundaries to be located close to the study domain in order to apply a uniform wind profile with some confidence. If placing the boundaries more offshore should provide better results in term of circulation at Gulf entrances essentially, it would also induce problems we did not face. Buoys deployment would be required in order to get sea level data and all the open boundary cells could not be forced with the same data set because of the phase shift induced by the stretching of the boundary. The use of smoothing process in very narrow fast bathymetry-changing bays dramatically impacts the absolute values of both speed and overall fluxes. Therefore, speed current values, when required for operational purposes (diving operation for example), must be used with caution. The assessment of this process, which was necessary not to increase the number of cells significantly and hence decrease an already very small time step, should request further study.

Despite these shortcomings, the baroclinicity of the circulation was pinpointed and the channels joining St Andrew Bay to both West and East Bays have clearly been identified as being two-layered. Notice that, even though no rivers are present on scene, the freshwater input from underground seepage was characterized in the model as originating from rivers. It is then reasonable to estimate that the fact the two-layered flow is confined in two areas takes its origin in this bias. This result alone is sufficient for using a 3D baroclinic model. However, the magnitude of the freshwater input does not really influence the flux itself neither did the accuracy of the wind field or of the tidal constituent amplitude. Nevertheless, the impacts of wind on vertical stratification and those of tidal residual on the flow are important, particularly for operational purposes, if all forcing mechanisms are not taken into account.

The baroclinicity was not however an outmost feature in the CHEMMAP applications. Because the chemical data embedded provided substances which were either immediately dissolved into water after their release, like ethylene glycol, or into

the sediment, like tetraethyl lead, or even too volatile for remaining into the water, we could not study the differences implied by releases at surface and bottom. We plainly proved the furthest importance of the wind in the pollution drift, particularly in St Andrew Bay system where the shallowness gives an outstanding weight to the wind in driving the flow. Because the water flows inward at Gulf entrances and splits asymmetrically mostly towards West Bay, the dependence of the chemical dispersion on the release point is strong and East Bay is hardly impacted unless the pollution takes source in the bay itself or when winds are blowing eastward. The chemical clearly propagates westward during the simulation with a concentration generally damping away from the source except in very shallow zones where some accumulation can occur with favorable winds. These accumulations are finally responsible of secondary pollution events. It is, at last, obvious that these results were biased, again, by the bathymetry smoothing process. However, it is reasonable to conclude that, as East Bay presents a rather uniform depth, this bias impact was not so crucial in this area and also that most of the pollution drift relied on the wind.

Furthermore, the description of different salt diffusion processes during ebb and flood tides besides the observation that spring tides were globally causing a general freshening of the system by pumping fresh water while neap tides let salt to diffuse from the saltier St Andrew Bay towards both East Bay and particularly West Bay constituted two central resulting outcomes. The tidal impact study finally described an estuarine circulation with imbalanced ebb and flood periods.

X. LIST OF REFERENCES

Atkinson,L.P., Lee,T.N., Blanton,J.O. and Chandler,W.S., 1983. *Climatology of the southeastern United States continental shelf waters*. J. Geophys. Res., 88, 4705-4718.

Blumberg Alan F. and B. N. Kim, 2000. *Flow balances in St. Andrew Bay revealed through hydrodynamic simulations.* Estuaries Vol. 23, No. 1, p. 21–33.

Davis, R.A., 1994. *Barriers of the Florida Gulf peninsula*. Davis, R. A., ed., Geology of Holocene Barrier Islands: Springer-Verlag, Berlin, p. 167-205.

Fischer H.B., E.J. List, R.C.Y. Koh, J. Imberger and N.H. Brooks, 1979. *Mixing in Inland and Coastal Waters*. Academic Press, 483 pp, San Diego.

Ichiye, T. and M. L. Jones. 1961. *On the hydrography of the St. Andrew Bay system, Florida.* Limnology and Oceanography 6, p.302–311.

Jain Manta, Mehta A. J., van de Kreeke J. and Dombrowski M. R., 2004. *Observations on the stability St. Andrew Bay inlets in Florida*. Journal of coastal research, Vol. 20 (3), pp 913-919.

Kantha, L, H and Clayson, C A (2000). *Numerical models of ocean and oceanic processes*, Academic Press, 940pp, San Diego, CA.

Lohrenz, S. E. and P. G. Verity. *Regional Oceanography: Southeastern United States and Gulf of Mexico (2,W)*. The Sea, Vol. 13, The Global Coastal Ocean: Interdisciplinary Regional Studies And Syntheses (A. R. Robinson and K. H. Brink, Eds.), John Wiley & Sons, New York, in press (2004).

Madala, R. V. and Piacsek, S A. (1977). *A semi-implicit numerical model for baroclinic oceans.* Journal of Computational Physics, Vol. 23, pp167-178.

McCay D.P.F. and T. Isaji, 2004. *Evaluation of the consequences of chemical spills using modeling: chemicals used in deepwater oil and gas operations*. Environmental modeling & software Vol 19 (7-8), p. 629-644.

Muin, M. and M. L. Spaulding, 1996. *Two-dimensional boundary fitted circulation model in spherical coordinates.* Journal of Hydraulic Engineering, 122 (9), 512-520.

Musgrove R. H., J. B. Foster, and L. G. Toler, 1965. *Water resources of the Ecofina Creek basin area in northwestern Florida.* Report of Investigation No. 41. Florida Geological Survey. United States Geological Survey, Florida.

Pritchard, D. W., 1952. *Estuarine hydrography.* Advances in geophysics I. New York: Academic Press, pp. 243-280.

Roberts,H.H., McBride,R.A. and Coleman,J.M. (1999). *Outer shelf and slope geology of the Gulf of Mexico: An overview*. The Gulf of Mexico Large Marine Ecosystem (Kumpf,H., Steidinger,K. and Sherman,K., Eds.), pp. 93-112. Blackwell Science, Malden, MA.

Solis,R.S. and Powell,G.L., 1999. *Hydrography, mixing characteristics, and residence times of Gulf of Mexico estuaries*. Biogeochemistry of Gulf of Mexico Estuaries (Bianchi,T.S., Pennock,J.S. and Twilley,R.R., Eds.), pp. 29-61. John Wiley & Sons, Inc., New York.

Spaulding, M. L., D. Mendelsohn, and J. C. Swanson, 1999. *WQMAP: An integrated three-dimensional hydrodynamic and water quality model system for estuarine acoastal applications.* Marine Technology Society Journal, invited paper, Special issue on state of the art in ocean and coastal modeling, Vol. 33, No. 3, p. 38-54.

U. S. Army Corps of Engineers. *National Shoreline Study - Regional Inventory Report*. South Atlantic Division, Atlanta, Georgia, August 1971.

Van de Kreeke J., Mamta J., Ashish J. Mehta and Michael R. Dombrowski, 2004. *Observations on the Stability St Andrew Bay Inlets in Florida*. Journal of Coastal Research, Vol. 20 (3), pp 913-919.

Weisberg, R.H., Z. Li, and F.E. Muller-Karger, 2001. *West Florida shelf response to local wind forcing: April 1998*. J. Geophys. Res., 106, 31239-31262.

Wiseman,W.J.,Jr. and Sturges,W., 1999. *Physical oceanography of the Gulf of Mexico: Processes that regulate its biology*. The Gulf of Mexico Large Marine Ecosystem (Kumpf,H., Steidinger,K. and Sherman,K., Eds.), pp. 77-92. Blackwell Science, Malden, MA.

XI. INITIAL DISTRIBUTION LIST

1. Defense Technical Information Center
   Ft. Belvoir, Virginia

2. Dudley Knox Library
   Naval Postgraduate School
   Monterey, California

3. Mary L. Batteen
   Department of Oceanography
   Naval Postgraduate School
   Monterey, California

4. Peter C. Chu
   Department of Oceanography
   Naval Postgraduate School
   Monterey, California

5. Steven D. Haeger
   Naval Oceanographic Office,
   Stennis Space Center, Mississipi

6. Matthew Ward
   Applied Science Associates, Inc.
   Narragansett, Rhode Island

7. Etablissement Principal du Service Hydrographique et Océanographique de la Marine
   Brest, France